NTNU
Norwegian University of
Science and Technology

Approaches to Numerical Simulations of Causal Sets

Conor Andre Kelly

MSc in Physics
Submission date: July 2018
Supervisor: Jan Myrheim, IFY

Norwegian University of Science and Technology
Department of Physics

Acknowledgements

Summary

This project explores the prospect of fundamental causal set events and whether or not there exist classes of fundamental event types. By considering so-called *Feynman posets*, where each vertex has a maximum degeneracy of three, this project aims to initiate the study by introducing vertex degeneracy as a defining property of fundamental events. The natural next step is to generalize by constructing posets containing n-degenerate vertices.

The first part of the project includes a classical growth model that simply constructs a sample of Feynman posets subject to no dynamic constrictions. In the second part, an action principle was introduced to drive the construction process away from the entropic space of posets and towards the most manifoldlike posets in the subspace of Feynman posets, if they exist. Unfortunately, the action-driven growth algorithm suffers from serious conceptual and implementational defects and offers little more than insights into what *not* to do when calculating the action on a causal set and does not produce interesting posets at this stage. However, the algorithm may prove useful in further studies under different contexts.

The analysis includes statistical considerations of poset height, level structure, total ordering fractions, and poset d-rigidity (a test for the existence of local regions and therefore a condition for manifoldlikeness). The analysis also includes results from coarse-graining the posets at a number of different levels. Finally, this document also provides an insight on internal interval observables within each poset along with Hasse diagrams of selected subintervals.

In addition to the computational study of Feynman posets, this document includes an expansive (although far from exhaustive) review of literature on causal sets, a discussion on the philosophical approaches to the study, and a technical discussion on several theoretical obstacles that arise in the study. Of critical importance are the scripts that were developed to carry out the project, which have been made publicly available for further study and are presently being improved through new releases. It is hoped that the literature review provided by this document proves useful for prospective causal set researchers in the future as well.

This study provides partial evidence for the manifoldlikeness of *some* Feynman posets. So-called *no holes* posets satisfy several manifoldlikeness conditions, including the agreement of dimension estimators and the existence of local regions at larger scales after coarse-graining. On the other hand, the so-called *holes* posets are found to be more diverse and preliminary investigations reveal no manifoldlikeness at this stage. While the results for the *no holes* posets are encouraging, a conclusive statement awaits further study with more tests for manifoldlikeness.

Preface

An adventure lacking in prospect or a rush made blindly, however, would in most cases end in failure. The adventure that really trains the theory and leads to correct cognition must have an accurate prospect more than anything else. The perspective adventure, even if it fails, is able to teach certainly lessons from the failure and secures the success in the next adventure.

- Shoichi Sakata, 1948

I don't know how radical you are, or how radical I am. I am certainly not radical enough. One can never be radical enough; that is, one must always try to be as radical as reality itself.

- V.I. Lenin

Contents

List of Tables

List of Figures

Units and Conventions

This document will use *natural units*, i.e. the speed of light, the gravitational constant, and the Planck constant are set to unity:

$$c = 1$$
$$G = 1$$
$$\hbar = 1$$

unless otherwise specified.

This document uses the *spacelike* metric signature convention,

$$(-,+,+,+,...)$$

Throughout this document, the terms *Minkowski spacetime* and *Lorentzian manifold* will frequently be used interchangeably. The Lorentzian manifold is typically defined as any manifold with the above signature, while Minkowski spacetime is typically defined to be a flat Lorentzian manifold with the metric

$$\eta_{\mu\nu} = \begin{pmatrix} -1 & 0 & 0 & 0 \\ 0 & 1 & 0 & 0 \\ 0 & 0 & 1 & 0 \\ 0 & 0 & 0 & 1 \end{pmatrix}$$

in four dimensions. Since this document makes explicit reference to whether or not the manifold in question is flat or curved, this convention will not be observed.

1

Introduction

This chapter will deal with quantum gravity in general and some of the justifications behind the causal set approach to quantum gravity, including a brief background in general relativity and Einstein's field equations to motivate the project. Following a philosophical overview of the methodology of the field, the last section will provide an orientation for the project and outlines the remaining sections.

1.1   Quantum Gravity

The search for a "theory of everything" is perhaps the most highly anticipated development in the field today, whether it is a subsequent task underlying Grand Unification or a goal in its own right. It suffices to say that one of the biggest embarrassments in physics is the incompatibility of two equally empirical properties of our universe: general relativity and quantum field theory. Unifying gravity with the three other forces has been a task since the late 1970s and is a noble, if not lofty, pursuit if we are to finally move beyond the Standard Model and into Planck's realm. Yet, for this author, the pursuit for this "theory of everything" seems a little premature, just as it was at the turn of the last century. More explicitly formulated, making general relativity and quantum field theory agree means having a theory of gravity that does not break down on the small scales that hold for the other forces in quantum field theory. How could we ever hope to achieve this so-called "theory of everything" if we do not start with the first step? That first step is quantum gravity.

What is quantum gravity? Most definitions are fairly straightforward, although it must be noted that the specific formulation will favor different approaches. This project will adapt David Reid's working definition:

> *quantum gravity is a theory that describes the structure of spacetime and the effects of spacetime structure down to sub-Planckian scales for systems containing any number of occupied states* [44].

Perhaps the most contentious part of Reid's definition is that the theory must describe "the structure of spacetime and the effects of spacetime structure". It favors those approaches that place primacy on geometry as the property from which the gravitational force arises, unlike approaches like string theory that propose fundamental gravitational "bosons" that define the interaction, rather than identifying the geometry itself as the carrier of the gravitational force. Moreover, the diction of *structure* evokes imagery of fundamental point-like discreteness, in contrast to Causal Dynamical Triangulation. Taking general relativity seriously means entertaining its literal interpretation, that *gravity is geometry*. While most of the literature simply cites the metric tensor $g_{\mu\nu}$ and the Einstein field equations and calls it a day, this document will trace this logic in more detail, despite its tedium, but stopping short of fully deriving the Einstein field equations. It is so fundamental to the argument behind causal sets that this author believes that it is worth the effort. It will also help to provide a clear understanding of the tools that are so central to causal set theory outlined in Chapter 2. The following discussion on the Einstein field equations and how the gravitational field arises from the source it describes follows Hartle [26].

1.1.1   Einstein Field Equations

The Einstein field equations are given by

$$R_{\mu\nu} - \frac{1}{2}Rg_{\mu\nu} + \Lambda g_{\mu\nu} = 8\pi T_{\mu\nu} \tag{1.1}$$

where $R_{\mu\nu}$ is the Ricci curvature tensor, R is the Ricci scalar curvature, $g_{\mu\nu}$ is the metric tensor, Λ is the cosmological constant, and $T_{\mu\nu}$ is the stress-energy tensor. Before going further, it's worth noting that the field equations express the fundamental principle that *gravity is geometry*. On the left-hand side of Equation (1.1), $R_{\mu\nu}$, R, and $g_{\mu\nu}$ all characterize the geometry, while $T_{\mu\nu}$ on the right-hand side serves as the source for the gravitational field. In turn:

The metric tensor is given by the *line element*,

$$\mathrm{d}s^2 = -g_{\mu\nu}\,\mathrm{d}x^\mu\,\mathrm{d}x^\nu$$
$$= -g_{00}\,\mathrm{d}t^2 - g_{11}\,\mathrm{d}x^2 - g_{22}\,\mathrm{d}y^2 - g_{33}\,\mathrm{d}z^2 - ... \tag{1.2}$$

where $\mathrm{d}x^\mu$ gives the infinitesimal displacements between two points in the metric space for the coordinates labeled by μ and $\mathrm{d}s$ is the line element. The line element can be thought of as the length of some curve defining the trajectory between the two points in the metric space.

The Ricci curvature tensor is given by

$$R_{\mu\nu} = \frac{\partial \Gamma^\gamma_{\mu\nu}}{\partial x^\gamma} - \frac{\partial \Gamma^\gamma_{\mu\gamma}}{\partial x^\nu} + \Gamma^\gamma_{\gamma\delta}\Gamma^\delta_{\mu\nu} - \Gamma^\gamma_{\nu\delta}\Gamma^\delta_{\gamma\mu} \tag{1.3}$$

where Γ, the Christoffel symbols, define the geodesic equation, describing the trajectory of a particle in curved spacetime:

$$\frac{\mathrm{d}^2 x^\mu}{\mathrm{d}s^2} = -\Gamma^\mu_{\nu\gamma} \frac{\mathrm{d}x^\nu}{\mathrm{d}s} \frac{\mathrm{d}x^\gamma}{\mathrm{d}s} \tag{1.4}$$

If one imagines a collection of points in spacetime that form some closed object with some volume, then $R_{\mu\nu}$ expresses the rate of change of that object's volume along its line element as it moves through the metric space.

The Ricci curvature tensor is generalized by the *Riemann curvature tensor*, and the former may be derived by taking the trace of the latter:

$$R_{\mu\nu} = R^\alpha_{\ \mu\alpha\nu} = g^{\alpha\beta} R_{\alpha\mu\beta\nu} \tag{1.5}$$

Physically, one may think of the Riemann tensor as describing not only the rate of change of the *volume* of our ball of test points, but also its *shape*. In a completely empty region of spacetime, $R_{\mu\nu} = 0$, but the Riemann curvature tensor is, in general, nonzero. The details will not be given in this document, but the Riemann curvature tensor can be decomposed into three parts; in an empty region of spacetime, all but one–the *Weyl tensor*–vanish. While the other two parts encompass gravitational effects from immediate non-gravitational forces and matter, the Weyl tensor encodes information about "everything else" that may contribute to the curvature of the region (e.g. gravitational waves). This is introduced only to emphasize that "empty spacetime" should not be thought of as equivalently flat spacetime.

In the context of Equation (1.4), it is also natural to define the Christoffel symbols with respect to the metric tensor:

$$\Gamma^\gamma_{\mu\nu} = \frac{1}{2} g^{\gamma\delta} (\partial_\nu g_{\delta\mu} + \partial_\mu g_{\delta\nu} - \partial_\delta g_{\mu\nu}) \tag{1.6}$$

where the notation

$$\partial_\mu = \frac{\partial}{\partial x_\mu} \tag{1.7}$$

has been introduced and will be used throughout the remainder of this document.

The second term on the left-hand side of Equation (1.1) must be a rank two tensor, which can be constructed from the scalar curvature and the metric tensor.[1] The former is the scalar analogue of the Ricci curvature tensor and assigns a value corresponding to this change at each point (furthermore, it is the trace of the Ricci curvature tensor and can thus also be expressed in terms of Christoffel symbols).

As for the last term on the left-hand side of Equation (1.1), for the purposes of this project, Λ, the cosmological constant, will be interpreted as vacuum contributions to the

---

[1]If this addition seems ad hoc, it's because it is in this treatment. As promised, I will not derive the Einstein field equations in this space, but only briefly mention that without this term, the field equations would violate conservation of energy and momentum. A full(er) treatment is given in [40]. Furthermore, Lovelock's Theorem states that this is the only possible form for this second "conservation-preserving" term [11].

stress-energy tensor and will be subsumed into the term on the right-hand side,[2] such that Equation (1.1) now reads:

$$R_{\mu\nu} - \frac{1}{2}Rg_{\mu\nu} = 8\pi T_{\mu\nu} \tag{1.8}$$

The stress-energy tensor, $T_{\mu\nu}$, expresses the total energy and momentum density and flux in spacetime. More specifically, it is the contribution of all matter, radiation, and any other non-gravitational fields. E.g. for some fluid, the contravariant stress-energy tensor is given by

$$T^{\mu\nu} = \rho u^{\mu} u^{\nu} \tag{1.9}$$

where ρ is the energy density and u^{μ} is the four-velocity of the fluid.

Finally, using the Einstein field tensor defined by

$$G_{\mu\nu} = R_{\mu\nu} - \frac{1}{2}Rg_{\mu\nu} \tag{1.10}$$

the Einstein field equations reduce to the simple form

$$G_{\mu\nu} = 8\pi T_{\mu\nu} \tag{1.11}$$

The Stress-Energy Tensor as a Source for Gravitational Fields

If the stress energy tensor is truly the source of gravitational fields, then the Einstein field equations should reduce to the Newtonian field equation for gravity in the limit of an approximately flat geometry and nonrelativistic matter:

$$G_{\mu\nu} = 8\pi T_{\mu\nu} \qquad \text{Einstein Field Equations}$$
$$\nabla^2 \Phi = 4\pi\rho \qquad \text{Newtonian Field Equation for Gravity}$$

where Φ is the (Newtonian) gravitational potential and in this context, ρ is the mass density.

The limit of an approximately flat geometry implies a weak gravitational field, such that the metric can be approximated by $\eta_{\mu\nu}$, the metric for a flat geometry,

$$\eta_{\mu\nu} = \begin{pmatrix} -1 & 0 & 0 & 0 \\ 0 & 1 & 0 & 0 \\ 0 & 0 & 1 & 0 \\ 0 & 0 & 0 & 1 \end{pmatrix} \tag{1.12}$$

plus a small metric perturbation, $h_{\mu\nu}(x)$:

$$g_{\mu\nu} = \eta_{\mu\nu} + h_{\mu\nu}(x) =$$
$$\begin{pmatrix} -(1+2\Phi) & 0 & 0 & 0 \\ 0 & (1-2\Phi) & 0 & 0 \\ 0 & 0 & (1-2\Phi) & 0 \\ 0 & 0 & 0 & (1-2\Phi) \end{pmatrix} \tag{1.13}$$

---

[2]This is justified because it satisfies local energy-momentum conservation, $\nabla_\nu T_{\mu\nu} = 0$ where ∇_ν is the covariant derivative. Alternatively, one may impose $\Lambda = 0$ and define the Einstein tensor without this term, which is the typical treatment in the literature and reflected here in Equation (1.10).

Inserting this expansion into the Einstein tensor, Equation (1.10), and using Equation (1.6) gives [26]

$$G_{\mu\nu} = G_{00} = 2\nabla^2\Phi + \mathcal{O}(\Phi^2) \tag{1.14}$$

The Newtonian limit also implies that the stress energy is dominated by rest energy, because for nonrelativistic matter, $v \ll c$, and to maintain consistency with the weak field approximation, ρ, the rest energy density, must also be small. Then $u^\mu = (1, \vec{0})$ and using Equation (1.9), the first order of the stress energy tensor is simply

$$T^{\mu\nu} = T^{00} = \rho \tag{1.15}$$

Lowering the indices for the stress-energy tensor and inserting these into the Einstein field equations, Equation (1.11),

$$\nabla^2\Phi = 4\pi\rho \tag{1.16}$$

The result is the *linearized gravitational field equation*, equivalent to the Newtonian field equations for gravity.

In analogy to electromagnetism, compare the field equations:

$$\nabla^2\Phi = 4\pi\rho \qquad \text{Linearized gravitational field equation}$$
$$G_{\mu\nu} = 8\pi T_{\mu\nu} \qquad \text{Einstein's Field Equations}$$
$$\nabla_\mu F^{\mu\nu} = 4\pi J^\nu \qquad \text{Maxwell's Equations}$$

where in the latter equation, $\mu_0 = \frac{2\alpha h}{e^2 c}$ and in natural units, $e = \sqrt{\alpha}$ is the charge of an electron, $h = 2\pi\hbar = 1$ is Planck's constant, and α is the fine structure constant, i.e. $\mu_0 = 2\pi$.

Towards a Fundamental Unit of Spacetime

Order + Number = Geometry
- Rafael Sorkin

As J^ν is the source of electromagnetic fields, $T_{\mu\nu}$ is the source of gravitational fields. As $F^{\mu\nu}$ is the electromagnetic field, $g_{\mu\nu}$ is the gravitational potential,[3] identically characterizing the geometry of some spacetime. For some spacetime geometry–perhaps one like the familiar 4-dimensional, smooth, connected Lorentzian manifold that describes our own universe–what could be more fundamental than its causal structure? What more is needed to specify the geometry than a light cone at each and every point? This is an instance of the causal metric hypothesis, a term introduced by Dribus which states that "the observed properties of the physical universe arise from causal relationships between pairs of events, or more generally, from causal relationships among families of events," and furthermore that "the hypothesis takes the familiar relationship between cause and effect to be the fundamental building block of this structure [19]."

---

[3]N.B., not $G_{\mu\nu}$ nor $R_{\mu\nu}$. In Maxwell's equations, the left-hand side is the *derivative* of $F^{\mu\nu}$. Lovelock's Theorem implies that the only possible solution is proportional to the metric tensor, $g_{\mu\nu}$ [11]. The gravitational *field* is a more complicated matter involving the so-called *exterior derivative* in mathematics, but this is more than is needed for this document.

This exposition places certain demands on causal set theory. As long as the action is approximately extremized such that the scale can be compared to the continuum limit, causal sets must [39] :

1. Give a spacetime dimension of 4 at the continuum limit.
2. Produce a light cone given by the metric according to $g_{\mu\nu}dx^\mu dx^\nu \leq 0$ everywhere.
3. Satisfy $R_{\mu\nu} = 0$ in a vacuum.

1.1.2 Malament's Theorem and Kleitman-Rothschild

This account of the story does little justice to the history. A theorem by David Malament states

> Suppose (M, g) and (M', g') are spacetimes and $f : M \longrightarrow M'$ is a bijection where both f and f^{-1} preserve future directed continuous timelike curves. Then f is a conformal isometry [37].

Malament furthermore concludes in a corollary that the causal structure (represented by ordered sets–a mathematical object) is enough to recover the spacetime geometry up to a conformal factor. This is often referred to as the *Hauptvermutung*, or central conjecture of causal set theory. It served as the motivation for Rafael Sorkin's aforementioned claim: "Order plus Number equals Geometry", where order is the binary relation on a causal set, i.e. Malament's family of curves, while the number is a volume corresponding to the above missing conformal factor. In his 1978 preprint, Myrheim suggests a counting measure as a means of quantifying volume by proposing the assumption of a discrete spacetime [41]. By taking an arbitrary region of spacetime as the starting point, it has been possible to model causal sets that are approximated by the continuous Lorentz manifold in a process referred to as *sprinkling*. Sprinkling has been the leading strategy for developing the kinematic tools needed to describe causet observables.

Pedestrian experience informs us that space and time are continuous, yet the discreteness of its fundamental units is central to causal set theory. These units are proposed to be Planckian, and we therefore expect the dynamics to be governed by an action principle as in quantum mechanics. In the same way a continuous drop of water approximates an abundance of discrete atoms, spacetime approximates the causal set; in the same way the classical trajectory arises from an infinite sum over its absurd (and reasonable) paths, the familiar manifold arises from a sum over of causal structures that look nothing like it. The task that lies before causal set theory is thus to develop 1) an analogous quantum measure that assigns to each spacetime structure an amplitude and 2) a configuration space of causal sets to sum over.

The main obstacle in this endeavor is the *Kleitman-Rothschild Theorem*, which states that the proportion of non-manifoldlike topologies on ordered sets containing N elements approaches 1 in the asymptotic limit, $N \longrightarrow \infty$, and furthermore that this dominant space of sets contains three-layered configurations (more specifically, sets with roughly half of the events in the middle layer) [33, 32]. Such sets are often referred to as *Kleitman-Rothschild orders*, or *KR orders*. Needless to say, such sets are decisively not like spacetime because they represent an infrared universe that is extremely vast while being extremely short-lived. The Kleitman-Rothschild theorem is the key contributor to what is

known as the Entropy problem in causal set theory. It has also been shown in [55, 43] that there exist a subdominant entropic space of two- and four-layered orders that for similar reasons are non-manifoldlike.

1.2 Dialectics of Nature[4]

Quantum gravity is a difficult idea for us to grasp. It combines the unobservability of sub-Planckian nature with our sense of familiarity with the strangeness of quantum physics; the lack of empirical results has given causal set theory the stigma of being a "solution without a problem", and this has been enough for many to claim that the theory evolves in an entirely different manner than the rest of scientific development. In much of the seminal literature on causal set theory (see e.g. [7]), Taketani's *Doctrine of the Three Stages of Scientific Development* has been cited in an effort to organize the theory, with notable adjustments made to reflect the perceived uniqueness of quantum gravity in physics. Tracing Taketani's three stages back to its inspiration, one finds that there is nothing particular about causal set theory in the development of our understanding of nature. There are two reasons for correcting this position.

The first is that the study of quantum gravity needs more discipline. The historical approaches to causal set theory amount to little more than (expertly) groping in the dark, and causal set theory is in turn just one of dozens of approaches to quantum gravity. Even this project is not exempt from this dilemma. This is not necessarily a bad thing, but even when a fuse is blown in one's house, there is an implicit strategy for navigating around the room in search for a flashlight or better yet: the circuit breaker. Taketani's three stages embody this strategy in physics and there are therefore one of two ways to move forward: we ensure that they are well understood and take them seriously, or we fundamentally reorganize our strategy.

Feynman is purported to have said that "the philosophy of science is as useful to scientists as ornithology is to birds". Although the apocryphal retort is admittedly salient, no squabbles between physicists and philosphers could ever supersede Marx's timeless jibe on both: "Philosophers have hitherto only *interpreted* the world in various ways; the point is to *change* it." In other words, to lift a line from Dribus, "physics should seek not to prescribe what may be, but to describe what is [20]." We would do well to keep this in mind when we search for *some* theory for *our* structure, lest we discover that we have found little more than *our* theory for *some* structure. Thus, the second reason: that "we must clearly distinguish physics itself from interpretations of physics given by physicists. They often state things which are different from what they have done," as Sakata affirms in [62].

---

[4]Readers allergic to political and/or philosophical discourse may skip this section, but the author implores those who entertain its contents to consider the following appeals to *ethos* before evaluating its *kairos*: 1) this philosophy of science is cited in much of the literature in causal set theory, particularly the seminal literature on the topic; in some places it is even used to define terms, as in [44, 7, 8, 50, 38], and 2) Taketani Mitsuo, the author of this philosophy of science, was an important contributor to the discovery of the meson, a development he cited when establishing this interpretation of Marxist dialectics.

1.2.1 Dialectic Materialism

In addition to being a renowned physicist, Taketani was a Marxist and his approach was explicitly grounded in dialectic materialism. The triad *thesis, antithesis, synthesis* (read: a phenomenon, its logical negation, their reconciliation), revealed first by Hegel, is the backbone of both Taketani and Marx's scientific approach. To apply it to causal sets, we must make a brief detour.

From Hegel arise three laws of dialectics:

1. *The law of the unity and conflict of opposites.* An object exists only insofar as it is the realization of the unity of opposites, i.e. for each thesis there exists a contradictory antithesis: the logical negation of the thesis.

2. *The law of the passage of quantitative changes into qualitative changes.* The conflict between opposites is never in perfect balance, which gives rise to small quantitative changes to the object. Over time, these quantitative changes abruptly give way to a qualitative change in the *synthesis* of contradictions to form a new thesis with its own antithesis.

3. *The law of the negation of the negation.* The original antithesis that negated the original thesis is itself negated. After cyclces of synthesis, the dialectic process has returned the original thesis, now governed by new laws of development. While Hegelian dialectics maintain that there is an "ultimate" negation of the negation–a deterministic Absolute to end all conflicts of opposites[5],dialectic materialism states that the absence of conflict is the absence of existence.

While Hegel's concept of the Absolute is deterministic, dialectic materialism is stochastic (although decidedly not Markovian) and the dialectic process never terminates. The Hegelian dialectic is *idealist*, in that the process is driven by the Spirit. On the other hand, dialectic materialism declares that the laws of motion are strictly material. In *Das Kapital*, Marx writes

> The mystification which dialectic suffers in Hegel's hands, by no means prevents him from being the first to present its general form of working in a comprehensive and conscious manner. With him it is standing on its head. It must be turned right side up again, if you would discover the rational kernel within the mystical shell...

> My dialectic method is not only different from the Hegelian, but is its direct opposite. To Hegel, the life-process of the human brain, i.e. the process of thinking, which, under the name of 'the Idea', he even transforms into an independent subject, is the demiurgos of the real world, and the real world is only the external, phenomenal form of 'the Idea'. With me, on the contrary, the ideal is nothing else than the material world reflected by the human mind, and translated into forms of thought.

In summary, the dialectic materialism adapted by Taketani is just that: 1) *material*, such that phenomena exist independently of the knowledge of nature and 2) *dialectic*,

---

[5]Incidentally, Hegel himself claimed that this Absolute was the Prussian monarchy.

such that theory is no more than the "temporary, relative, approximate character of [the] *milestones* in the knowledge of nature". As Lenin describes it in his *Materialism and Empirio-Criticism*, "The electron is as *inexhaustible* as the atom, nature is infinite, but it infinitely *exists* [58]."

The sharpest resolution of dialectics today is Maoist dialectics,[6] from which just one additional law must be presented: the distinction between the principal contradictions and secondary contradictions. "If in any process there are a number of contradictions, one of them must be the principal contradiction playing the leading and decisive role, while the rest occupy a secondary and subordinate position." According to Mao, "the principal and the non-principal aspects of a contradiction transform themselves into each other and the nature of the thing changes accordingly [60]."

Consider, e.g. a train. For a steam engine, the primary contradiction is the friction between the wheels and the track, while air resistance is only secondary. Its motion is the unity of opposites: the friction that enables acceleration and the very same force that simultaneously hinders it. The synthesis of this unity of opposites is realized by the Maglev. Yet, this gives rise to another unity of opposites; the friction between the train and the tracks (whether mechanical or electromagnetic drag) becomes secondary, while air resistance becomes primary. This process continues *ad infinitum*, with vactrains, and so on! Critically, the motion of this development is driven at all points by the frictional force, only taking different forms with each successive synthesis. Likewise, the Maglev does not move faster than the steam engine because the mind wills it: it moves faster because the objective material conditions allow it. Perhaps some new form of transportation arises that is entirely frictionless: a negation of the negation (although, as physicists, we ought to agree with Lenin in that nature is infinite). Even then, this mode of transportation exists only as a unity of opposites, and the dialectic continues according to new rules.

I have surely not done justice to these principles. The preceding background is designed only to give a very rough outline for the basis of the methodology used in several fields, but in particular in causal set theory. Although I would sincerely like to expand this discussion, this document is simply not the space for an in-depth discussion on the matter. Readers who are interested in this topic can refer to the supplementary bibliography provided at the end of this document. Without further ado, I will demonstrate the relevance for the patient reader who may be wondering where this digression is going.

1.2.2 Taketani's Three Stages

Sakata describes Taketani's stages in the following manner:

> The first is the phenomenological stage [thesis] in which the [object] is described as it is. The second is the substantialistic stage [antithesis] in which it is investigated what structure the object has. The third is the essentialistic stage [synthesis] in which it is clarified by what interactions and under what laws of motion the object moves [62].

---

[6]Incidentally, Taketani could very well have been a Maoist, at least philosophically speaking. The two come to an identical conclusion almost concurrently, but likely semi-independently (the former in January 1936; the latter in August 1937): that the unity of contradictions is the only fundamental law, and the other laws are just its manifestations.

Essential to understanding this theory is Taketani's discussion on quantum mechanics and dialectics in [63], in which he posits that "[science] is, at every point, accomplished by dialectics," its main point "the unification of antagonisms". We begin with observation of an object, e.g. Malament's theorem: that the spacetime structure can be recovered from an ordered set. Then, we make an investigation of the object's substantial properties which contradicts our initial observation, e.g. the Kleitman-Rothschild theorem: that the space of ordered sets is dominated almost entirely by sets whose topologies look nothing like spacetime.

Finally comes recognition, the essentialistic stage, or synthesis: "the copying of Nature..." which "penetrates deep into, and still deeper into, the essence of Nature..." This stage is "the process of bringing the copy into agreement with the object...[rather than an] arbitrary 'production' of the [observation]." Taketani seems to have come to a similar conclusion as Lenin when he identifies the synthesis with analysis and stresses that "observation itself is not recognition." At the risk of redundancy, this author offers another example: 1) the Hegelian thesis of nuclear fusion in stars and 2) its logical negation–our understanding of Coulomb forces. The observation of heavy elements is not identically the recognition of quantum tunneling. It is only with the analysis provided by quantum mechanics that the antagonism between nuclear fusion and Coulomb forces is unified in the synthesis.

Bombelli writes in [7] that "quantum gravity, however, is forced to skip virtually all of the first stage and tackle the second and third stages simultaneously, hoping that the resulting theory will enable us to recognize with hindsight what features of already-known physics can serve as its 'phenomenology'." In this author's opinion, this is a misunderstanding of Taketani's theory, where the dialectic has again been turned on its head. It is true that causal set theory today seeks to phenomenologically identify the nature of the causal set's fundamental unit, but it is incorrect to suppose that this has been its original thesis. For Bombelli, it is the geometrical properties of the causal set that is the antithesis (which he refers to as the *kinematics*), while the synthesis (which he refers to as the *dynamics*) is the mechanism by which the causal set gives rise to the "higher-level structure" of the continuum.

A philosophical flaw in causal set theory is demanding that the phenomenology amounts to a direct measurement of the object. This is the same form of dogmatic and mechanical empiricism that Taketani decries in [63]. The phenomenological stage has *already* been completed: it is Malament's theorem (or more precisely, its corollary: that causal structure specifies the spacetime geometry). Alternatively, taken from the perspective of causal set theory, the thesis is that ordered sets are approximated by the spacetime manifold. The unhappy empiricist can be satisfied with sprinklings if a more concrete phenomenonology is needed. The antithesis is then its negation, the Kleitman-Rothschild theorem: that the distinct topologies on ordered sets are overwhelmingly non-manifoldlike.

My purpose is not to appear flippant (or worse yet–*Hegelian!*). As a materialist philosophy, this dialectic *requires* a certain level of empiricism, at least at some point. Were we to be indefinitely content with sprinklings without speaking to the nature of the fundamental units of gravity, we would not be doing physics (or dialectic materialism for that matter), but rather something else entirely! Yet, as physicists, the very act of sprinkling presupposes a claim–albeit a temporarily immeasurable one–about some physical *thing*

that the object we construct represents. The phenomenology of causal set theory is certainly weak, but far from nonexistent. The quantitative changes to causal set theory are not so difficult to identify in this context, and one finds that they are the result of two contradictions, alternating in their primacy:[7]

1. The class of causal sets was once the class of all ordered sets: a *phenomenological* whole. The *substantialistic* existence of spacelike separated points demands an object that reflects incomparable elements. The principal contradiction is kinematic. In the first iteration of Taketani's third stage then, the *essentialistic* reconciliation of the contradiction between the whole and its irreconcilable parts has reduced it to a subclass of ordered sets: the class of *partially* ordered sets. This is itself a whole, but again the unity of contradictions: the *phenomenological* whole of its members and the *substantialistic* non-manifoldlike topologies on a large portion of its sets.

2. *Phenomenologically*, we presume that the events in the single causal set that describes our universe are on the order of Planck's length. *Substantialistically*, we find that objects on such scales are more "fuzzy" than they appear macroscopically; that the object itself is not a singular entity, but rather the superposition of its various states. The principal contradiction is dynamic. In this iteration, the *essentialistic* reconciliation leads to the recognition of quantum mechanical rules that govern the causal set. It will take many small quantitative changes before causal set theorists find an appropriate way to sum over causal sets.

With each iteration, the laws become more and more complex, from lower levels to higher levels of structural complexity. These small quantitative changes lead to a qualitative leap, radically changing the character of the theory. One cannot be definitive about what this revolution looks like, simply because the theory hasn't reached a level where it will undergo a qualitative change quite yet. I certainly don't know what the fundamental unit of gravity looks like today.

The substantialistic stage is then both the kinematics and the dynamics as defined by Bombelli–the identification of that which makes these topologies non-manifoldlike. Or more precisely, the kinematics and dynamics are the kernel of the *contradictions* between the thesis and the antithesis: realized between Taketani's first and second stages, made apparent in his third. It is the struggle between the thesis and antithesis (where the principal contradiction alternates between kinematics and dynamics) that informs the synthesis. The synthesis may be the kinematic removal or addition of topologies on sets considered, the dynamical rules by which the topologies on the sets give rise to the manifold, or some union of these developments. In sum, each iteration tells us more about the phenomenology of the fundamental unit of gravity, and perhaps there will come a qualitative leap in causal set theory's future that reveals to us how to satisfy the gentle experimentalist!

The unity of contradictions in causal set theory can be rephrased once more by appropriating Dowker's brilliant language:

Causal set theory is described by the dialectic process arising from the antagonism between Action and Entropy.

---

[7]The Maoist concept of *One Divides Into Two* may also be of use here. The term originates from Lenin, who writes "The splitting of a single whole and the cognition of its contradictory parts ... is the essence ... of dialectics [59]."

Every successful theory, whether it be the theory of making revolution or QCD, has been systematized and dialectical. It is this author's belief that causal set theory has suffered such a long hiatus in development precisely because it has failed to properly identify the principal contradiction between Taketani's first and second stages, a stumbling block introduced due to the misunderstanding of the dialectics of nature and an inability to recognize the universal property of the unity of contradictions.

1.3   Overview of this Project

This project introduces the class of *Feynman posets* as a toy model for exploring the effects of kinematic restrictions on the object approximated by continuous spacetime. By placing strict restrictions on the properties of the set's elements and exploring the properties of the resulting geometries, such an approach may inform us about what the set approximated by the continuum may look like (or may not look like). On the other hand, by making statements about the properties of a causal set's elements, we can begin to scratch the surface of synthesis: a phenomenological characterization (however incomplete), or at the least a categorization, of gravity's fundamental units.

The impetus for the toy model was an open question posed by Jan Myrheim in a colloquium talk given in October 2017, "Is there only one kind of elementary event, or is there a periodic table [39]?" Referring to their namesake, Feynman posets are inspired by the (strictly figurative) analogy to particle interactions, whose vertices contain three lines. As such, the vertices of a Feynman poset are always three-degenerate, but one may imagine that if elementary events are distinguished by their degeneracy, then three-degeneracy is likely to be but one type in a family of n-degenerate events.

Chapter 2 outlines the fundamentals of causal set theory in greater detail and introduces the tools and vocabulary that will be used in the remainder of the thesis. It also includes a cursory overview of current approaches in the literature that are relevant for this project. Chapter 3 outlines the specific methodology chosen to construct causal sets in this project, as well as a discussion regarding the logic behind these choices. Chapter 4 includes the immediate results from the constructions. Chapter 5 includes an in-depth discussion on the manifoldlikeness of the causal sets constructed, a critical review of this project's methodology, and current and planned work moving forward. Chapter 6 is a summary of the findings of this project and contains a few closing remarks. Readers interested in the computational implementation who find Chapter 3 lacking can refer to Appendix C for a more detailed description of the MatLab scripts used in this project.

Open source scripts adapted from this project can be found on GitHub. Ongoing work includes making the script user-friendly, automated and more efficient, as well as migrating the script to Python. The link can be found in Appendix C.

2

The Fundamentals of Causal Sets

As a somewhat novel theory, the conventions and terms used in causal set theory often differ from author to author. Moreover, the field has a fair degree of overlap and inconsistencies with terms used in mathematics, particularly in set and graph theory. This is a modest attempt to organize the basic ideas in the field without cluttering the document with technical jargon by maintaining consistency and avoiding the introduction of extraneous terminology.

Section 2.1 will introduce the the basic concepts of causal sets, along with some tools that are used to represent them. It includes everything that makes a causal set a causal set, or in other words the *phenomenology* in this author's estimation, with a discussion on axioms and representations. Section 2.2 will deal with what the literature refers to as the *kinematics* of the theory. This entails the properties of the causal set as a mathematical object and the geometric information that can be extracted from it without having to embed it within the manifold. Section 2.3 will address the *dynamics* of the theory, including the path integral formulation and the continuum approximation. Finally, Section 2.4 will provide a (far from exhaustive) summary of the past and present work in the theory.

2.1 Phenomenology

2.1.1 Causal Sets

An *ordered set* is a mathematical object containing a collection of elements and their ordering relations. If the ordering relations are specified by the *direction* of the order (i.e. the relation indicates not only that two elements are related, but that one of the elements *causally precedes* or is *causally preceded* by the other), the ordered set is said to be a *partially ordered set*, or *poset*. Consider the sets illustrated in Figure 2.1. Figure 2.1a is an ordered set containing no information about the direction of the ordering relation. On the other hand, Figure 2.1b is a poset, where the directions of the ordering relations have been indicated by the arrow heads. In the partially ordered set, the two top elements have no relation to each other, while all of the elements in the ordered set are related to each other. Two events that are related to each other are said to be *comparable* and otherwise *incomparable*. The *cardinality* of the set is given by the number of elements in the set.

Causal set theory states that continuous spacetime is an approximation of a partially ordered set. In this context, a *causal set* or *causet* is nothing more than a poset whose elements are conceptualized as *spacetime events* and their partial ordering relations that the continuum manifold approximates. With this interpretation, the causet must be:

(a) Ordered set   **(b)** Poset
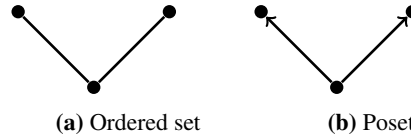
Figure 2.1: Ordered set vs. partially ordered set.

1. *Connected*, i.e. it is not the union of more than one non-empty disjoint set, as in Figure 2.2, and

2. *Locally finite*

A subset of the poset whose elements are all causally related to its *endpoints* is said to be an *open* interval. An open interval of finite cardinality is said to be an *Alexandrov interval*. Likewise, a *closed* interval is the union of any closed interval with its endpoints. The endpoints are defined as the *extremal* elements of the subset, where an element is said to be *minimal* if there exist no elements that causally precede it and *maximal* if there exist no elements that it causally precedes. A poset is *locally finite* if every interval in the poset is an Alexandrov interval. Figure 2.2 illustrates the distinction between closed and open intervals.

It is trivial to ensure that all constructed causets are connected. However, in the intermediate stages of the growth process of a causet or after coarse-graining (see Section 2.3.2), the poset may become a *disconnected set*. In this case, the poset is understood to be a *subinterval* of a larger connected poset. Moreover, the causet need not be a closed interval. However, the kinematic tools introduced in Section 2.2 are considerably simplified when the set is a closed interval. For this reason, the posets constructed in this project will also be understood as the subinterval of a connected *and* closed poset.
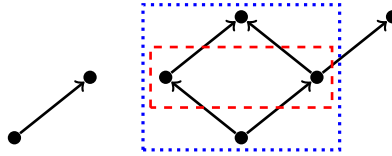
Figure 2.2: An example of a *disconnected* poset. Taken independently, each subset is a *connected* poset; note that not all elements need be causally related for the poset to be connected, as in the subset on the right-hand side. The dashed red line indicates an *open interval*, while the dotted blue line indicates a corresponding *closed interval* between the same endpoints.

The partial order relation is written as $\prec$, read as *causally precedes*, or $\succ$, read as *is causally preceded by*. For any two events a and b, $a \prec b$ if b is in the future light cone of a. The partial order relation may occasionally be referred to as a *relation* throughout this document.[1]

Care should be taken to not interpret this statement as "a causes b". Suppose event a is located at the origin of its light-cone and that event b is located in the future light-cone of event a. The presence of these two events does not imply the existence of any physical trajectory along the world line connecting them. Nor does the presence of either event imply the existence of any physical object located at the points. In fact, the existence of the causal relation between the two does not even imply that some occurrence at a causes an occurrence at b.

This semantic difficulty is unfortunate, as the concept of causality is what tethers the theory to physical reality. Adding insult to injury, events do not have a concrete definition either, which is particularly frustrated by the proposition that there are potential families of events (not to mention by divergent interpretations of quantum mechanics). The issue is severe enough that some authors have opted to use the more agnostic "spacetime atoms" to refer to events. In this author's opinion, the best compromise to resolve this issue is twofold: (1) the event is defined in the same way as its typical usage in relativity: it is a point in spacetime where something occurs (where an occurrence is extended to include "nothing happens" on the same footing as any other conceivable occurrence) and (2) the partial ordering relation $a \prec b$ can be read as "an occurrence at a could potentially, but does not necessarily, cause an occurrence at b".

As Bombelli emphasizes,

> if we look for observational consequences of the theory, we must not try to attach any operational meaning to the individual relationships between elements in the causal set, nor relate the intrinsic discreteness of the theory with any notion of discreteness that may arise from ordinary experience of lab ex-

---

[1]The partial order relation can also be denoted $\preceq$ or $\succeq$ if the reflexive formulation is used and more recently, $\prec\!\prec$ and $\succ\!\succ$ where the acyclic formulation is used–see the remainder of this section for more on these formulations. In general, I believe that this serves only to complicate matters and I am a strong proponent of simply using the canonical $\prec$ and $\succ$ symbols, regardless of the formulation being used, as long as it is the only relevant formulation and the convention being used is clearly stated in the document. This document will use only $\prec$ and $\succ$ to denote the order relation. Although most of the content in this document is based on the acyclic formulation, if the subject matter concerns any other formulation, it will be noted explicitly.

periments: any observational consequences of this framework will have to come through properties of the continuum approximation to it... [7]

This is not to say that the events in a causet are nothing but coordinate labels. If causal set theory is correct, then these events are more than just abstract mathematical objects: they are the very physical fundamental units of the gravitational force. To date, there is no single definition of these objects founded on a physical interpretation (although there are many theoretical proposals that have been offered), an unwieldy obstacle that lies in causal set theory's near future.

There is a wide diversity of poset-like objects in set theory, which offers many options for causal set researchers. In fact, the poset is generalized by the *ordered set*, and as seen in the preceding chapter, causal set researchers have sharpened the causal set by demanding that the set contains incomparable elements: hence the poset. This project deals with a particular class afforded by what mathematicians may refer to as *labeled reachability-ordered vertex sets of 3-degenerate directed acyclic graphs*, which will be referred to as *Feynman posets* for the remainder of this document. Below are some definitions that may be useful in understanding this object:

- *Covering relations* are the ordering relations between an element and its nearest neighboring elements, i.e. those ordering relations not implied by transitivity (later they will be introduced as *links*).

- *Directed Acyclic Graphs (DAGs)* are the graphs of partially ordered sets and their covering relations, where no element may precede itself by transitivity. Mathematically, the events are referred to as *nodes* or *vertices* and their relations are referred to as *edges* in this context.

- *Vertex Sets* have as their elements the *vertices, nodes* or *events* in the DAG.

- *Reachability-Ordered* sets additionally contain the covering relations of its vertex elements (i.e. the transitive reduction of the DAG).

- *n-Degeneracy* means that the vertices of the DAG have a maximum of n covering relations. Moreover, one may define the *indegree* and *outdegree* of a vertex as the number of its incoming and outgoing covering relations, respectively.

- *Labeled* graphs have integer labels assigned to their vertices.

In other words, *Feynman posets* are posets such that all of its elements have three or fewer covering relations. Although this mathematical definition may appear cumbersome, defining the set in this manner is a step in the right direction towards systematizing future research. Several classes of ordered sets have been studied in great detail, and organizing the objects we use may prove rewarding in the future, especially if there happens to be a "periodic table" of fundamental events.

As indicated, these posets (and nearly every other poset encountered in the prior literature) are *labeled* as a computational tool. In general, the observables of the causet are *label invariant* and thus the causets as they exist in nature are unlabeled, a condition reflecting the discrete analogue of general covariance [15].

Causal set theory is motivated by the construction of a causal set $(\mathcal{C}, \prec)$ that can be faithfully embedded[2] into a continuous manifold $(\mathcal{M}, g)$, where g are smooth Lorentzian metrics. If the embedding is faithful, then its image is a high probability Poisson distribution in $(\mathcal{M}, g)$ [54]. This is the very essence of Malament's theorem and the causal set program and is known as the *Hauptvermutung* of causal set theory.

2.1.2 Axioms

While the overwhelmingly dominant approach to causal sets (see [8], [47]; but many more examples abound) adheres to a single standard for defining set axioms (which I will refer to as the *transitive axioms*), a novel approach offered by Dribus in [20] (which I will refer to as *acyclic axioms*) has enjoyed recent popularity (see e.g. [54]). Despite some technical, albeit largely esoteric disclaimers, all of the causal set literature reviewed by this author agrees that the *causal set* is a set whose elements are events and their (typically partial) ordering relations.

The *transitive axioms* are given by:

1. **Irreflexivity**: $\forall a \in \mathcal{C} : a \nprec a$, i.e. all events are incomparable with themselves.

2. **Antisymmetry**: $\forall a, b \in \mathcal{C} : \left\{ \nexists a, b | a \prec b; b \prec a \right\}$, i.e. there exist no events that can precede one another (in this document, this is occasionally referred to as a "loop").

3. **Transitivity**: $\forall a, b, c \in \mathcal{C} : \left\{ (a \prec b; b \prec c) \implies a \prec c \right\}$, i.e. if event a precedes event b and b precedes event c, then a precedes c.

4. **Local Finiteness**: $\forall a, c \in \mathcal{C} : \mathbf{Card} \left\{ b \subset \mathcal{C} | a \prec b \prec c \right\} < \infty$, i.e. the number of events between any two given events (a subset of the causal set) must be finite.

These four axioms comprise the very basic foundation of causal set theory introduced from the very start. There are furthermore three more implicit axioms of causal sets that arise from the causal set program [20]:

5. **Binary**: The elements of a causal set are not only the events, but also the binary relations between them.

6. **Measure**: The volume of a spacetime region approximating a subset of the causal set is proportional to the cardinality of the subset up to Poisson fluctuations.

7. **Countability**: The cardinality of the causal set is countably infinite.

Technically speaking, irreflexivity (taken with transitivity) implies antisymmetry. In fact, irreflexivity and antisymmetry may be incorporated in a more general axiom of *acyclicity*,

$$\forall a, b, c...z \in \mathcal{C} : \left\{ \nexists a | a \prec b \prec ... \prec z = a \right\}. \tag{2.1}$$

Although the distinction may seem trivial, only the conjunction of irreflexivity and transitivity implies acyclicity. In most cases, this condition is ensured by considering *partially* ordered sets. However, it may be possible to study causal set theory with the more general

---

[2]Dribus generalizes this further by promoting causal sets from a set theory to a category theory, and thereby the faithful embedding to a *morphism* in [20].

ordered set, as Dribus proposes in [20], in which case acyclicity is an important addition. The axioms used in this project are:

1. **Irreflexivity**

2. **Transitivity**

3. **Acyclicity**

4. **Local Finiteness**

Acyclicity will have *no* practical consequences in this project, and is included here simply to prepare the study for future work, where the space of sets may be generalized.

On a minor note, there are two formulations used in the causal set literature that are more or less equivalent. The *irreflexive formulation* was used to write the axioms in Page 18 and in this formulation, each event is incomparable with itself.

By contrast, in the *reflexive formulation* the partial order relation is written as $\preceq$ and is read as *precedes or is equivalent to* and the axioms are then given by:

1. **Reflexivity**: $\forall a \in \mathcal{C} : x \preceq x$

2. **Antisymmetry**: $\forall a, b \in \mathcal{C} : \big\{ a \prec b; b \prec a \Longrightarrow a = b \big\}$

3. **Transitivity**: $\forall a, b, c \in \mathcal{C} : \big\{ a \preceq b; b \preceq c \Longrightarrow a \preceq c \big\}$

4. **Locally finite**: $\forall a, c \in \mathcal{C} : \mathbf{Card} \big\{ b \subset \mathcal{C} | a \preceq b \preceq c \big\} < \infty$

The implicit axioms mentioned previously also follow for the partial order formulation.

Summary of Formulations

The key distinction between the irreflexive and partial order formulations rests within the definition of antisymmetry, but this is a trivial distinction that will have no bearing on the information contained by the sets they govern.[3] This project will use the *acyclic axioms* in the *irreflexive formulation*.

2.1.3   Hasse Diagram and Matrix Representation

Causal sets are most commonly represented by Hasse diagrams (in mathematics, a Hasse diagram is often referred to as the DAG of the transitive reduction of a poset). Constructing a Hasse diagram is straightforward: each event in the causal set is represented by a point in the diagram, and the partial ordering relation between events is represented by a line connecting the points. Most authors will typically denote the direction of the partial order relation by either including arrows on the lines, choosing a convention such that time is oriented upwards along the vertical axis, or as in the case of this document, both. Unlike light cones, Hasse diagrams have no axis scales, and therefore $45°$ lines have no special meaning.

---

[3]Dribus points out in [20] that the latter technically does not imply acyclicity and therefore admits for structure-breaking mappings that might otherwise be faithful embeddings (or morphisms). However, there are simple ways to deal with this issue and [4] and [25] simply press on with the reflexive condition.

The partial ordering relation is necessarily a binary relation, and as such, the matrix representation of a causal set is equally straightforward. The matrix representation of a causal set $\mathcal{C}$ containing N events is an $N \times N$ matrix and for the relation $a \prec b$, the row labels of this matrix correspond to a and the column labels of this matrix correspond to b. The partial order relation $\prec$ is denoted by 1, while the relation $\succ$ is denoted by -1. The absence of a partial ordering relation (i.e. $\not\prec$ and $\not\succ$) between two events is denoted 0. As a consequence of irreflexivity, the diagonals of such a matrix are 0. All matrix representations of causal sets are also antisymmetric as a consequence of the binary nature of the ordering relation.[4]

Consider the Hasse diagram and table in Figure 2.3. The matrix representation for this causal set is given by

$$
\begin{array}{c@{\hspace{1em}}ccccc}
 & 1 & 2 & 3 & 4 & 5 \\
1 & 0 & 0 & 1 & 0 & 1 \\
2 & 0 & 0 & 1 & 0 & 1 \\
3 & -1 & -1 & 0 & 0 & 1 \\
4 & 0 & 0 & 0 & 0 & 1 \\
5 & -1 & -1 & -1 & -1 & 0
\end{array}
$$

where the labels on the borders refer to the number labeling the events in the causal set.

$1 \prec 3$	$3 \succ 1$
$1 \prec 5$	$5 \succ 1$
$2 \prec 3$	$3 \succ 2$
$2 \prec 5$	$5 \succ 2$
$3 \prec 5$	$5 \succ 3$
$4 \prec 5$	$5 \succ 4$
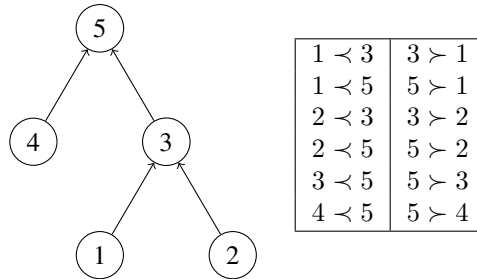
Figure 2.3: A Hasse digram for a causet with 4 elements and the table enumerating its relations.

This particular representation is a *relation matrix* and is the convention that most of the literature on causal sets uses. Variations on the relation matrix include 1) the Seidel adjacency matrix, where the element labeled by (a, b) has 0 on the diagonal, -1 for adjacent vertices, and $+1$ for non-adjacent comparable vertices and 2) the distance matrix, where the element labeled by (a, b) has the smallest number of intermediate events between a and b minus one. The latter will be used in this project; the former may be useful for future studies, as it may reduce computation time.

---

[4]The reader may notice that the matrix representation is redundant, as the ordering relation is by definition binary and this representation is trinary. As far as this author is aware, the trinary representation is the convention, but as others have found, converting to a binary representation makes computations simpler–see for instance Appendix C and [5]. Computations in this project will use both trinary and binary matrix representations.

It is also useful to define an *adjacency matrix* expressing only the covering relations of the set. The adjacency matrix for the causal set in Figure 2.3 is then given by

$$
\begin{array}{c}
\\
\begin{array}{cccccc}
& 1 & 2 & 3 & 4 & 5
\end{array}\\
\begin{array}{c}1\\2\\3\\4\\5\end{array}
\left(
\begin{array}{ccccc}
0 & 0 & 1 & 0 & 0\\
0 & 0 & 1 & 0 & 0\\
-1 & -1 & 0 & 0 & 1\\
0 & 0 & 0 & 0 & 1\\
0 & 0 & -1 & -1 & 0
\end{array}
\right)
\end{array}
$$

On a final note, it is worth mentioning that the Hasse diagram in Figure 2.3 and its two representation matrices reflect *natural labeling*, such that the numerical ordering of event labels reflects the causal ordering of the events themselves. In other words,

$$x_i \prec x_j \Longrightarrow i < j \tag{2.2}$$

There is no reason that causal sets must be naturally labeled (or labeled at all, for that matter) and this convention can even artificially restrict the construction of a causal set.[5] The same causal set represented by Figure 2.3 can very well be represented by the Hasse diagram in Figure 2.4 with no change in the causal structure, and the two are said to be *automorphic*.

The relation matrix then becomes

$$
\begin{array}{c}
\\
\begin{array}{cccccc}
& 1 & 2 & 3 & 4 & 5
\end{array}\\
\begin{array}{c}1\\2\\3\\4\\5\end{array}
\left(
\begin{array}{ccccc}
0 & -1 & -1 & -1 & -1\\
1 & 0 & 0 & 0 & 0\\
1 & 0 & 0 & 0 & 1\\
1 & 0 & 0 & 0 & 1\\
1 & 0 & -1 & -1 & 0
\end{array}
\right)
\end{array}
$$

This project does not use natural labeling, although future changes to the growth model that make growth parameters explicit may feature natural labeling.
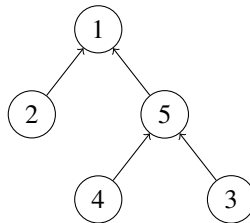
Figure 2.4: Hasse diagram without natural labeling. This Hasse diagram represents the same causal set as the Hasse diagram in Figure 2.3.

---

[5]Rideout and Sorkin, among others, have availed themselves of natural labeling as a matter of pure computational convenience. Natural labeling is particularly useful for *sequential* growth models. See [29, 47, 5] and Section 2.4. Since causets are unlabeled in nature, labeling conventions do not affect the underlying physics.

2.2 Kinematics

2.2.1 Properties of the Causal Set and Definitions

The *future* of an event is defined as the set of events that it precedes, i.e.

$$T^+(a) \equiv \{b \in \mathcal{C} : a \prec b\} \tag{2.3}$$

Likewise, the *past* of an event is defined as the set of events that precede it, i.e.

$$T^-(a) \equiv \{b \in \mathcal{C} : b \prec a\} \tag{2.4}$$

A *link* is any causal relation between two events that cannot be deduced by transitivity, i.e. there exist no intermediate relations between them. In mathematics, the link is also referred to as a *covering relation*. A link $\mathcal{L}$ is some subset of the causal set

$$\mathcal{L} \equiv \{a, b, (a \prec b)\} \subset \mathcal{C} : \{\nexists c \in \mathcal{C} | a \prec c \prec b\} \tag{2.5}$$

A *chain*, C, or a *totally ordered* subset is a subset of the partially ordered set such that

$$C \equiv \{c_i, i = 0, 1, \ldots, N - 1\} : c_i \prec c_{i+1} \tag{2.6}$$

i.e. it is a sequence of links that form a straight line. The *maximal chain* of a subset is the chain that contains the greatest number of events and the *length* of any subset is equal to the number of links in its maximal chain. It has been shown in [41] that the proper length of a *geodesic* curve in the continuum is given by the length of the chain between the two events that define its endpoints.

An Alexandrov interval, $I(a, b)$, between events a and b is a subset of events resulting from the intersection of the future of a with the past of b, *not* including a or b, i.e.

$$I(a, b) \equiv \{I \subset \mathcal{C}; a \prec b; I(a, b) = [T^+(a) \cup T^-(b)]\} \tag{2.7}$$

The interval is said to have *volume* equal to its cardinality, i.e. the number of points in the interval.

The *height* of a causal set is the length of the maximal chain(s) in the entire set.

A *layer* (or *level*; the two terms will be used interchangeably in this document) is a subset of the causet resulting from the partition of events that have the same chain length between a given "root" element. In mathematics, each layer is given with respect to the chosen root element, but causal set theory offers some natural choices for a designated root event, i.e. the causet's extremal elements.

As this project uses the graphical tools offered by MatLab to determine the layer structure of the causets, this document will opt for an informal definition illustrated by Figure 2.5. The specifics of assigning layers to the elements of a poset are rather complicated and unnecessary for our purposes. Typically, the treatment depends on identifying the *antichains*, subsets of incomparable events in the poset, *antilinks*, subsets containing exactly two incomparable events in the poset, and the poset *width*, the number of links in the largest antichain. Readers interested in strategies for defining layers in the context of causal set theory are referred to [29].
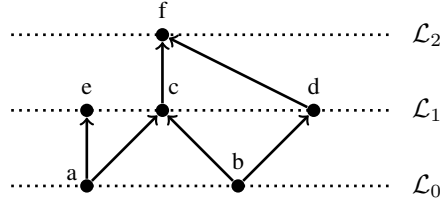
Figure 2.5: An illustration of a causet's layers. Elements a and b are assigned layer $\mathcal{L}_0$, while elements e, c, and d are assigned to layer $\mathcal{L}_1$. Layer $\mathcal{L}_2$ contains only element f. This document admits only an approximate assignment of layers in place of a rigorous mathematical assignment. Moreover, since one is free to designate any root element, the assignment of layers is somewhat arbitrary.

Volume, Length, and Metric

Consider the proper distance between two timelike points in Minkowski spacetime, a and b, which we have identified as the height of the Alexandrov interval $I(a, b)$:

$$L(a, b) = \int_C \mathrm{d}s = \sqrt{-g_{\mu\nu}(a^\mu - b^\mu)(a^\nu - b^\nu)} \tag{2.8}$$

where C is the geodesic connecting the two points (compare with Equation (1.2) on Page 2).

Suppose now that the events a and b are infinitesimally separated and parameterize C as $x^\mu(u)$, where u is some intermediate event such that $a \prec u \prec b$ and $(a, b) \to u$. Equation (2.8) can then be written as

$$L = \int_a^b \mathrm{d}u \sqrt{-g_{\mu\nu} \frac{\mathrm{d}x^\mu}{\mathrm{d}u} \frac{\mathrm{d}x^\nu}{\mathrm{d}u}} \tag{2.9}$$

Moreover, the volume of the interval $I(a, b)$ is given in the continuum as

$$V = \int_\Omega \sqrt{-g} \, \mathrm{d}^n x \tag{2.10}$$

where Ω is some n-dimensional volume and $g = \det(g_{\mu\nu})$. For a flat manifold, the metric tensor is given by

$$g_{\mu\nu} = \eta_{\mu\nu} = \mathrm{diag}(-1, 1, 1, ..., 1) \tag{2.11}$$

and the volume becomes

$$V(a, b) = C_n L^n \tag{2.12}$$

where the prefactor C_n is given by the volume of the intersection of two conical hypersurfaces in an n-dimensional flat Lorentzian manifold (see Figure 2.8 on Page 35):

$$C_n = \frac{\pi^{\frac{n-1}{2}}}{2^{n-2} n(n-1)\Gamma\left(\frac{n-1}{2}\right)} \tag{2.13}$$

Prefactor for the volume of two conical hypersurfaces for various dimensions						
n	1	2	3	4	5	6
C_n	1	$\frac{1}{2}$	$\frac{\pi}{12}$	$\frac{\pi}{24}$	$\frac{\pi^2}{160}$	$\frac{\pi^2}{360}$
As decimal	1	0.5	0.262	0.131	0.062	0.027

Table 2.1: Reference table for comparing the volume prefactor, C_n, for a flat spacetime to the dimension, n, of the spacetime considered. Copied from a colloquium presentation given by Jan Myrheim [39].

where Γ is the gamma function,

$$\Gamma(n) = (n-1)! \tag{2.14}$$

Table 2.1 shows the prefactor C_n for various dimensions of Lorentzian manifolds.

Myrheim postulates in [41] that the volume can be expressed with a counting measure as

$$V = k^n N \tag{2.15}$$

where N is the number of events in the interval, n is the Minkowski dimension, and k is the fundamental discreteness length scale. Moreover, it is postulated that

$$\left(\frac{h}{L}\right)^n \propto \frac{N}{V} \tag{2.16}$$

where h is the length of the maximal chain in the poset and using Equation (2.15),

$$L = hk \tag{2.17}$$

These results hold for flat spacetime only. To generalize Equations (2.12) and (2.17), one must return to Equation (2.10) and consider a more general metric tensor. The derivation can be rather complicated, and considerable care must be taken to observe the appropriate sign convention. To avoid introducing conflicting conventions, the derivation will not be carried out in this space, and the result simply cited from [41, 40] as:

$$V = \frac{\pi L^4}{24}\left\{1 + L^2\left[\frac{1}{30}R_{00}(0) - \frac{1}{180}R(0)\right] - \mathcal{O}(L^3)\right\} \tag{2.18}$$

for 4D curved spacetime, although the expression can be generalized to any n dimension. Note that in an empty region of spacetime, $R_{\mu\nu}(0) = 0$, $R(0) = 0$ and Equation (2.18) reduces to Equation (2.12), as expected. Readers interested in the details of the derivation may refer to [41] for the original derivation and [9] for a more detailed derivation.

It is worth taking a moment to fully appreciate this result. Since Equation (2.18) must hold for any orientation of the time component of a given interval in curved spacetime, *all* components of the Ricci curvature tensor, $R_{\mu\nu}$ may be recovered from the causal information in the continuum alone [28, 21].

2.2.2 Action and Locality

Benincasa-Dowker Action

Consider the Einstein-Hilbert action,

$$S = \int \left[\frac{1}{16\pi}(R - 2\Lambda) + \mathcal{L}_M \right] \sqrt{-g} \, \mathrm{d}^n x \tag{2.19}$$

where R is the Ricci curvature scalar, Λ is the cosmological constant, $\mathcal{L}_M$ is the Lagrangian density describing matter fields, $g = \det g_{\mu\nu}$, and n is the dimension. By imposing

$$\delta S = 0 \tag{2.20}$$

one may use Equation (2.19) to derive Einstein's field equations, Equation (1.11).

Suppose now that $\Lambda = \mathcal{L}_M = 0$, such that the action,

$$S = \frac{1}{16\pi} \int R \sqrt{-g} \, \mathrm{d}^n x \tag{2.21}$$

describes some empty region of spacetime. In other words, Equation (2.21) is the gravitational action, with the gravitational Lagrangian density given by

$$\mathcal{L}_g = R\sqrt{-g} \tag{2.22}$$

This integral is very similar to that encountered in Equation (2.10), although now the integrand contains a factor of R, a quantity that we have no simple way of measuring within in the discrete causal set. The motivation for this section is then to find some alternative definition of R for a causal set that can be computed from the causal information alone, then insert it into Equation (2.21) to define the action on a causal set.

Given this background, let's reconsider the meaning of a manifold. Mathematically, a *manifold* is defined as a *topological space* covered by an *atlas* of at least one *map* [40]. Simply put: we have some set of points and their neighborhoods (the topological space), along with a collection (the atlas) of at least one function (the map) that assigns to each element in the set a corresponding point in $\mathbb{R}$ (the manifold), such that the structure of the set is preserved. To be more clear about how this will help us, we can consider continuous spacetime to be our manifold, our topological space to be the causal set (we may as well choose a discretized 2D Minkowski lattice space in light-cone coordinates with lattice spacing l_p to serve this purpose), and some scalar function, $\phi(u, v)$ that assigns some point in $\mathbb{R}$ to each lattice site.

What should this scalar function look like? *Synge's world function*, $\sigma(x, y)$, gives half of the square of the geodesic distance between some points x and y. In flat Minkowski spacetime,

$$\sigma(x, y) = -\frac{1}{2} \eta_{\mu\nu}(y^\mu - x^\mu)(y^\nu - x^\nu) \tag{2.23}$$

so we may as well choose

$$\phi(x) = \Box \sigma(0, x) \tag{2.24}$$
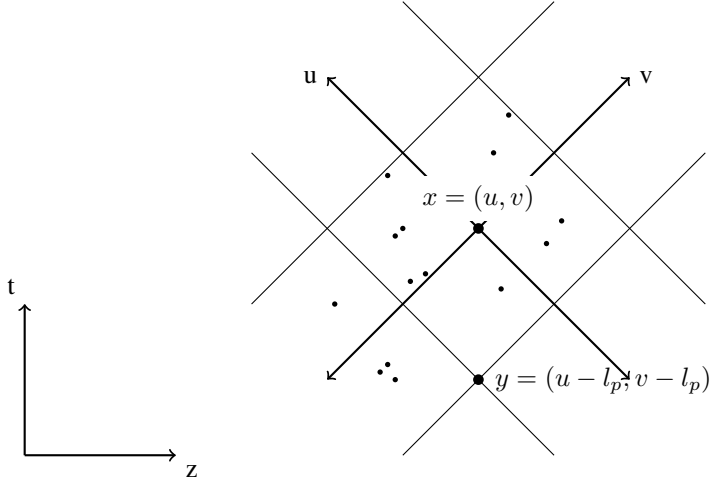
Figure 2.6: A discretized 2D Minkowski space represented by a light cone lattice and some sprinkled events. The lattice need not consist of straight lines, and in the more general case, the coordinate axes will be curved.

where 0 is the origin. In the flat case, this is

$$\phi(x) = -4 \tag{2.25}$$

For a curved spacetime, $\phi(x)$ is not constant, and from this, one may characterize the curvature scalar. It has been shown that [28]

$$\boxed{R(0) = \Box\Box\sigma(0,x)|_{x=0}} \tag{2.26}$$

For the discrete case, Equation (2.21) becomes a sum, and we are immediately confronted with the fact that any given point in the space, 0, has an infinite number of x along the null surface of its past light cone.

In Appendix A, it is shown that the discrete approximation of the d'Alembertian is given by

$$\Box\phi \approx \frac{2}{D} \frac{\phi(u,v) - \phi(u,v-b) - \phi(u-a,v) + \phi(u-a,v-b)}{ab} \tag{2.27}$$

The limit $a \longrightarrow 0$ with ab constant gives the infinitesimally skinny interval between $x = (u,v)$ and some event $y = (u-a, v-b)$ along its past light cone extending to infinity, and it is easy to see that in this limit, Equation (2.27) approaches 0, such that contributions to the d'Alembertian of intervals extending infinitely down the light cone can be neglected [54]. Note that this is a completely general result.

Sorkin has proposed a discrete version of Equation (2.27), a general expression for the d'Alembertian ([3, 4] citing [49]):

$$B^{(d)}\phi(x) = \frac{1}{l^2}\left(\alpha_d\phi(x) + \beta_d\sum_{i=1}^{n_d} C_i^{(d)} \sum_{y\in L_i} \phi(y)\right) \tag{2.28}$$

d	α_d	β_d
1d	-1	2
2d	-2	4
3d	$-\frac{1}{\Gamma(\frac{5}{3})}\left(\frac{\pi}{3\sqrt{2}}\right)^{2/3}$	$\frac{1}{\Gamma(\frac{5}{3})}\left(\frac{\pi}{3\sqrt{2}}\right)^{2/3}$
4d	$-\frac{2}{\Gamma(\frac{6}{4})}\left(\frac{\pi}{6}\right)^{2/4}$	$\frac{2}{\Gamma(\frac{6}{4})}\left(\frac{\pi}{6}\right)^{2/4}$
5d	$-\frac{1}{\Gamma(\frac{7}{5})}\left(\frac{\pi^2}{20\sqrt{2}}\right)^{2/5}$	$\frac{1}{\Gamma(\frac{7}{5})}\left(\frac{\pi^2}{20\sqrt{2}}\right)^{2/5}$
6d	$-\frac{2}{\Gamma(\frac{8}{6})}\left(\frac{\pi^2}{45}\right)^{2/6}$	$\frac{2}{\Gamma(\frac{8}{6})}\left(\frac{\pi^2}{45}\right)^{2/6}$

Table 2.2: Reference table for the coefficients of α_d and β_d for 1-6 dimensions. Copied from Dowker and Glaser's table in [17].

where d is the dimension, l is a discreteness length scale (i.e. the "lattice spacing" of the approximating space), and $\phi(x)$ is the scalar field. The derivation of this expression will not be explored in this space, but the author will offer some brief comments. Rather than summing over each nearest neighbor, the prescription becomes to sum over the layers, L_i, with event x as the root, residing to the causal past of event x, as reflected in the second summation. The discreteness length scale is typically set equal to

$$l = l_p = 1 \tag{2.29}$$

The limit of the first summation, n_d, may be infinite, but it is minimally bound by

$$n_d = \begin{cases} \frac{d}{2} + 2 & d \text{ even} \\ \frac{d-1}{2} + 2 & d \text{ odd} \end{cases} \tag{2.30}$$

This condition is imposed by the cutoff limit $V = l_p^2$, c.f. Equation (2.17) on Page 23. This limit is justified by the preceding discussing on the vanishing contribution to the d'Alembertian from distant layers. Note also that the $\frac{2}{D}$ from Equation (2.21) is expressed in Equation (2.28) as α_d and β_d, coefficients characterizing the dimension of the space, and $C_i^{(d)}$, characterizing the curvature of the space [4, 17, 24]. Table 2.2 gives the values for α_d and β_d in up to 6 dimensions and Table 2.3 gives the values for $C_i^{(d)}$ in up to 7 dimensions. The closed-form expressions for β_d and α_d are given by

$$\beta_d = \begin{cases} \frac{2\Gamma(\frac{d}{2}+2)\Gamma(\frac{d}{2}+1)}{\Gamma(\frac{2}{d})\Gamma(d)}c_d^{\frac{2}{d}} & d \text{ even} \\ \frac{d+1}{2^{d-1}\Gamma(\frac{2}{d}+1)}c_d^{\frac{2}{d}} & d \text{ odd} \end{cases} \tag{2.31}$$

d	C_1	C_2	C_3	C_4	C_5
1d	1	$-\frac{1}{2}$			
2d	1	-2	1		
3d	1	$-\frac{27}{8}$	$\frac{9}{4}$		
4d	1	-9	16	-8	
5d	1	$-\frac{215}{16}$	$\frac{225}{8}$	$-\frac{125}{8}$	
6d	1	-34	141	-189	81
7d	1	$-\frac{6307}{128}$	$\frac{14749}{64}$	$-\frac{10633}{32}$	$\frac{2401}{16}$

Table 2.3: Reference table for the prefactors $C_i^{(d)}$ for 1-7 dimensions.
Copied from Dowker and Glaser's table in [17].

and

$$\alpha_d = \begin{cases} \dfrac{-2c_d^{\frac{2}{d}}}{\Gamma(\frac{d+2}{d})} & d \text{ even} \\[2ex] \dfrac{-c_d^{\frac{2}{d}}}{\Gamma(\frac{d+2}{d})} & d \text{ odd} \end{cases} \tag{2.32}$$

while the closed-form expression for the coefficients $C_i^{(d)}$ is given by

$$C_i^{(d_{\text{even}})} = \sum_{k=0}^{i-1} \binom{i-1}{k} (-1)^k \frac{\Gamma(\frac{d}{2}(k+1)+2)}{\Gamma(\frac{d}{2}+2)\Gamma(1+\frac{dk}{2})} \tag{2.33}$$

$$C_i^{(d_{\text{odd}})} = \sum_{k=0}^{i-1} \binom{i-1}{k} (-1)^k \frac{\Gamma(\frac{d}{2}(k+1)+\frac{3}{2})}{\Gamma(\frac{d+3}{2})\Gamma(1+\frac{dk}{2})} \tag{2.34}$$

Note that the lower case c_d in Equations (2.31) and (2.32) are not to be confused with coefficients $C_i^{(d)}$, but rather

$$c_d = S_{d-2} \frac{1}{d(d-1)2^{\frac{d}{2}-1}} \tag{2.35}$$

where S_{d-2} is in this context the volume of a $d-2$ dimensional unit sphere:

$$S_{d-2} = \frac{\pi^{\frac{d}{2}}}{\Gamma(\frac{d}{2}+1)} \tag{2.36}$$

Table 2.4 shows the S_d for $d = [1,6]$.

The discrete d'Alembertian provided by Equation (2.28) is very valuable in causal set theory for a number of reasons. The first thing to note is that the $C_i^{(d)}$ introduce an alternating parity in the first sum, which allows it to converge. Secondly, although the expression is dependent on the dimension, d, the d'Alembertian is the same regardless

of the causal set it is applied to. One will need to use some estimator to approximate the continuum dimension; the Myrheim-Meyer dimension discussed in Section 2.2.3 is an excellent candidate. This project will instead impose a dimensionality *a priori*.

Prefactor for the volume of a d-ball for various dimensions					
d	1	2	3	4	5	6
S_d	2	π	$\frac{4\pi}{3}$	$\frac{\pi^2}{2}$	$\frac{8\pi^2}{15}$	$\frac{\pi^3}{6}$

Table 2.4: Reference table for comparing the volume prefactor, S_d and the dimension d for a d-ball.

Recall Malament's theorem, which states that the bijective map between two spacetimes that preserves their causal structure is a conformal isomorphism. In other words, as long as the ordering relations between points in the causal set are preserved, any other arbitrary causal set may describe the same spacetime, up to local volume fluctuations. To see this, consider again Figure 2.6. In the depicted scenario, the interval I(y,x) contains just one point. Yet, when subject to a Lorentz boost, the interval will become "stretched" downwards while containing a fixed volume, while the position of the points remain invariant. We have already shown what happens when the interval is stretched infinitely along the light cone. What about the more immediate relations? A coordinate transformation leaves the metric (and therefore the geometry) invariant, and yet in the limit of an infinite density of points, even the most modest Lorentz boosts will change the number of points within the interval with a probability that approaches 1. The operator in Equation (2.28) will then fluctuate, yielding a different result for the d'Alembertian (and therefore for the action) on causal sets that purportedly describe the same spacetime [23].

To address this issue, Sorkin introduces a non-locality scale, ξ, over which the d'Alembertian is "smeared" to correct for these fluctuations, providing a more reliable average over the causet. The resulting expression for the d'Alembertian is then given by

$$B^{(d)}\phi(x) = \frac{1}{l^2}\left(\alpha_d\phi(x) + \beta_d\sum_{i=1}^{n_d} C_i^{(d)}\sum_{y\in L_i}\phi(y)\right) \qquad (2.28)$$

$$\bar{B}^{(d)}\phi(x) = \frac{1}{\xi^2}\left(\alpha_d\phi(x) + \beta_d\epsilon\sum_{y\prec x} f_d(n(x,y),\epsilon)\phi(y)\right) \qquad (2.37)$$

where the *smearing function*, $f_d(n,\epsilon)$, is given by

$$f_d(n,\epsilon) = (1-\epsilon)^n\sum_{i=1}^{n_d} C_i^{(d)}\binom{n}{i-1}\left(\frac{\epsilon}{1-\epsilon}\right)^{i-1} \qquad (2.38)$$

and

$$\epsilon = \left(\frac{l}{\xi}\right)^d \qquad (2.39)$$

and n is the chain length between events x and y.

Note that the latter summation in Equation (2.28) has now been replaced in Equation (2.37) with a summation over all $y\prec x$. Naturally, we will require this non-locality

scale, ξ, to be larger than the discreteness scale. After all, this would also render the correction useless, as in the limit $l \rightarrow \xi$, Equation (2.37) simply reduces to an enumeration of events in the interval and there is no effective smearing. Suppose we have some interval of height h. In essence, ξ tells us that for the $h - 1$ layers to the causal past of the maximal event in this interval, elements in up to ξ of these layers might be assigned to the first layer under Lorentz transformations. Clearly, the first condition must be

$$l < \xi \tag{2.40}$$

$$\tag{2.41}$$

Moreover, it can be readily seen that for $\xi < nl$, $f(n, \epsilon) \approx 0$, which means that the smearing only accounts for intervals of cardinality less than $1/\epsilon$, potentially leading to infrared errors [55]. An additional condition is then given by

$$nl^d > \xi^d \tag{2.42}$$

We therefore demand

$$\frac{1}{n} < \epsilon < 1 \tag{2.43}$$

where $n = h$ is the length of the maximal chain in the set (i.e. the height). It is satisfying to note that for $n \longrightarrow \infty$, the lower bound on ϵ effectively vanishes–as expected–and in the limit $\epsilon \longrightarrow 0$, Equation (2.37) reduces to Equation (2.28).

It has been shown in [49] that

$$\lim_{\rho \to \infty} \bar{B}^{(d)} \phi(x) = \Box^{(d)} \phi(x) \tag{2.44}$$

for flat spacetime, where ρ is the density of events, i.e. the discrete d'Alembertian is successful approximated by its continuum counterpart.

The question is now whether or not this this operator holds for *curved* spacetime. Dowker and Glaser demonstrate in [17] (as well as in [4] and [49] by Benincasa and Sorkin, respectively) that in the case of a curved spacetime, there is a correction term:

$$\boxed{\lim_{\rho \to \infty} \bar{B}^{(d)} \phi(x) = \Box^{(d)} \phi(x) - \frac{1}{2} R \phi(x)} \tag{2.45}$$

Finally, one can recover the Ricci curvature scalar, provided the test field, ϕ, is appropriately chosen. What is ϕ? Thus far, we have simply identified it as some function that takes points from the discrete lattice and assigns them a value in continuous Minkowski space; the d'Alembertian of Synge's world function was given as a suitable scalar field. Unfortunately, expanding on this discussion in detail is simply not a detour that this author is equipped to provide in this document. Suffice to say that in the context of Equation (2.25) and (2.23), σ is constant for an approximately flat spacetime and $\phi = \Box\sigma(0, x)$ is a scalar, as required. There are a few more considerations that must be made when choosing ϕ, but these details will not concern us in this space and [3] will simply be cited for this purpose. Before this final step, it is worthwhile to review what has been done.

First, it has been demonstrated that the operator B may indeed be used to approximate the continuum d'Alembertian, which may in turn be used to define the Ricci curvature scalar. Moreover, despite expectations, the operator is useful in curved spacetimes as well. Second, it has been demonstrated that despite the radical non-locality of causal set theory, causal relations extending infinitely along the light cone of some causal event provide vanishing contributions to the d'Alembertian and can be ignored. This allows us to apply a volume cutoff limit for the sum over layers, making the expression more manageable for computations. Third, in addressing the non-trivial fluctuations arising from Lorentz transformations *not* extending to infinity, a smearing function was introduced to account for Lorentz invariance.

Using Equation (2.25) and selecting $\phi(x) = -4$, Equation (2.45) then becomes

$$\lim_{\rho \to \infty} \bar{B}(-4)|_x = -\frac{1}{2} R(-4) \tag{2.46}$$

Here is the long-awaited definition of R; the scalar curvature of a causal set at event x is given by

$$R(x) = -2\bar{B}|_x \tag{2.47}$$

Summing Equation (2.47) over all $x \in \mathcal{C}$ gives

$$\sum_{x \in \mathcal{C}} R(x) = -\frac{1}{\xi^2} \left(\alpha_d N + \beta_d \epsilon \sum_{n=1}^{N-2} N_n f(n, \epsilon) \right) \tag{2.48}$$

where the equations

$$\sum_{x \in \mathcal{C}} \phi(x) = \sum_{x \in \mathcal{C}} \delta_{xy} = N \tag{2.49}$$

and

$$\sum_{x \in \mathcal{C}} \sum_{y \prec x} \phi(y) = \sum_{n=1}^{N-2} N_n \tag{2.50}$$

were used and where

$$N_n = \begin{cases} \text{Number of links in the set} & n = 1 \\ \text{Number of intervals with volume n-1} & n \geq 2 \end{cases} \tag{2.51}$$

i.e. N_2 is the number of length-2 chains, N_3 is the number of length-3 chains *and* so-called diamond posets (two incomparable events in the middle layer), and so on.

With the d'Alembertian in hand, we can finally return to Equation (2.21),

$$S = \frac{1}{16\pi} \int R\sqrt{-g}\, \mathrm{d}^n x \tag{2.21}$$

Inserting Equation (2.48) (the factor $16\pi^{-1}\sqrt{-g}$ was added only to account for the continuum case, but since we now have a discrete expression, it can be removed) gives the *Benincasa-Dowker Action*:

$$S[\mathcal{C}] = \lim_{\rho \to \infty} \sum_{x \in \mathcal{C}} R(x) \qquad (2.52)$$

$$= \sum_{x \in \mathcal{C}} -\bar{B}|_x \qquad (2.53)$$

$$= -\left(\alpha_d \epsilon^{\frac{2}{d}} N + \beta_d \epsilon^{\frac{2+d}{2}} \sum_{n=1}^{N-2} N_n f(n, \epsilon) \right) \qquad (2.54)$$

Note that Equation (2.54) is written using natural units such that $\xi = \epsilon^{-\frac{1}{d}}$.

One final simplification will be made. Note that the smearing function, Equation (2.38), introduces a factor $(1 - \epsilon)^n$ for each successive term in the leading sum over n, and since Equation (2.43) provides $\epsilon < 1$, as long as an appropriately small ϵ is chosen, higher orders in n will be negligible (in fact, Sorkin himself suggests $\epsilon \ll 1$ in [49]). Thus, for this project, the summation limit $N - 2$ in Equation (2.54) will be replaced with the height of the causet and $\epsilon = \frac{1}{N}$.

Putting this all together, the final result is the *Benincasa-Dowker action*,

$$S^{(d)}[\mathcal{C}] = -\alpha_d \left[\epsilon^{\frac{2}{d}} N + \epsilon^{\frac{2+d}{d}} \frac{\beta_d}{\alpha_d} \sum_{n=1}^{\text{height}} N_n f(n, \epsilon) \right] \qquad (2.55)$$

where

$$f(n, \epsilon) = (1 - \epsilon)^n \sum_{i=1}^{n_d} C_i^{(d)} \binom{n}{i - 1} \left(\frac{\epsilon}{1 - \epsilon} \right)^{i-1} \qquad (2.56)$$

It is important to note that this action is *not* in general additive. As Benincasa points out in [3], if the action were additive, Equation (2.55) would simply be a sum of the contributions of each element and in effect, $S[\mathcal{C}] \propto N$. Rather, the action is *bi-local*, such that for some timelike partitioned subsets X and Y, the action of the causet $\mathcal{C} = X \cup Y$ is given by

$$S[\mathcal{C}] = S[X, X] + S[Y, Y] + S[X, Y] + S[Y, X] \qquad (2.57)$$

where $S[X, Y]$ refers to the action of the interval between the maximum point of subset X and the minimum point of subset Y. This behavior significantly frustrates the computational methodology, since few of the causets considered are Alexandrov intervals. To address this issue, this project adapts some simplifying assumptions about the causets. See Section 3.4 and Chapter 5 for more.

To conclude this section, the smearing functions, Equation (2.56), are given in up to

four dimensions:

$$
f_d =
\begin{cases}
(1-\epsilon)^n \left[1 - \frac{n}{2}\left(\frac{\epsilon}{1-\epsilon}\right)\right] & d = 1 \\[3mm]
(1-\epsilon)^n \left[1 - 2n\left(\frac{\epsilon}{1-\epsilon}\right) + \frac{1}{2}n(n-1)\left(\frac{\epsilon}{1-\epsilon}\right)^2\right] & d = 2 \\[3mm]
(1-\epsilon)^n \left[1 - \frac{27}{8}n\left(\frac{\epsilon}{1-\epsilon}\right) + \frac{9}{8}n(n-1)\left(\frac{\epsilon}{1-\epsilon}\right)^2\right] & d = 3 \\[3mm]
(1-\epsilon)^n \left[1 - 9n\left(\frac{\epsilon}{1-\epsilon}\right) + 8n(n-1)\left(\frac{\epsilon}{1-\epsilon}\right)^2 - \frac{4}{3}n(n^2 - 3n + 2)\left(\frac{\epsilon}{1-\epsilon}\right)^3\right] & d = 4
\end{cases}
$$

$$(2.58)$$

Locality

Suppose some event 0 at the origin of its light cone were causally related to some event b several decades and some light years along its future light cone with no intermediate relations between the two. In this case there is no way to distinguish this relation from, e.g. the relation between a and c, a third event timelike separated from a by a Planck time in a Hasse diagram from the causal information alone. Causal set theory is said to be *radically non-local*. What we need now is some Lorentz invariant quantity by which we can define a local region.

Thus far, we have encountered just two observables that are by definition Lorentz invariant: the proper distance (Equation (2.8)) and the volume (Equation (2.10)). As we have seen, neither of these observables contain the requisite information for defining a local region (if the poset is embeddable in a manifold, then the dimension estimators are also in theory Lorentz invariant, but this doesn't help us with our locality problem). Consider Figure 2.7, adapted from Glaser and Surya's paper in [25]. Both the points a and b form an Alexandrov interval with the origin and from the perspective of volume and length considerations, they may both be considered local regions in the causal set. Nonetheless, while ϕ
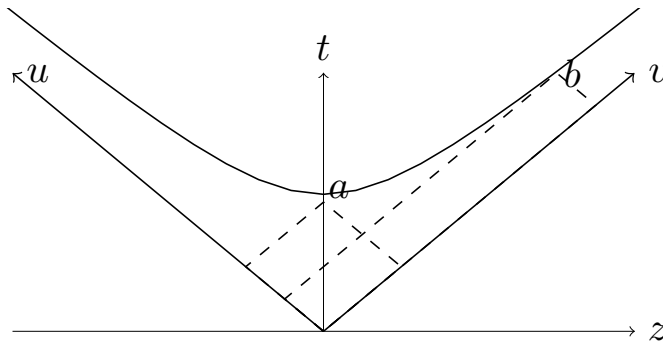
Figure 2.7: Point a resides in a region that is local to the origin, while b does not. Neither length nor volume may be used to distinguish local regions. Adapted from a figure provided in [25].

is constant at 0 and a, it is not constant at b; event a therefore lies in a local neighborhood of 0, while b does not.

The discrete operator (with the smearing function) is yet another Lorentz invariant observable, and while Equation (2.28) is non-local, Equation (2.37), in which the non-locality scale is taken to be equal to the discreteness length scale, is well suited to a definition of locality. In [25], Glaser and Surya give a definition of a local region in a causet using the abundance of intervals in a causet. Using sprinklings of local regions, Glaser and Surya define a *rigidity* criterion with $\langle N_m^d \rangle$ that candidate causets must satisfy in order to be local regions.

A poset is said to be *strongly d-rigid* if

$$N_m(\mathcal{C}) \sim \langle N_m^d \rangle (N \pm \sqrt{N}) \qquad n \neq 0 \tag{2.59}$$

where, $N_m(\mathcal{C})$ is the number of m element inclusive orders in the d-dimensional causet $\mathcal{C}$ (N.B.: Notice the change in convention!),[6] $\langle N_m^d \rangle$ is the expectation value of the number of n element inclusive orders over an ensemble of manifoldlike, d-dimensional $\mathcal{C}$ (obtained from analytic calculations, confirmed by simulated sprinklings), and N is the number of events in the set. A poset is said to be *weakly d-rigid* if it contains subsets that are strongly d-rigid. Strong d-rigidity is (one) condition for a causal set to be embeddable in flat d-dimensional spacetime and a strongly d-rigid causal set is said to be "local". Furthermore, the presence of a large family of strongly d-rigid subintervals in a weakly d-rigid causal set is a condition for its embeddedness in a curved d-dimensional spacetime.

The expectation value for each N_m over the dimensions arises from a geometric argument whose details will be subdued in this paper. A derivation of the concept can be found in the appendices of [25]. For the purposes of this paper, the behavior of the characteristic curve for the abundance of m order intervals will be compared qualitatively with those found in [25]. The closed-form expression for $\langle N_m^d \rangle$ can be found in Chapter 4.1.2.

2.2.3 Dimension

There are many ways to estimate the dimension of a causal set, and exploring them all is beyond the scope of this project. This project will primarily concern itself with the use of the ordering fraction, f, and the midpoint scaling dimension estimator.

Before proceeding, an important caveat must be mentioned. When considering causal sets, especially in this project, the dimension is only useful insofar as it is variable. By the end of this chapter, the reader will understand that the concept of an "overall" dimension for a given causal set should be taken with a grain of salt because:

1. For a discrete theory of spacetime, geometrical properties have statistical meaning only [41],

2. On the mesoscopic scale of a computationally accessible causal set, dimensional quantum fluctuations become increasingly relevant and at the limit of a single irreducible relation (i.e. a link), geometrical concepts become physically meaningless as quantum effects dominate completely, and

---

[6]N.B. despite earlier promises of simplicity, the convention has been changed here from $m + 1$ inclusive intervals to m inclusive intervals for consistency with [25]; this convention will also make the calculations for $\langle N_m^d \rangle$ a little simpler. For clarity: $m = 0$ refers to links, $m = 1$ are length-2 chains, etc.

3. The individual causal set need not be consistent with continuum geometry; the superposition of causal sets or some other phase transition process (i.e. the transition from Planckian discreteness to a continuum manifold) may return the appropriate geometry of the continuum using non-manifoldlike causal sets or subsets.

In general, the concept of an "overall" dimension only becomes relevant insofar as one considers a sufficiently large causal set, i.e. when one considers the continuum limit, as discussed in Section 2.3.2. For the same reason, it will also be of little use to consider relatively small intervals. However, dimension estimators for the microscopic scale have been recently developed that may shed new light on the geometry at this scale; see e.g. [25]. Moreover, it has been suggested by Carlip in [10] that the erratic (typically two-) dimensional behavior of infrared orders is a physical, rather than purely mathematical, phenomenon.

A final note of caution arises from terminology. It is important to distinguish between the *Minkowski dimension* (the dimension of the spacetime that approximates the causet at the continuum limit), the *Myrheim dimension* (the estimated Minkowski dimension of the causet using the ordering fraction), and the *order dimension*. In mathematics, the *(poset) order dimension* is defined by the smallest number of total orders whose intersection gives rise to the poset. This is in general *not* equal to the Minkowski dimension of the spacetime the poset is embedded into (if it can be embedded). However, it has been shown that a causal set can be embedded in 2D Minkowski (flat) spacetime iff it has a order dimension of at most two [38]. The order dimension will not play a large role in this project, but it has been useful when considering Monte-Carlo simulations [55].

The dimension estimators should not be interpreted for tests or even conditions for manifoldlikeness. However, the agreement of *several* scale-invariant dimension estimators is often considered an important preliminary condition for manifoldlikeness.

Myrheim-Meyer Dimension

The most popular method of estimating the dimension of the spacetime that approximates the causet uses the *Myrheim-Meyer dimension estimator*, first introduced as the *ordering fraction* by Myrheim in his 1978 CERN pre-print [41]. For a given Alexandrov interval, the ordering fraction, f, is given by

$$f \equiv \frac{R}{R_{\text{max}}} \tag{2.60}$$

where R is the number of order relations in the interval under consideration and R_{max} is the number of order relations of a totally ordered causal set constructed with the same number of events as the interval under consideration. For an interval with cardinality N,

$$R_{\text{max}} = \binom{N}{2} \tag{2.61}$$

such that the ordering fraction for a given interval of N events is given by

$$f = \frac{2R}{N(N-1)} \tag{2.62}$$

(a) Light cone for event c **(b)** Light cone for event c'
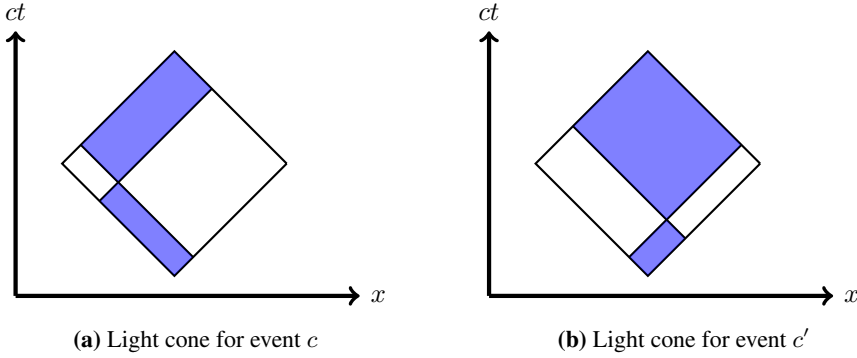
Figure 2.8: A visualization of the symmetry arguments exploited in order to estimate the dimension of the spacetime from the ordering fraction of an Alexandrov interval. This is a demonstration for 2D spacetime only; the symmetry arguments do not hold for arbitrary dimensions.

The dimension can then be estimated from the ordering fraction using Table 2.5. In general, the relationship between the ordering fraction and the dimension is given by [6] (citing [38])

$$f = \frac{3}{2} \frac{d!(d/2)!}{(3d/2)!} \tag{2.63}$$

Let $I(a.b)$ be the intersection of the past light cone of some point b with the future light cone of some second point a that is timelike separated from b and let $A(a,b)$ be the area contained by $I(a,b)$. Consider an ensemble of $I(a,b)$ containing some variable intermediate point c that is timelike to both a and b (i.e. within the area formed by $I(a,b)$). One element of this ensemble is given by Figure 2.8a (for two dimensions), where the union of the blue and white regions gives $I(a,b)$ and the sum of the areas of the blue and white regions gives $A(a,b)$. Let

$$I_R = I(a,c) \cup I(c,b) \tag{2.64}$$

be the intersection of the past and future light cones of c and $I(a,b)$. Let

$$A_R = A(a,c) + A(c,b) \tag{2.65}$$

be the area of I_R. In Figure 2.8a, I_R is given by the blue regions, while A_R is the area contained by the blue regions. The ordering fraction is then given by

$$f = \frac{\langle I_R \rangle_i}{\langle I \rangle_i} \tag{2.66}$$

where the subscript i denotes that the average is taken over all ensembles.

By symmetry, each event c has some corresponding event in the interval, c', as shown in Figure 2.8b, such that for two-dimensional spacetime, the ordering fraction is $\frac{1}{2}$. These arguments can also be generalized to higher dimensions, as in Table 2.5, although the symmetry arguments may only be exploited for the two-dimensional case. Intervals which are

identically links will of course always return an ordering fraction–and thus dimension–of 1 by construction. Intervals with a height of two do not fare much better for the purposes of this project. Consider the length-2 interval formed by the ordering of two vertices as in Figure 2.9. In theory, an event may have an infinite vertex degeneracy and thus the dimension of an interval constructed from such vertices is not bounded by any means. However, the rules imposed by the scheme this project uses allows for such intervals to have a dimension no greater than two (and in fact, such intervals will *always* have a dimension less than two when using the Myrheim-Meyer dimension estimator). Given the discussion of infrared dimensional reduction in [10], the vertex degeneracy restrictions of Feynman posets may have further physical justification.

Locality-Based Continuum Dimension Estimator

In introducing a definition of locality (and thereby a test for the manifoldlikeness of topologies on a causal set), Glaser and Surya also introduce a new dimension estimator that arises from their methods in [25]. Each of the $\langle N_m^d \rangle$ introduced in Section 2.2.2 return characteristic curves for the abundance of intervals in the causal set for each dimension. Although this approach presupposes a causal set describing a local region of spacetime, these curves can be used to estimate the dimension. Moreover, such an approach precludes fractal dimensions, although this should come as no surprise, given that the expectation value for the abundance of intervals is derived from the continuum and defined only for integer values of d.

Midpoint Scaling

Having established that the number of events in an Alexandrov interval embedded in a region of a Lorentzian manifold is proportional to the volume of that region in spacetime and then introducing the correspondence of the height of the interval with the proper distance of the geodesic in the continuum, one can use the cardinality of the poset to estimate the dimension. For a given Alexandrov interval, $I(a, b)$ containing some midpoint c, consider subintervals $I_1 = I(a, c)$ and $I_2 = I(c, b)$, where c is the event that maximizes the subintervals I_1 and I_2. Note that this partition need not result in exactly two subsets, but may result in I_1, I_2, and the remaining elements in the poset not contained in either of the two.

Ordering fraction of an interval in various dimensions of spacetime						
d	1	2	3	4	5	6
f	1	$\frac{1}{2}$	$\frac{8}{35}$	$\frac{1}{10}$	$\frac{128}{3003}$	$\frac{1}{56}$
as decimal	1	0.5	0.229	0.1	0.043	0.018

Table 2.5: Reference table for comparing the ordering fraction, f, to the dimension of the spacetime of the interval considered. Copied from a colloquium presentation given by Jan Myrheim [39].
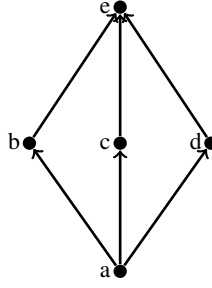
Figure 2.9: A 3-pronged vertex and its T-symmetric vertex ordered to create a length-2 Alexandrov interval. For arbitrarily large n, n-pronged vertices have $f = (0, 1]$, and $d = [1, \infty)$. For $n = 3$, the lowest possible value for f is 0.7.

Since $V(L) \propto L^n$, where n is the dimension (c.f. Equation (2.12)) the midpoint scaling dimension estimator is given by [45]

$$N_1 \simeq N_2 \simeq \frac{N}{2^n} \tag{2.67}$$

Inverting this equation, we have

$$n \approx \log_2\left(\frac{N}{N_2}\right) \tag{2.68}$$

where N_1 and N_2 are the number of events in I_1 and I_2, respectively, and N is the total number of events in the total interval $I(a, b)$.

Referring again to Figure 2.8, one may informally see that this approach holds in two dimensions.

A Cursory Look at Subinterval Dimension

Most of the literature reviewed by this author indicates that considering this ordering fraction for *any* causal set, regardless of whether or not it is an Alexandrov interval, is a close approximation to the original dimension estimator (see e.g. [5, 55, 45, 46]). As of writing, this author is unaware of any mathematical proof of this assumption. The validity of this assumption was subject to a great deal of attention throughout this project, and a cursory exploration into the issue is given in Section 3.3.2.

This approach is formulated in the following way: suppose there is some causal set $\mathcal{C}$, with N events containing $N_\mathcal{A}$ Alexandrov subintervals, labeled $\mathcal{A}_i$, each containing N_i events and R_i ordering relations as in Figure 2.10. The most naïve approach is to consider the average interval ordering fraction, given by

$$\langle f \rangle = \frac{1}{N_\mathcal{A}} \sum_{i=1}^{N_\mathcal{A}} \frac{2R_i}{N_i(N_i - 1)} \tag{2.69}$$
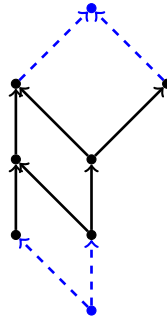
Figure 2.10: A causal set where two extremal points and their relations to the existing events within the set have been added to create an Alexandrov interval. The blue points are the extremal points a and b, and the blue dashed lines are the additional relations that are added.

Suppose now that the causal set $\mathcal{C}$ is a subinterval of some larger Alexandrov interval, $I(a, b)$, where a precedes all minimal events in $\mathcal{C}$ via links and b is preceded by all maximal events in $\mathcal{C}$ via links (i.e. a partial order is imposed between global extrema in the causal set and two additional events, then those relations implied by transitivity). The ordering fraction of the interval containing $\mathcal{C}$ as a subinterval is then given by

$$f = \frac{2(R + N + N + 1)}{(N + 2)(N + 1)} = \frac{2R + 4N + 2}{(N^2 + 2N + 2)} \tag{2.70}$$

where the number of relations and events in the subinterval are given by R and N respectively. After adding one event, a, the number of relations is first increased by the relation between this point and every other existing point in the subinterval. Adding the second point, b, introduces the same number of relations, plus the relation between a and b.

Meanwhile, the "total" ordering fraction of the subinterval, if one eschews the condition that the set considered must be an Alexandrov interval, is simply

$$f = \frac{2R}{N(N - 1)} \tag{2.71}$$

In the case of Figure 2.10, one finds $\langle f \rangle \approx 0.94$ when using the first method, Equation (2.69) (where links were not considered), and $f = 0.88$ using the second method, Equation (2.70). Meanwhile, the "total" ordering fraction using Equation (2.71) is $f = 0.60$. One may also note that in this case, it was possible to add only two additional points to complete the Alexandrov interval, but it need not be so straightforward. A causal set may include several more extremal events, and the growth dynamics may involve restrictive rules (as in this project), meaning that several orders containing many extraneous events may need to be added to create an Alexandrov interval containing the entire subinterval. Additionally, it is possible that the divergence explored in this extremely limited example may become less severe in the limit $N \longrightarrow \infty$.

A crude approximation can be made for a more general causal set if one considers the findings in [29], wherein the number of Alexandrov intervals, $N_{\mathcal{A}}$, and the typical number

of relations, R, can be estimated for the limit $N \longrightarrow \infty$ using the Kleitman-Rothschild theorem. Yet, this has a fairly limited application, as it characterizes the exact space of posets that one tries to avoid.

Upon closer review, it is rather obvious that the averaging of ordering fractions is a physically meaningless pursuit. When it comes to the total ordering fraction, a reasonable approximation may be made to apply the estimation to open intervals. This will be explored in greater detail in Section 3.2. As it abides by the same principles for estimating the dimension as outlined here, the discussion is better suited to methodology.

2.3 Dynamics

When considering the configuration space of all posets, the Kleitman-Rothschild theorem will restrict any given poset to an entropy space that is decidedly non-manifoldlike. As will be seen in Section 2.3.1, it is poset *space* that is presumed to give rise to the manifold, rather than a single poset. The topology on some superposition of posets over all poset space is proposed to give rise to the manifoldlikeness of spacetime at the continuum scale. Presented with the contradiction between Action and Entropy, there are two strategies for reaching synthesis:

1. *Limiting the configuration space* by ruling out sets whose topologies are non-manifoldlike (it is tempting to refer this as *Causal Dynamical Triangulation* (CDT), but this is already appropriated by another approach to quantum gravity; although the two are very similar, they have irreconcilably divergent interpretations of causal events and their relations), and

2. *Kinematic Schemes*,[7] where the entire configuration space of posets contribute to a sum over histories and give rise to the causal set. The strategy here is to then find the appropriate rules for the dynamics, presumably using some analogue of the action for a causal set to develop a *quantum measure*.

While causets are thought to be *unlabeled* posets, the Kleitman-Rothschild theorem technically applies to *labeled* posets. The distinction is however trivial in the context of the asymptotic limit, as regardless of the labeling convention, entropy space is nonetheless dominant. Recall that this project considers a specific class of posets whose vertices are three-degenerate. If the kinematic properties of this class, or other classes of posets based on this class, lead to sets that escape the scenario outlined by the Kleitman-Rothschild theorem, it may have important implications for the configuration space and perhaps even the amplitudes of sets.

---

[7]Again, this term has also already been appropriated by Dribus in [20], but at the very least, it is not radically different from the typical causal set theory treatment. In particular, kinematic schemes refers to expanding the configuration space from the space of posets to higher-level multidirected structures. In this context, it may be instructive to refer to this approach as *limited kinematic schemes*.

2.3.1 Path Integral Formulation

Sum Over Histories

Causal set theory has focused primarily on the *sum over causal sets* approach, an adaptation of the path integral, or *sum over histories* approach in quantum mechanics. In analogy to continuous quantum mechanics, the task has been to select classes of causal sets (conceptualized as the *histories* of some locally finite region of the universe's spacetime) according to a causal set action, i.e. its amplitude. By applying an analagous principle of least action, the superposition of these sets is expected to return the properties of a continuum geometry. The implementation of this approach has therefore been to "grow" causal sets stochastically, where partial order relations and/or new events are added according to this action. Each addition in this growth is referred as a *transition*.

Up until recently, the subject of defining this action and thus the amplitude on a given causal set and probability for transition remained unresolved. The focus has more or less been to prepare a classical growth model that could later be used for a fully quantized theory. While Rideout and Sorkin provide a dynamics for growth that produce sets that can be approximated by the manifold in [47], they emphasized that this is a classical model because the transitions do not depend on any parameters defined by this action. The Benincasa-Dowker action first gave a causal set version of the Einstein-Hilbert action in 2 and 4 dimensions and provided initial evidence that causal sets give rise to local physics [4]. It was later generalized by Dowker and Glaser in arbitrary dimensions in [17].

Despite this phenomenal success and breakthrough for the theory, causal set *growth* using amplitudes computed from this action have not yet been implemented, although Monte-Carlo simulations have been carried out by Surya in [55] (see Section 2.4 for more) with encouraging results. Cunningham and Krioukov have generated sprinklings of causal sets and computed the Benincasa-Dowker action on their paths in [12], but report prohibitive numerical limitations owing to the non-locality of the theory, although Glaser and Surya's working definition of locality may make simulations of local regions more accessible.

Despite having defined the action for causal sets, its implementation in a stochastic model is less obvious. In the Feynman path integral formulation, to find the classical trajectory of some particle between two fixed endpoints, one simply calculates the action, S, of all possible paths and integrates the contribution from each path given by

$$e^{iS[x]} \tag{2.72}$$

over path space, where the action can be easily calculated from the energy of the system, in turn defined in reference to some substantiative coordinates. The squared modulus of the resulting complex probability amplitude gives the probability for the trajectory to occur. In the classical limit where $S \gg 1$ and $\delta S \approx 0$, the classical path dominates and reflects the principle of least action. Mathematically,

$$Z = \int e^{iS[x]} \mathcal{D}x \tag{2.73}$$

where $\mathcal{D}x$ denotes integration over path space and Z is the path integral. The choice of Z as the label is for historic reasons: it has a striking similarity to the partition function

in statistical mechanics; in fact, it is often simply referred to as the partition function in this context. This resemblance will be exploited later. Each path is assigned an equal probability and it is the phase difference for each path that gives rise to deviations from classical behavior; interference terms enable modest non-classical behavior, but suppress extreme violations.

What is the analogy in causal sets? In this case, we are no longer dealing with the trajectory of a single particle, but rather the stochastic "growth" of a causal set arising from contributions from the whole of configuration space. Some (see e.g. [31], [28], and [14]) opt for an approach faithful to Feynman by modeling (point) particles in the causal set (generally referred to as the swerve model) in order to model discrete dynamics based on these path integrals. One approach has been the (analogous) Wiener integral, where the probability is assigned based on a class of Brownian paths passing through a small region of spacetime, but as pointed out by Dribus in [20] and Sorkin in [51] (and again in [50] and [53]), these approaches are necessarily classical.

The most recent approach has been to define some scalar field on the causal set, an endeavor spearheaded by Sorkin [52], with modest success for a handful of Monte-Carlo simulations. If the geometric meaning of spacetime is reinterpreted in a discrete Planckian theory (recall that save their continuum approximation, the posets have no correspondence to macroscopic geometric properties), then so too must be the field, a criticism that has been levied against this approach [39]. While the test field described in Section 2.2.2 has proved useful in developing a kinematics for causets, there is much work to be done in providing a reasonable physical interpretation for this scalar field. It is certainly founded on theoretical grounds, but without promoting the "event", a purely mathematical concept at the current stage, to some physical object, the theory remains partially undeveloped. Analagously, the electromagnetic wave is not a philosophical abstract: it fundamentally consists of real and physical photons; "mathematical object" is an ontologically unacceptable description of the fundamental units of the gravitational wave, at least where physicists are concerned. It should be emphasized that the scalar "field" defined on the causet is a temporary measure that cannot persist if there exists no physical interpretation that the mathematical formalism describes.

Returning from this digression to the path integral formulation, when generalizing to the configuration space of posets rather than the trajectories of the particles defined on them, the analogy shifts to that of integration in quantum field theory. In this context, the action is referred to as the *functional* and the key difference is that the contribution from each field (as opposed to path) is given by

$$e^{iS[\phi]},\tag{2.74}$$

i.e. the action is now a function of some scalar field, $\phi(x)$. The path integral then becomes

$$Z = \int \exp\left\{i\left[S[\phi] + \int \mathrm{d}^n x J(x)\phi(x)\right]\right\}\mathcal{D}x\tag{2.75}$$

where n is the Minkowski dimension. The integration of amplitudes over fields in QFT is mathematically imprecise due to the imaginary exponential term, as is the integration over configuration space in causal set theory, and more will be said about analytic continuation

in the following chapter. The second exponential term in Equation (2.75) is the source function, or more precisely

$$S_{\text{source}} = \int d^n x J(x)\phi(x). \tag{2.76}$$

In the context of causal set theory, the first term in the exponential of Equation (2.75) can be identified with pure gravitation, while the source function encompasses other non-gravitational forces. As the source may be defined arbitrarily, allowing $S_{\text{source}} \longrightarrow 0$ (i.e. an approximately empty region of spacetime), and subsuming long distance physical source effects into an effective Lagrangian that approximately vanishes (this is in essence the procedure carried out in Equation (2.30)), Equation (2.75) can be expressed as

$$Z = \int e^{iS[\phi]} \mathcal{D}\phi \tag{2.77}$$

Yet for this application, the path integral does not consider fields, but causal sets and while the former space is continuous (and, perhaps more importantly, uncountably infinite), the latter is discrete (and countably infinite), such that the action is now $S[\mathcal{C}]$, the action of a causal set, and the integral in Equation (2.77) is now a summation

$$Z = \sum_{\mathcal{C} \in \Omega} e^{iS[\mathcal{C}]} \tag{2.78}$$

where the sum over Ω, the sample space of causal sets, replaces the functional integration over $\mathcal{D}\phi$.

Configuration Space

The question is now: what is the sample space of causal sets that the path sum should consider? A possible interpretation arising from the original formulation of path integrals would suggest that the sample space should be the space of *all* posets (as these are, we recall, the class of sets purported to specify spacetime structure). Why stop there? Perhaps the summation should be taken over the space of all ordered sets–any mathematical object that can represent any arbitrary geometry, no matter how absurd. After all, path integration is taken over the space of all trajectories, no matter how classically absurd. One may be tempted to argue that surely there are restrictions on the space of paths that are integrated over; is Equation (2.73) taken over loop space or Cauchy surfaces?[8] The answer, which can be stated without having to engage in the lengthy ongoing debates on the interpretation of quantum mechanics, is emphatically *no*: there are, for the most part, no limitations on

---

[8]Respectively: trajectories that begin and terminate at one point (i.e. closed loops) and trajectories of super-luminal particles (i.e. spacelike sections of a light cone). This author has been tempted to include Skorokhod space, the space of discontinuous paths, as well. Upon closer review, there are some limitations to including discontinuous paths in QM. The subject of selecting an appropriate *measure*, or space of paths, is an unresolved, but by no means notorious problem in physics. Physicists have more or less accepted the lack of mathematical rigor in defining the configuration space and have been content with starting with an abstract Wiener space and generalizing from there [51]. This project will simply defer to precedence and assume that the space is bounded by nothing but our imagination [3]. Dribus has also proposed a more rigorous, albeit much more involved, definition of the measure using kinematic schemes–see [19, 20].

the configuration space. Those regions are more than non-classical: they are kinematically prohibited, and yet are included in the path integral (in the Feynman formulation at the very least). The phase difference simply erases these trajectories in the classical limit, but they are very much still there in the entirety of *configuration space*, the integration space. By analogy, the configuration space of causal set theory should include ordered sets whose topologies are not only non-manifoldlike, but "perverse".

Sumati Surya has provided evidence for manifoldlike causal sets when summing over Ω_{2D}, the sample space of 2D partial orders grown using the Benincasa-Dowker action in [55]. However, as Surya points out, such a model is more akin to causal dynamical triangulation (and compares the results with that of Ambjørn, et. al. in [2], concerning the sample space of 4D partial orders, but without the use of the Benincasa-Dowker action), which features Metropolis-Hastings modeling over a restricted region of poset space. The resulting posets in Surya's model are just broad enough to allow for non-manifoldlike topologies, but tend towards manifoldlike posets using the quantum measure provided by the action. The goal is to use the Benincasa-Dowker action in generalized dimensions to formulate a quantum dynamics for causal set growth, and perhaps to broaden the configuration space even further.

In the limit $S[\mathcal{C}] \gg 1$ and $\delta S \to 0$, any dynamics governed by the action must give rise to classical behavior, forming an effective litmus for the validity of the Benincasa Dowker action; it should effectively pick out those posets that are most manifoldlike from a sea of non-manifoldlike topologies. Conversely, the phase difference of classically absurd topologies should make their contributions negligible in the classical limit. Yet, it is the cross terms of the integration over these absurd paths that contributes to the experimentally (and theoretically) observed interference phenomena at the classical limit. This is precisely why the path space contains such strange paths: it is a *decoherence functional*.[9] The analogy to causal set theory further strengthens the argument that the sample space must include the most comprehensive configuration space available. It has been shown that a single poset suffices to reproduce the spacetime structure of some region, but one is tempted to conjecture that more exotic (known or unknown) phenomena arise only in the superposition of objects in a space encompassing non-manifoldlike posets. Following Dowker and Halliwell's work on analogous decoherence functionals in [18], perhaps the next step is to reinterpret the classical limit as a maximally decoherent (i.e. approximately diagonal decoherence functional) set of histories and look there for non-classical behavior within the causal set.

Implementation

Having an expression for the action of a causal set and some ideas for the sample space, all of the pieces are in place to use Equation (2.78) to grow a causal set. As the Kleitman-Rothschild theorem has made clear, the number of topologies on a set of N elements is *at least* $2^{N^2/4}$, such that growing a set with 100 elements involves summing over a sample space of 10^{752} sets, of which no more than 0.09% are manifoldlike (and this situation de-

---

[9]There is a deeper and somewhat sinister ambiguity lurking in here, arising from the interpretation of quantum mechanics, but following this thread will quickly unravel the organization and goals of this project, so for the time being, they will be ignored. It will simply be noted that this author is following a *consistent histories* generalization of the Copenhagen interpretation and save the diatribes for some other space.

terioriates asymptotically). Furthermore, growing the set by adding one element at a time would mean enumerating those remaining sets in the space that the set at its current stage could still reproduce (and this is not to mention a given set's isomorphisms, which need to be accounted for since the causet is technically an unlabeled poset), a computational obstacle even if the sample space shrinks with each iteration.

A promising approach can be found in [55]. Starting with some arbitrary poset and using a Metropolis-Hastings algorithm, Surya exchanges relations one at a time with some probability determined by the change in the action. In [55], the move is accepted if it reduces the causal set action and rejected if the change in action is too extreme. In review, Bergtun was on the right track with his Monte-Carlo simulations in [5], but without a way to implement quantum dynamics, it is natural to expect this model to reproduce non-manifoldlike topologies on sets. The next step would be to expand this Metropolis-Hastings algorithm to allow for a larger domain in the sample space, i.e. to arbitrary dimensions (and perhaps even arbitrary classes of mathematical sets). In this case, the Benincasa-Dowker action would need to be generalized such that the probability for exchange is based on the action for any generalized dimension. One possible strategy would be to use some other scale invariant measure of dimensionality, like the Myrheim-Meyer dimension discussed in Section 2.2.3, compute first the estimated dimension of the causal set after an exchange, and then use the most appropriate expression of the d-dimensional Benincasa-Dowker action to assign a probability for the exchange. As Section 2.2.3 alluded to and as will be seen in Chapter 3, this introduces some theoretical hurdles that will need to be navigated before a full dynamics can be developed. Namely, as Glaser discusses in [23], it is difficult to specify rules that do not inappropriately change the causal structure.

Aside from Metropolis-Hastings algorithms, one may also apply these general principles to stochastic growth models, where posets are constructed by adding one event at time, rather than through exchanges. This will form the second phase of this project.

2.3.2 The Continuum Approximation

Most of the numerical approaches to causal sets reviewed by this author grow causal sets with no greater than 5000 points. If the causal set hypothesis is correct and these events are Planckian, even if these causal sets were totally ordered (which one would hope they were not, as this would not be a very fruitful endeavor), they would describe a spacetime region on the order of at most 10^{-40} seconds, while the spatial extent of such a spacetime would be at most 10^{-70} times the size of a proton. The region of spacetime in which a single, stationary grain of sand exists contains 10^{146} events (not to mention the roughly $10^{10^{290}}$ other configurations of posets containing the same number of events), when the discreteness scale is taken to be Planckian! A gargantuan task for the machines at this author's disposal, but not even remotely approaching the continuum limit. Each causal set must then be "smoothed out", or *coarse-grained* in order to represent a larger scale region of spacetime at the continuum limit.

Another complication arises when ensuring that this process returns a coarse-grained causal set that preserves the structure of the original causal set, although as Rideout points out, "one would not expect the topology of spacetime to be four dimensional all the way

down to the Planck scale... [and] it is likely that even the continuum approximation itself will break down at Planck distances... [46]" Perhaps one can expect other types of kinematic differences as well. Hence, at the current stage of development in the theory, any definitive statement about a rigourously defined limit is bound to be ill-defined. No matter which method is used to "smooth out" the causal set, there is always a risk of losing geometrical information or changing the structure and these issues will be discussed in Chapter 5.

As with dimension, there are several approaches to coarse-graining, but they will not be explored in this space. The simplest method is the *event decimation* approach used by Rideout and Sorkin in [48], where a subset of events and their relations are selected at random and removed from the set. The cardinality of the resulting set is determined by some probability $P \in [0, 1]$. Even at the upper limit of causal set simulations, coarse-graining seldom returns a "continuum limit", although the resulting sets are often treated as fair approximations. The specifics of the coarse-graining procedure used in this project will be addressed in Section 3.

2.3.3 Manifoldlikeness

This document has covered quite a bit of ground when it comes to characterizing and measuring the poset. Somehow, with such an abundance of tools at our disposal, we still have no way of saying whether or not the set is approximated by the manifold. So far, we are equipped to answer what the dimension of the manifold is, if it is curved or flat, how large it is, and if it has local regions, *provided* the causet is actually embeddable in the manifold. The absence of this discussion is a partial reflection of the lacuna in the current literature.

While some manifoldlikeness tests have been developed, some are extremely recent (at the time of writing, at least one of these is only a few weeks old), others are very stringent and do not allow for small deviations, and other are simply beyond the scope of this project. Chapter 5.1.1 will deal with the matter of determining manifoldlikeness is greater detail, but it bears mentioning at this stage that the machinery introduced until this point collectively serve as *conditions* for manifoldlikeness (as opposed to tried and true tests). The agreement of dimension estimators after coarse-graining, for instance, is a highly cited requirement for manifoldlikeness [28]. The existence of local regions as proposed in [25] is another. A much weaker case for the composite of indicators as a test for manifoldlikeness is given by the Kleitman-Rothschild theorem. As such an overwhelming region of the configuration space is occupied by posets that do not meet the requirements for embeddedness, it may be argued that posets that pass them have a fair likelihood of being approximated by the manifold.

2.4   Current Approaches Within Causal Sets

Sprinkling

This approach deals with producing a causal set that can be embedded into a manifold by simply sprinkling points into a Lorentzian manifold according to a Poisson distribution. This is bound to return a causal set that can be faithfully embedded into the manifold, as it necessarily does by construction. This procedure cannot reveal any new information about the dynamics of the construction of a causal set, and is therefore a strictly classical model. However, sprinkling has been critical for causal set theory, as it has enabled the development of the kinematic tools outlined throughout this chapter.

Classical Sequential Growth

The fundamental principle behind the Classical Sequential Growth (CSG) model is to construct a set by adding one relation at a time according to a set of rules, i.e. to develop a dynamics for causal sets. This diction can be misleading because strictly speaking, all constructions of causal sets are decidedly static. The addition of events to a causal set does not occur in the same Minkowski "time" that the causal set itself precipitates, but rather in some artificial, external measure of "time". The motivation is to develop a model that classically produces non-entropic posets in preparation for a quantum measure that can later be applied to the model to select out manifoldlike causets. The most successful of these models was developed by Rideout and Sorkin in [47], whose dynamics yielded causets that were almost entirely not KR orders.

Moreover, as Fay Dowker points out in [16], the most promising paradigm for CSG models is transitive percolation (TP), wherein the additions to the causal set are governed by a single parameter, p, the probability that the new event will be related to the events in the existing causal set. According to Dowker, the TP family is conjectured to be the only CSG model that is CPT invariant.

Although it was introduced earlier, the Kleitman-Rothschild theorem is worth mentioning once more, this time with the appropriate preliminaries established. The Entropy problem that the Kleitman-Rothschild theorem introduces is a more specific discretized manifestation of the Cosmological Constant Problem that is encountered in every approach to quantum gravity. As Dowker explains it,

> classical behaviour results when the amplitudes of the paths in the path integral which are not close to a classical path cancel out and do not contribute... [I]n the primal struggle between Action and Entropy, Entropy looks like it will overcome a local Action. In other words, an amplitude given by exponentiating a local action that grows linearly with N, the number of spacetime atoms, cannot overcome the entropic weight of the vast number of non-manifold-like discrete configurations. These will then dominate the path sum and there will be no continuum approximation [16].

To illustrate the scope of these entropically favored orders, for causal sets with just 5000 elements, the Kleitman-Rothschild theorem states that 99.98% of all causal sets that

can be constructed will form these three-layered configurations.[10] Regardless of how the layers are defined, a KR order will have a height no greater than two, which provides a very weak test for manifoldlikeness; if the posets are of height greater than two, they avoid an overwhelming space of non-manifoldlike topologies.

Although the Kleitman-Rothschild theorem offers a quick check of the causal set, having a height greater than two does not necessarily imply that the causal set can be embedded in a Lorentzian manifold. Furthermore, a causal set that has more than three layers may not necessarily have more than three layers after continuum approximations are made (e.g, after coarse-graining). In any event, if a causal set avoids the situation described by the Kleitman-Rothschild theorem, it can be said to have passed a first "test" which many other dynamics have failed.

As Surya points out in [54], there exist more sub-dominant classes of (non-KR-like) causal sets with non-manifoldlike topologies that have been identified by Dhar in [13], and similar concerns have been voiced by Loomis in [34]. After 3-layered KR-orders, the entropically favored orders are 2- and 4- layered posets (trailed by a declining number of layers as one moves down the hierarchy [43, 13, 54]). That said, the transitive percolation model has experienced modest success as a "halfway house" to quantum dynamics, even if the causets were not entirely manifoldlike in [47].

Quantum Mechanical Growth

The strength of causal set theory is that it provides a model in which spacetime is defined by (and thus arises solely from) events and their relations, rather than existing as an *a priori* manifold in which events "live", a defining characteristic of Dribus' "causal metric hypothesis". This is a radically different interpretation of physics: Feynman diagrams, for instance, and the probability amplitudes for some interaction they describe, presuppose some pre-existing substantiative manifold in which objects interact. The challenge is then to define some rules governing growth according to quantum mechanical interaction probabilities independent from models that depend on spacetime locality and even physical coordinate systems. In this light, the aforementioned growth models have been purely classical.

While Rideout and Sorkin offer a toy model in [47], they point out that the dynamics of transitive percolation cannot produce a manifold that holds at the quantum level because "it is stochastic only in the purely classical sense, lacking quantum interference," and "the future of any element of the causet is completely independent of anything 'spacelike related' to that element".

The backdrop of general relativity and Einstein's field equations suggests that the only way to develop a quantum growth dynamics is to allow Action itself to guide causal set growth. With the closed-form expression for the d'Alembertian for a causal set in d-dimensional spacetime given by Glaser in [24], an open call for causal set researchers has been made for studies of the causal set action in different dimensions. While it will not be explored in this project, this author takes the position that there should be made

---

[10]To make things more explicit once and for all: a closed-form algorithm for the enumeration of the number of partial orders on a (labeled or unlabeled) N-element set is an unsolved problem in combinatorics, with the exception of exact results for $N \leq 18$ (labeled posets) and $N \leq 16$ (unlabeled posets); and, of course, the results from [33] in the asymptotic limit, to which $N = 5000$ is considered here to be a reasonable approximation.

no *a priori* assumptions about the domain of dimensionality contributing to the path sum of causal sets. Therefore, the proposition may be to study the causal set action in *all* dimensions.

Thus far, only Monte-Carlo simulations of an ensemble of causets with a fixed number of points and dimensionality have been carried out (see [55]). Stochastic growth models should also provide an opportunity to study causet dynamics. The goal is to find a means by which to select posets that are approximated by the manifold and both of these approaches satisfy this task. While stochastic growth models are, in theory, the only means by which a "true" *dynamics* can be developed (i.e. swerve models and defining fields in direct reference to non-gravitational forces on a causal set), Monte-Carlo simulations are a perfectly reasonable (and in many ways superior, as will be seen) means to develop a dynamics of the type described herein.

3
Methodology

Underlying the project is a conjecture about the kinematics of causets, arising from Myrheim's suggestion that there could be a set of elementary event types, in the way hadrons are organized by the Eightfold Way, or elements in the periodic table [39]. Myrheim's suggestion forms the *ansatz* of the Feynman posets that were chosen for this project. The central hypothesis is then that there are elementary event types and that they are characterized by their number of links. The first leg of this voyage, likely to inform whether or not to continue on this path, is the consideration of events with exactly three links. The task of this project is not to actually prove this hypothesis, as even encouraging results may not offer proof, nor may discouraging results necessarily preclude their existence as elementary events.

Thus, the hypothesis ought to be reformulated. Rather than determining whether or not this class of posets is approximated by 4-dimensional spacetime, the focus is on whether or not such events could–either on their own or in conjunction with some other features–contribute to a configuration space whose superposition is approximated by 4-dimensional spacetime. Moreover, one may ask if such three-degenerate events could conceivably exist in abundance in a 4-dimensional spacetime.

There are two parts in this chapter, corresponding to two different stages in the project. In the first, a large collection of Feynman posets is constructed with a classical stochastic model and their kinematic properties are explored. By organizing an overview of the posets' ordering fractions, heights, d-rigidity, Hasse diagrams, and so on, a partial litmus for embeddability is established. Of particular interest is determining whether or not this class is abundantly populated by KR orders and if they provide evidence of local regions.

The second stage is motivated by a more stringent hypothesis rejection criteria for the first stage in light of recent reviews of the work of Surya, Benincasa, Dowker, and Glaser (see [55, 18, 25, 17, 4]) by implementing quantum dynamical principles in the causet growth by applying an action principle. Avoiding the entropic space of posets, the

agreement of dimension estimators, and the existence of local regions are all conditions for a poset's embeddedness in the manifold. Nonetheless, these conditions still cannot conclude whether or not this *class* of posets are inherently embeddable. A path sum over the space of classically acceptable paths will of course return classical results. On the other hand, a path sum over classically absurd paths is unlikely to produce a classical approximation. By the same token, if this particular class never returns posets that can be approximated by the manifold, it would serve as partial and suggestive evidence that its elements are not "fundamental", or at the very least that they are not the only fundamental events that make up a physically realistic manifold.

This chapter outlines both the classical and quantum growth models with an expanded discussion on approximating methods to deal with open intervals that arise during construction.

3.1 Classical Stochastic Growth

The classical stochastic model takes a fixed number of events that initially have no ordering relation, save for two totally ordered events. Covering relations are then added randomly (hereafter referred to as a *transition*) between two events subject to only two constraints:

1. The causal set always satisfies the four axioms of causal sets as stated on Page 18 at each step in the iteration.

2. Every event vertex may have a degeneracy of *at most* three and furthermore

   (a) *For the special case of the "no holes" script,* an event vertex may have an indegree of at most 2 and an outdegree of at most 1, *or* an outdegree of at most 2 and an indegree of at most 1.

   (b) Any event that has a degeneracy less than three is assumed to be linked to some other event outside of the subset considered, with the direction of the ordering relation determined by the presently existing links.

On a theoretic level, it should be noted that the resulting causal set is in reality a *subset* of the causet that the spacetime approximates, i.e. the resulting set is *at most* a finite region of spacetime, even after coarse-graining. Each resulting causet is then expected to contain at least one event that is related to some other event not included in the set (with the exception of special configurations that arise when considering Feynman posets–see Chapter 5 for more).

Vertices

The vertex degeneracy rule was selected as an *analogy* to Feynman diagrams, and the Hasse diagrams that result are *not* intended to represent particle interactions in the literal sense of Feynman diagrams. The model then allows only for two types of vertices formed at each event: "Y" shaped vertices inspired by the fundamental Feynman vertices for a particle interaction as in Figure 3.1, and "fork" shaped vertices that will be referred to as *holes*, inspired by the Feynman diagram for a white/black hole (where some liberties have
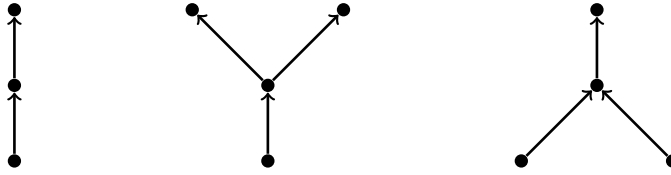
Figure 3.1: Three event vertices inspired by Feynman diagrams. The subclass of Feynman posets that allows for these events only is referred to as *no holes posets*.

Figure 3.2: Two additional event vertices inspired by "Feynman" diagrams for black/white holes. Both the Feynman and Hasse diagrams for such a situation are much more complicated, and it cannot be overstated that these vertices do not literally describe holes in either of the representations. The subclass of Feynman posets that allows for these events, plus those in Figure 3.1 is referred to as *holes posets*.

certainly been taken in this analogy), as in Figure 3.2.

Although it must be admitted that the divergence from the TP paradigm is fairly extreme (more will be said about this shortly, but suffice to say, this model is by no means *sequential*), one may note that transitions are governed by an (implicit, over explicit) parameter dependent on the probability that a new event will be related to the events in the existing causal set. In other words, the probability of transition is governed by the number of "non-saturated" events which have fewer than 3 existing links.

Dealing with Transitivity

Transitivity introduces a number of computational hurdles that can only be resolved by storing two matrices for the causets at each iteration. At each step, one link is added to the adjacency matrix, but any additional relations implied by transitivity are not added. Meanwhile, an auxiliary relation matrix keeps track of the relations and thus "adds in" transitivity, as this is the only means to establish a condition for avoiding loops (and in the case of *no holes* posets, for avoiding holes). This allows for a greater degree of freedom in the causal set construction, as the direction of the transition is no longer restricted by an extraneous relation. Consider, for instance, Figure 3.3a. If a link is added between the free point and the maximal event in this causal set, transitivity imposes an ambiguity in the Hasse diagram. The Hasse diagram may reflect the relations in the causal set, as in Figure 3.3b, or it may reflect the links in the causal set, as in Figure 3.3c.

If the poset in Figures 3.3 are *no holes* posets, transitivity will preclude otherwise permissible future transitions, and therefore unnaturally restrict the space of posets. Consider

(a) Three events in an initial configuration, where no transitions have been introduced.

(b) A Hasse diagram that inadvertently expresses the relations in the causal set and thus restricts future transitions.

(c) A Hasse diagram expressing only the links in the causet
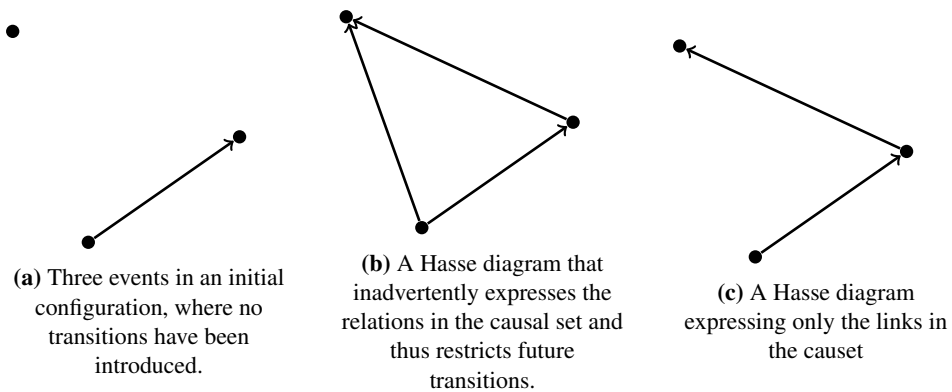
Figure 3.3: Depiction of causal set construction using two matrix representations and the Hasse diagrams constructed from such matrices.

Figure 3.4, a copy of Figure 3.3b where potential transitions are visualized. Despite the fact that the dashed red line is a perfectly acceptable transition, transitivity precludes it.
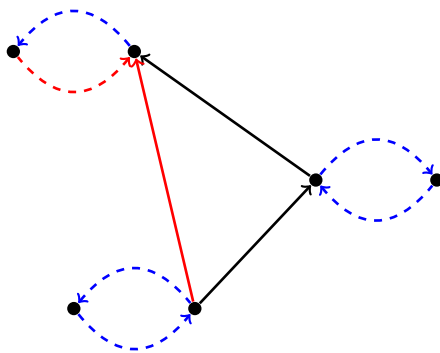
Figure 3.4: Transitivity restricts the growth process. The solid red line shows the offending relation. The dashed blue lines show allowed transitions, while the dashed red line shows the acceptable transition that is precluded by transitivity.

Technically, Figure 3.3b is not a Hasse diagram at all, as Hasse diagrams reflect links only.[1] However, the matrix representation remains ambiguous unless there are two concurrent matrices in use. Without a corresponding matrix for Figure 3.3b, there would be no restriction on a transition that maps the set depicted in Figure 3.3c to the target depicted in Figure 3.5, a clear violation of the axioms of causal sets.

The program is then given as follows: 1) impose a transition between two events (subject only to degeneracy and acyclicity constraints), 2) update both the adjacency and relation matrices with this single link only (as in Figure 3.3c), and 3) update the relation matrix by "drawing in" transitivity, as in Figure 3.3b to establish the restrictions for avoiding loops (and holes, if applicable). The significance of this feature of the model should not be overstated. It is simply a computational tool for constructing the causet, rather than a statement about causet kinematics. The presence of two concurrent matrices should not be interpreted as a statement about causet axioms. Ultimately, it is the relation matrix replete with the transitive axiom

---

[1]Recall that in graph theory, a Hasse diagram is the *transitive reduction* of a DAG, which by definition would include only the covering relations of a poset.

that serves as the causal set in the strictest sense.

When the causal set has been completely constructed, transitivity is imposed a final time to reflect the properties of a causal set. During the aforementioned process, if transitivity is suspended in one of the matrices, the resulting causal set may contain extraneous relations, as in Figure 3.6a. Since transitivity is suspended only as a matter of computational convenience, it is imposed later and therefore this direct link is demoted to a relation that is already implied, as in Figure 3.6b. On the other hand, the presence of two chains in Figure 3.6c does *not* mean that the poset contains extraneous links and this poset remains unchanged in the final analysis.

Figure 3.5: A loop that results from neglecting transitivity arising from the relation matrix.

Readers interested in an alternative view on the business of "suspending transitivity" are referred to [20], where Dribus proposes *modes of influence* governing the distinction between each vertex's covering relations versus the relations implied by transitivity. In this approach, the two causets indicated in Figures 3.6a and 3.6b are *not* automorphic and are therefore distinguishable configurations.

(a) Hasse diagram expressing only links with an extraneous relation.
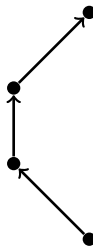
(b) Hasse diagram with the offending relation removed.
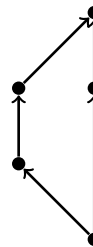
(c) Hasse diagram with two chains in the path. The links in this poset are *not* considered to be extraneous and are not removed.

Figure 3.6: There is an extraneous relation in Figure 3.6a indicated by the dashed red line. In the script, this relation is removed as a link, as it is already implied by transitivity and the result is given in Figure 3.6b. This is not to be confused with the situation indicated in Figure 3.6c, where there are two chains between the extremal points in the path. Since the right-most path is not a link, it is not considered extraneous and no changes are made.

Comparison to Other Approaches

Although this project originally took Rideout and Sorkin's CSG model as its starting point, it is clear that the only point of similarity between the two is that they are both transitive growth models that deal with complex networks. While CSG is a percolation model that features sequential growth, the causets in this project do not "percolate", nor is the process by any means sequential. In this case, the growth dynamics have been drastically simplified because they no longer treat a strictly classical approach. Although the dynamics described in the preceding section do describe a classical model, they may be applied to a quantum model without having to devise of any analogy for the Bell causality condition.

In [47], each transition occurs "in a definite order with respect to some fictitious 'external time'", and the authors go to great lengths to emphasize that the order of transitions in the growth model is purely fictitious. It is therefore difficult to understand the justification behind their condition of internal temporality, in which "no element can arise to the past of an existing element..." as "it would mean that an event occurred 'before' another which intrinsically preceded it [47]." For this author, it seems as though such an event would occur "before" the other only in the external, fictitious sense, in which case there is no physical contradiction present. This author would like to offer the possibility that the distinction between intrinsic and external time has not been treated in its complete nuance in this space, and the topic will be tabled, as it will not be relevant for this project.

Unlike the original CSG model, the more generalized 'dynamics' of this project abandon Bell causality as Rideout and Sorkin suggest for an inherently non-local theory like causal sets, a choice that will have further consequences in the second stage of this project. For the classical case, the properties of growth dynamics are less important, as the first stage of this project aims only to construct "complete" regions of spacetime subject to kinematic constraints only; in other words, the phenomenological question of how the causet comes into being is ignored in this stage. It should be emphasized that the choice to abandon Bell causality without an in-depth consideration of the consequences it has for Bell's theorem was not taken lightly, but this discussion is better suited for another space. While the phenomenological question is dropped in this consideration and the action principle therefore does not indicate the physical "growth" of a causet, this author argues that this will bear no impact on the quantum growth model offered in the next section. Each transition undertaken in the scripts should not be interpreted as a physical process, but rather a means by which to produce a large and random collection of action-minimized posets.

It may also be noted that the parameter p, the probability that a new event will be related to the events in the existing causal set, is implicit rather than explicit in this project. In the original CSG model, this parameter serves to restrict the configuration space of posets, with the additional implication that a quantum theory will provide some function that assigns p its appropriate values. For this project, such a parameter is unnecessary, as the posets considered presumably already occupy a rather restricted region of poset space.[2]

---

[2]Admittedly, this is just a conjecture, as the enumeration of posets in this class is not available at the time of writing. It may be interesting to explore classes of posets that *have* been enumerated and occupy a small region of poset space. Yet, this is not the space for such an exploration. Readers interested in this direction are offered the following resources from OEIS, an encyclopedia of integer sequences containing sequences for poset enumeration (`http://oeis.org/wiki/Index_to_OEIS:_Section_Pos#posets`) and digraph enumera-

In the second stage of this project, the quantum behavior of this parameter is encoded in the action, while the role of p is subsumed by β, an analagous thermalization temperature.

3.2 Quantizing the Classical Growth Model

It has been established that the space of Feynman posets cannot and does not represent the configuration space of topologies on posets. Initial results using the classical growth model returned a notable collection of potentially manifoldlike posets, although most were decidedly unlike 4D Minkowski spacetime. However, one may conjecture that the class suffers from a more specific entropy problem leading to non-manifoldlike dominance. This stage of the project is therefore an attempt to insert the class of Feynman posets into a quantum growth model guided by an action principle. This process introduces significantly higher computational demands, such that the set cardinality must be considerably reduced. The general prescription for quantizing the model is as follows:

1. Begin as usual with the set of two partially ordered events. Determine the Myrheim-Meyer dimension, d, of the causet (unless the dimension was specificied *a priori* as it is in this project, it is trivially 1) and its Benincasa-Dowker action in d dimensions.

2. Impose a transition either:

   - between two existing events,
   - between one existing event and an additional event introduced to the set as in Figures 3.7a and 3.7b, or
   - between two new events introduced as in Figure 3.7c.

   Each transition is selected according to the phenomenological (axioms) and kinematic (Feynman posets) rules enumerated in Section 3.1.

3. Before accepting the transition, determine the new Myrheim dimension of the causet and calculate the new action of the system after the transition. Accept if $\Delta S \leq 0$, reject if

$$e^{-\beta|\Delta S|} < r \tag{3.1}$$

   where $r \in [0, 1)$ is a random number that ensures that the system is approximately stationary (i.e. $\Delta S \to 0$) and β is a thermalization constant.

It is well known that the integral in Equation (2.77) (as well as the sum in Equation (2.78)) does not converge. Equation (3.1) is the result of Wick rotating Equation (2.78) by making the time coordinate imaginary, i.e.

$$e^{i|\Delta S|} \longrightarrow e^{(i\beta)i|\Delta S|}$$
$$e^{-\beta|\Delta S|} < r \tag{3.2}$$

---

tion (https://oeis.org/wiki/Index_to_OEIS:_Section_Di#digraphs), some of which are replete with closed algorithms, or at least asymptotic limits. More on this will be mentioned in Chapter 5.3.

(a) Transition $c \prec a$ is automorphic to $b \prec c$.

(b) Transition $a \prec c$ is automorphic to $c \prec b$.

(c) $2(N-2)$ automorphic transitions.
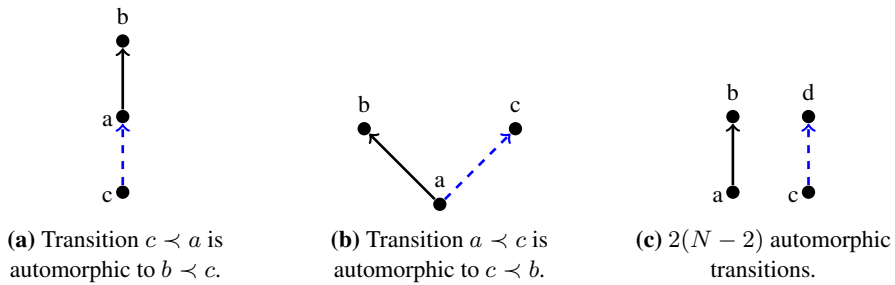
Figure 3.7: $2N$ initial transitions, where N is the maximum cardinality of the causet considered.

The thermodynamic transition parameter, β, has been introduced in order to frame the causal set partition function as a thermodynamic partition function to avoid non-manifoldlike behavior [55, 22]. While Monte-Carlo simulations have been effective in probing the effects of β, it is more computationally demanding to reproduce phase transitions in a stochastic growth model. This project will consider only coarse intervals of β, sweeping its value from $\beta = 0.2$ to $\beta = 1.4$ in intervals of 0.2.

3.3 *Intermezzo*: Theoretical Obstacles

At this point one encounters some additional theoretical questions that must be addressed before proceeding. The development of this project was rather dialectic, and went through several stages before landing on a suitable prescription for quantizing the model. It must also be admitted that the resulting methodology still needs improvements (a critical review of the model used in this project is given in Chapter 5.2). Rather than discarding these developments, the reader is offered an insight into this dialectic process, so as to illuminate potential pitfalls for future researchers. Moreover, Section 3.3.2 contains a theorem regarding the approximation of an Alexandrov interval by means of an open interval. The resulting methodology used in this project is given in Section 3.4 on Page 61, and the reader may safely skip to this page to continue the methodology report.

There arise two important questions at this stage:

1. How does one calculate the Benincasa-Dowker action of a causet if it is not an Alexandrov interval?

2. How does one determine the dimension of the causet in the intermediate stages of the growth model?

3.3.1 Large or Small, the Poset Must be a Causet

The title of this section is at odds with the original philosophy adapted for the classical growth model. In the classical growth model, it was assumed that the poset, a purely mathematical object, remained so until the completion of the growth process; it is not until "completion" that the poset is theoretically promoted to a causet. However, the action is
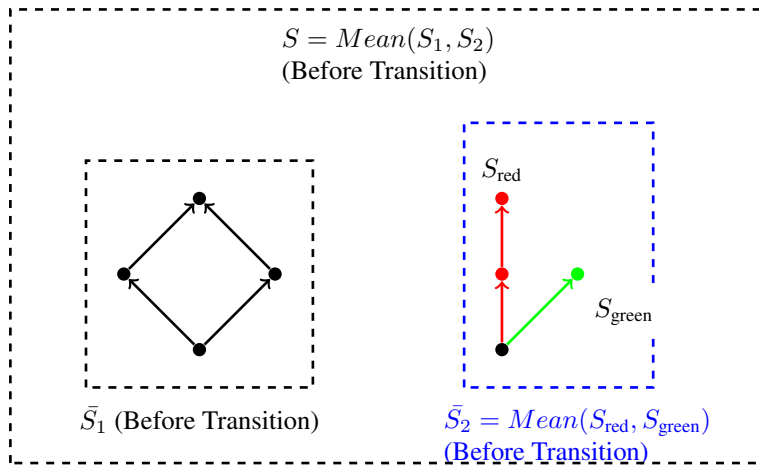
Figure 3.8: The first step of the naïve additivity for the Benincasa-Dowker Action

strictly *physical*. Thus, if one is to apply an action principle to the growth model, it must be applied to a physical object. The simplifying assumption of the classical growth model will not work here.

An earlier version of the scripts used in this project applied a naïve additivity for the Benincasa-Dowker action, where two events were randomly selected for transition and the dimension(s) and action(s) for the subset(s) containing the events were calculated, then added. If any of the subsets containing the relevant events are not Alexandrov intervals, then a sample of closed intervals from the subset is selected and their actions calculated, then averaged to return a subset action. The 'total action' is then given by the sum of subset actions. The transition is then imposed, and the action(s) calculated a second time. Figure 3.8 provides a sketch of the first step of this process. Naïve additivity makes the model simple, as only those subsets containing the relevant events require calculation (since we are only interested in their difference).

Unfortunately, as seen in Section 2.2.2, the causet action is *bi-local*, such that for a causal set $\mathcal{C} = A \cup B$, the total causet action

$$S[\mathcal{C}] \neq S[A] + S[B] \tag{3.3}$$

but is rather given by

$$S[\mathcal{C}] = S[A, A] + S[B, B] + S[A, B] + S[B, A] \tag{3.4}$$

where $S[X, Y]$ is the action of the interval formed by the maximum of subset X and the minimum of subset Y. Moreover, this addition presupposes that the causet has been partitioned along a timelike surface.

At the least one must identify the intervals in the set one wishes to use to calculate the action, preferably some appropriately partitioned collection of intervals such that their union returns the entire set. Alternatively, one may consider the open set to be a subinterval

of some larger closed Alexandrov interval and assume that the abundance of intervals will approximately retain its distribution. This is the approach adapted in this project. Any open Feynman poset $\mathcal{C}$ with cardinality $N_{\mathcal{C}}$ may always be a subinterval of some Alexandrov interval $\mathcal{A}$ with cardinality $N_{\mathcal{A}}$, where

$$N_{\mathcal{A}} = N_{\mathcal{C}} + M \tag{3.5}$$

where M is the smallest number of additional events that would be needed to construct $\mathcal{A}$. For Feynman posets (and any other class of posets with kinematic restrictions of the same nature), it is straightforward to see that M is a function of 1) the kinematic vertex restrictions of the class and therefore the indegree, $\deg^-(v)$, and outdegree, $\deg^+(v)$, for a given vertex v in the set and 2) the number of extremal events in the set.

First, we introduce V, the *net vertex degree*, the allowed difference between the indegree and outdegree of any given vertex

$$V = |\deg^-(v) - \deg^+(v)| \tag{3.6}$$

For Feynman posets, this is given by

$$V = \begin{cases} 1 & \text{No Holes posets} \\ 2 & \text{Holes posets} \end{cases} \tag{3.7}$$

With a little thought, one finds that for any given poset containing $N_{\text{ext}} = N_{\text{min}} + N_{\text{max}}$ extremal events, the number of elements that must be added is given by

$$\begin{aligned} M &= (N_{\text{min}} - V) + (N_{\text{max}} - V) \\ &= N_{\text{ext}} - 2V \end{aligned} \tag{3.8}$$

For a poset with no vertex restrictions, M is of course vanishingly small for large N:

$$M \approx \begin{cases} 0 & N_{\text{ext}} = 1 \\ 1 & N_{\text{ext}} = 2 \\ 2 & N_{\text{min}} \geq 1, \quad N_{\text{max}} \geq 1 \end{cases} \tag{3.9}$$

Referring to Equation (2.55), one must now determine how to define N_n and ϵ. The natural choice is of course to find $S[\mathcal{C}]$ with respect to $\mathcal{A}$, as doing so avoids the need to partition the set to add the action. Computationally, this means not only enumerating the number of extremal events for each subinterval at each transition, but also explicitly imposing the additional causal structure of $\mathcal{A}$. Instead, this project opts to use $\mathcal{C}$, assuming that this will serve as a fair approximation. A similar approximation will be made for the Myrheim dimension. This author is not aware of any rigorous proof to justify such an approximation, and much of the literature reviewed does not make any explicit reference to the issue. Yet, there appears to be a precedence for its application. The analysis of the time-asymmetry of the causets in [55] for instance implies the application of the action to a causet containing open intervals. The matter is very briefly mentioned in [46], where it is claimed that "because this measure of dimension associates a dimension to any ordering

fraction, it is sometimes used heuristically to specify the 'dimension' of a causal set as a whole, without regard to whether it represents an Alexandrov set or whether the region is small enough not to see the spacetime curvature." The question will be explored on a preliminary basis in the following section, but the reader should be aware that the following proof is subject to a number of limitations.

It is in theory possible to consider individual intervals, devising of an algorithm to apply the bi-local property of the action, and this is likely to be a fruitful strategy suitable for future work. However, this project will simply assume that the causet is at all points a subinterval of some larger Alexandrov interval to serve as a preliminary exploration of the quantum dynamics of Feynman posets.

3.3.2 The Dimension of a Subinterval

Having established that the causet is at all stages a subinterval of some larger Alexandrov interval, one is forced to confront the dilemma that arose in Section 2.2.3 when discussing the Myrheim dimension of a causal set.

Theorem 1. *Suppose $\mathcal{C}$ is an open partially ordered set of cardinality $N = N_\mathcal{C}$ containing N_{ext} extremal events. Suppose $\mathcal{A}$ is a closed partially ordered set of cardinality $N_\mathcal{A}$ and suppose $\mathcal{C} \subset \mathcal{A}$. Let $f_\mathcal{C}$ be the ordering fraction of $\mathcal{C}$ and $f_\mathcal{A}$ be the ordering fraction of $\mathcal{A}$. In the limit $N \longrightarrow \infty$,*

$$f_\mathcal{C} \approx f_\mathcal{A} \tag{3.10}$$

and in the limit $\frac{N_{ext}}{N} \longrightarrow 0$

$$\Delta f = |f_\mathcal{C} - f_\mathcal{A}| \longrightarrow 0. \tag{3.11}$$

Proof.

Postulate 1. *The number of chains in a finite set containing N elements is given by [42]*

$$R = \frac{4N!}{2(\log 2)^{N+1}} \tag{3.12}$$

$\square$

If $f_\mathcal{C} \approx f_\mathcal{A}$, then

$$\frac{2R_\mathcal{C}}{N(N-1)} \overset{?}{\approx} \frac{2R_\mathcal{A}}{(N_\mathcal{A})(N_\mathcal{A}-1)} \tag{3.13}$$

where $R_\mathcal{C}$ is the number of relations in $\mathcal{C}$ and $R_\mathcal{A}$ is the number of relations in $\mathcal{A}$. Using Proposition 1 and Equations (3.5) and (3.8), we have

$$\frac{4(N-2)!}{\left(\log(2)\right)^{N+1}} \overset{?}{\approx} \frac{4(N + N_{ext} - 6)!}{\left(\log(2)\right)^{N+N_{ext}-4}}$$

$$\frac{(N-2)!}{(N + N_{ext} - 6)!}\left(\log(2)\right)^{N_{ext}-4} \overset{?}{\approx} 1 \tag{3.14}$$

where the case $V = 2$ has been assumed, although in the asymptotic limit, the results can be generalized to arbitrary values of V. In the asymptotic limit, $N \gg 1$, and denoting $\alpha = \frac{N_{\text{ext}}}{N}$, the approximation becomes

$$\frac{N!}{[N(1+\alpha)]!} \left(\log(2) \right)^{(\alpha N - 5)} \overset{?}{\approx} 1 \tag{3.15}$$

Since $\log(2)^N \ll \frac{N!}{[N(1+\alpha)]!}$, then

$$\lim_{N \to \infty} \left(\log(2) \right)^{(\alpha N - 5)} \approx 1 \tag{3.16}$$

and

$$\frac{N!}{[N(1+\alpha)]!} \overset{?}{\approx} 1 \tag{3.17}$$

Clearly, if only a very small fraction of elements are extremal (for a closed Alexandrov interval, for example), then the subinterval is a very good approximation. Despite expectations, the approximation even holds in cases where the number of extremal points approaches the cardinality of the set. Series expansions at $N = \infty$ to first order give

$$\frac{N!}{[N(\alpha+1)]} \approx \begin{cases} 0.71 & \alpha = 1 \\ 0.75 & \alpha = 0.8 \\ 0.79 & \alpha = 0.6 \\ 0.85 & \alpha = 0.4 \\ 0.91 & \alpha = 0.2 \\ 0.95 & \alpha = 0.1 \end{cases} \tag{3.18}$$

$\square$

Therefore, for sufficiently large sets, the subinterval will serve as a suitable approximation for the interval. While this approximation remains unproven for small orders, it has been suggested that the so-called "dimensional reduction" of posets at this scale may be an acceptable and even expected behavior [10].

Provided the appropriate conditions on the poset are met, one may now use the following methodology for quantum dynamics:

1. Estimate the Myrheim dimension of the interval with respect to its subinterval relations and cardinality.

2. Calculate the action using the appropriate form of the Benincasa-Dowker action with respect to the subinterval.

3. Introduce a transition and repeat steps one and two for the target causet.

4. Accept if $\Delta S \leq 0$ and reject if $e^{-\beta |\Delta S|} < r$.

3.4 Resulting Methodology Used In This Project

In the preceding section it has been argued that the ordering fraction of some causal set may be approximated by conceptualizing the set as a subinterval of some larger interval. However, this approximation needs further study for infrared orders; while the approximation is well suited for Monte-Carlo simulations, its application to a stochastic growth model is questionable (consider e.g. the initial set containing a total order of two elements when $N = 2$–although this is itself a closed interval, the immediate transitions that follow are unlikely to be). This project will therefore table the exploration and simply prescribe the dimension of the poset *a priori*, testing at 4 dimensions. Although this simplifies the methodology considerably, doing so has led to significant loss of a so-called "quantum" quality, as it may be recalled that a truly quantum dynamics should make no *a priori* assumptions about the dimensionality of posets.

In this project, the poset will be assumed at all stages to be a subinterval of some larger interval with fixed cardinality.

Finally, the procedure adapted in this project is given as follows:

1. Begin with a set of two partially ordered events, the subinterval of some larger interval. Prescribe the dimension *a priori*; this project will consider $d = 4$. Determine the action of the subinterval using Equations (2.55) and (2.58), where

$$\epsilon = \frac{1}{N} \tag{3.19}$$

   where N is the cardinality of the subinterval (i.e. those that have already been "introduced", i.e. $N = 2$ before any transitions have been made, $N = 3$ after the first transition and so on).

2. Introduce a transition between any of the $N_{\mathcal{C}}$ events in the interval (i.e. the "total" number of events that will be included in the final poset) and calculate the action of the resulting target set.

3. Accept the transition if $\Delta S \leq 0$ and reject if ΔS satisfies Equation (3.1).

Classical Model

The resulting analysis of the classical growth model now features two approaches. In the first, the posets are taken at face value and rather than conceptualizing the resulting objects as subintervals, a sampling of intervals in each poset will be considered in their own right. While this approach precludes the study from answering more interesting questions regarding their embeddedness in a manifold, it does provide an opportunity to study the internal structure of the posets in this class. This approach also allows us to understand, as has been suggested by Myrheim, Sorkin, Bombelli, and others, the Planckian causal structure as a complex system with exotic behavior that is never observed at the continuum limit. We observe, for instance, only static and integer dimensionality at the continuum limit, although Planckian subintervals of a causet approximated by the manifold may ex-

hibit fractal dimensions, and may wildly fluctuate along its chains (i.e. along the causal analogues of a continuum geodesic), a natural consequence of statistical geometry. In this part, the qualitative properties of the causet's intervals will also be explored with Hasse diagrams. For each of the causets constructed, a total of N_{sample} intervals *with heights greater than or equal to 3* are randomly selected, where

$$N_{\text{sample}} = \frac{N_{int}X}{X + N_{int} - 1},\qquad (3.20)$$

N_{int} is the number of intervals in the causet, and X is given by

$$X = \frac{\hat{p}(1 - \hat{p})z^2}{M^2},\qquad (3.21)$$

$\hat{p} = 0.25$ is the sample proportion (chosen to maximize Equation (3.20)), $z = 1.96$ is the z-score for a 95% confidence interval, and $M = 0.05$ is the margin of error.

The sample of intervals excludes intervals with a height less than 3 to avoid overrepresenting those intervals that have a Myrheim dimension of 1 by construction. A total of four samplings are taken: once for each poset with 1800 and 4500 elements. The intervals in each sampling are measured for their volume, ordering fraction, and length. These results are used twice. In the first, the measures of a statistically representative sample of intervals from *one* poset of each class at each cardinality is stored to explore potential relationships between kinematic properties for infrared subintervals. In the second, the measures of a statistically representative sample of intervals from *50* posets of each type are *averaged* in order to understand the diversity of subinterval properties across posets. Since an enumeration of the length of each interval in the set is required for further computation, the distributions of interval length are given as *absolute* values, rather than representative samples.

In the second approach, the posets are understood to be subintervals of a larger Alexandrov interval. This includes an analysis of the estimated Minkowski dimension of the "total" set, using both the midpoint scaling estimator and the Myrheim dimension. Both the strong and weak d-rigidities of the causets are calculated in this part, again using the open interval as a suitable approximation to the larger closed interval that it is a subset of.[3] The heights of the causets are also calculated in this analysis, as well as a crude approximation of the level structure of the causet.

The benefit of this division of the approaches is that one is now in a position to make a computational comparison between the Myrheim dimension of the open interval and the Myrheim dimension of the closed interval that contains it. An interesting task for future studies would be to impose the additional events and relations that are needed to construct the interval given the subinterval and compare the ordering fractions to provide a numerical verification of the approximations made in Section 3.3.2.

Lastly, the single poset containing 4500 elements was coarse-grained five times for each subclass of Feynman posets, removing roughly 20% of the set's events at each iteration. The resulting sets contain (roughly) 80, 64, 51.2, 40.96, and 32.77% of their original values. Although a more effective coarse-graining might be desired given the cardinality

---

[3]Technically Theorem 1 does not apply to the abundance of intervals in the open poset, but this issue will be ignored for the time being.

of the sets, the algorithm used in this project is at this current stage unstable for large coarse-graining parameters. While some change in the causal structure is to be expected, it is a good practice to reject coarse-grainings with extreme deviations in structure. For each coarse-graining, the kinematic properties were calculated again to explore changes to the causal structure.

Quantum Model

Due to time constraints, only the *holes* posets were selected for the quantum model. The constructed posets from this class contained the most manifoldlike between the two types, with a significant portion of causets featuring a Myrheim dimension of 4. As the script no longer needs to look for holes before imposing transitions, the computation time is significantly reduced when compared with the *no holes* posets. In this project, a total of 7 causets are constructed using the action principle at each transition, once for each value of β in 4 dimensions. Initial results using the action principle returned incomplete posets, where several elements could not be introduced by transitions, resulting in very small and disconnected posets. Therefore, coarse-graining and detailed computations were not carried out on the resulting posets.

Coarse-Graining

The *event decimation* approach was introduced in Chapter 2.3.2. The procedure is given as follows: for each vertex in the poset, select a random number between 0 and 1; if the number is less than the coarse-graining parameter, promote the relations between its outgoing and incoming relations to links and remove the vertex and its relations from the set. Repeating this process five times (using the poset from the previous coarse-graining) gives a causal set that contains only approximately 33% of its original vertices, while representing a region of spacetime comparable to roughly 3 times larger than the original causal set. Figure 3.9 shows the first step of this process.

(a) Original poset containing 12 elements. The events that are removed in the coarse-graining process are indicated in red.

(b) Poset that results after the first coarse-graining at 50%.
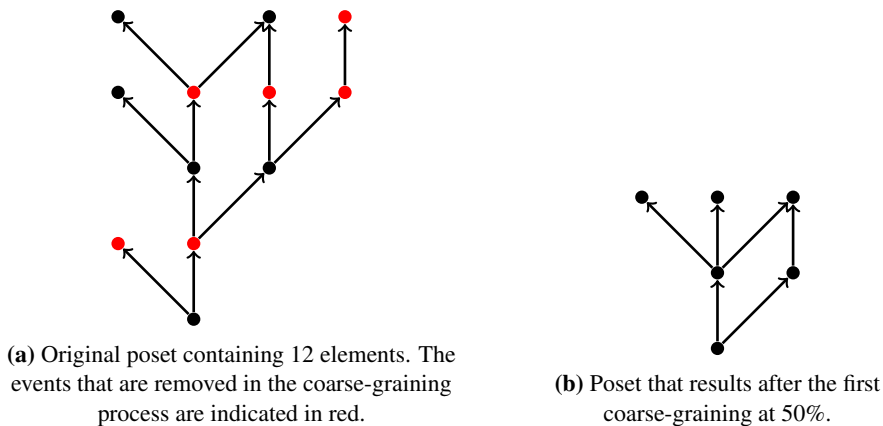
Figure 3.9: Event decimation approach to coarse-graining.

4
Results

The scripts used in this project provide a wealth of information that may be of use in future studies, but a portion of the data has proved extraneous for the purposes of this document. This section will only include the most insightful results in this author's estimation, while figures associated with additional data can be found in Appendix B. While some analysis will be provided in this section, a more in-depth discussion is given in Chapter 5. The aim of this chapter is simply to provide the immediate results from the constructions.

Section 4.1 offers the results from causets of both regimes constructed using the growth model. It includes first the interval sampling statistics where the posets are treated in their own right and explores potential relationships between the observables in the statistics in Section 4.1.1. Next, the posets are treated as subintervals of a larger Alexandrov interval, and Section 4.1.2 explores d-rigidity, level structure, and dimension estimators. Finally, a more in-depth report on the effects of coarse-graining is given in Section 4.1.3.

Section 4.2 gives the results for the quasi-quantum model and illustrates the scope of the shortcomings in the algorithmic implementation.

4.1 Classical Growth

In general, the results indicate that the *no holes* posets tend to be subintervals of 1- and 2-dimensional sets, while the *holes* posets tend to be subintervals of sets ranging between 4 and 6 dimensions. There exist no relationships between interval kinematic observables at this scale, although the scatterplot of interval volume and ordering fraction in the *no holes* posets is visually suggestive, offering a potential avenue for future exploration. Coarse-graining reveals a relationship between the two measures for the *no holes* posets.

The interval sampling analysis reinforces the results found in [10], as regardless of the overall ordering fraction of the set, the infrared orders within the larger intervals are

overwhelmingly 1- and 2- dimensional.

Tests for the d-rigidity of the constructed posets return mixed results. While the interval abundance curves of both the entire posets as well as their subintervals do not fit the characteristic curves provided by Glaser and Surya in [25], larger values of m are in close agreement and smaller values of m tend towards agreement after coarse-graining, similar to the results found in [25] for percolated causets. Moreover, the curves are markedly dissimilar from the curves of KR-orders.

4.1.1 Interval Sampling

Figures 4.1-4.3 give the distributions of mean interval length, volume, and ordering fraction for 50 causets containing 1800 elements for each subclass of Feynman posets. Although the distributions do not fit normal or half-normal distibutions, they offer somewhat reasonable standard deviations from the mean, suggesting some degree of normality across each poset. Figures 4.4-4.6 give the distributions of the length, volume, and ordering fractions for the intervals of one causet containing 4500 elements for each subclass of Feynman posets. Again, none of these distributions fit normal or half-normal distributions. Moreover, the standard deviations from the mean are quite large in this series with the exception of the ordering fraction, which is nearly negligible for the *holes* posets, but moderate for the *no holes* posets.

These results indicate that while there is a fair degree of consistency from poset to poset for each subclass (i.e. the distributions are typically similar for any given poset), the intervals within a single poset are rather varied. In the distribution of intervals for a single causet, one finds a positive skew for length and volume for both types of Feynman posets, but this should not come as a surprise. For any interval of cardinality N, the minimum skewness of the subinterval length distribution is realized by a total order, with $N - 1$ length-1 intervals (links), $N - 2$ length-2 intervals, and so on. As the interval deviates from a total order, there are more and more infrared subintervals available. The same logic can be applied to the skew of the volume distribution, where the skewness increases even more rapidly as it deviates from a total order than it does for length.

Figures 4.1-4.3 reveal that the distribution of interval volumes and lengths in the *holes* posets is flatter than the comparable distribution of *no holes* intervals. This indicates that the *holes* class exhibit a wider diversity across posets, which explains the topological diversity of the resulting sets.

For each type of poset, the scripts used in this project identified one subinterval with an ordering fraction corresponding with two dimensions and isolated their respective portions of the adjacency matrix. The Hasse diagrams for each type are given in Figures 4.10 and 4.11 on Pages 71-72. In each case, one finds very "skinny" orders that are only a few relations removed from a total order. More will be said about these Hasse diagrams in Chapter 5.
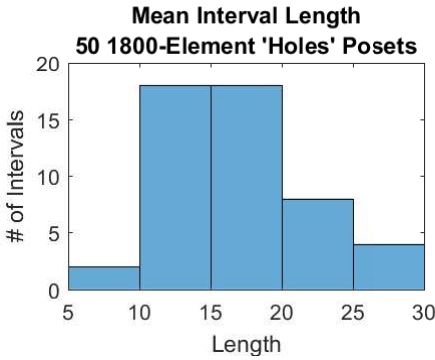
(a) Mean length = 16.83
Standard Deviation = 4.815
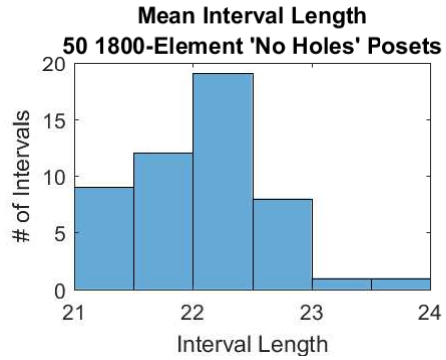
(b) Mean Length = 22.05
Standard Deviation = 0.54

Figure 4.1: Distribution of mean interval length across 50 posets
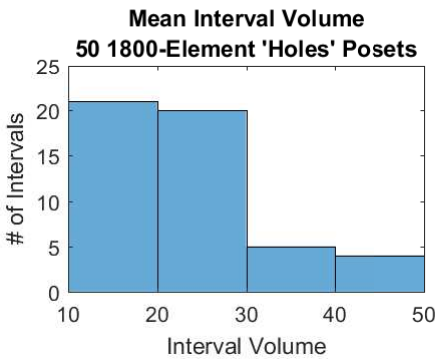
(a) Mean Volume = 23.49
Standard Deviation = 8.67
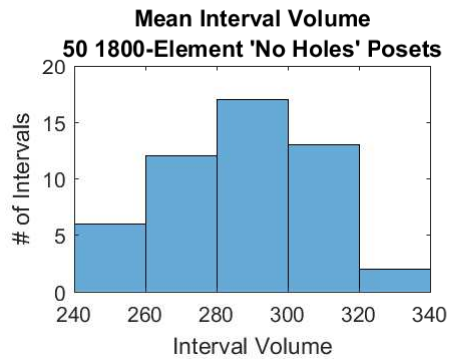
(b) Mean Volume = 287.48
Standard Deviation = 20.88

Figure 4.2: Distribution of mean interval volume across 50 posets
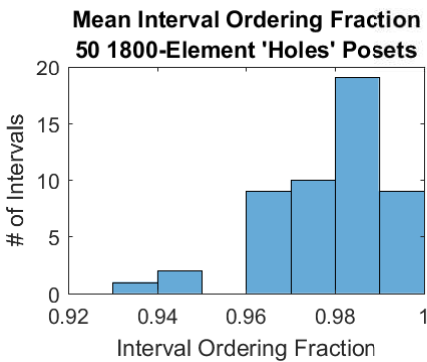
(a) Mean f = 0.98
Standard Deviation = 0.01
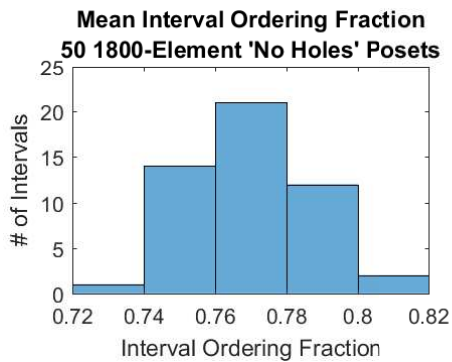
(b) Mean f = 0.77
Standard Deviation = 0.02

Figure 4.3: Distribution of mean interval ordering fraction across 50 posets

(a) Mean length = 17.07
Standard Deviation = 10.745

(b) Mean Length = 30.04
Standard Deviation = 14.19
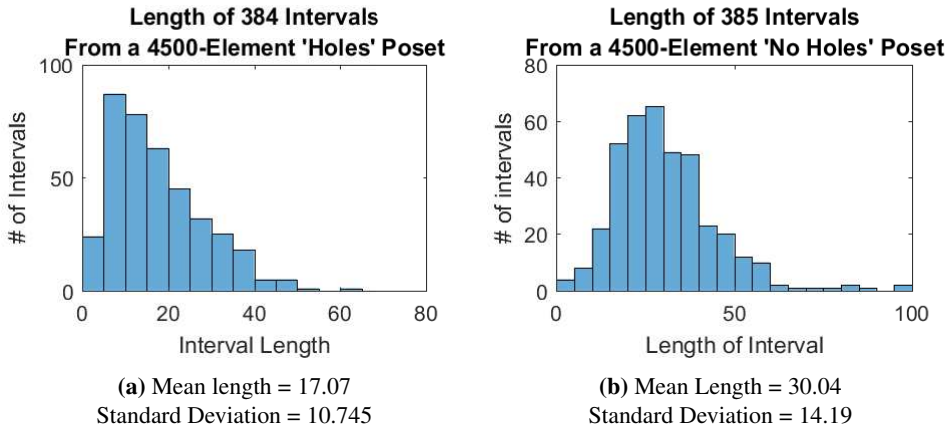
Figure 4.4: Distribution of interval length in one poset

(a) Mean Volume = 19.78
Standard Deviation = 13.19

(b) Mean Volume = 654.89
Standard Deviation = 596.87
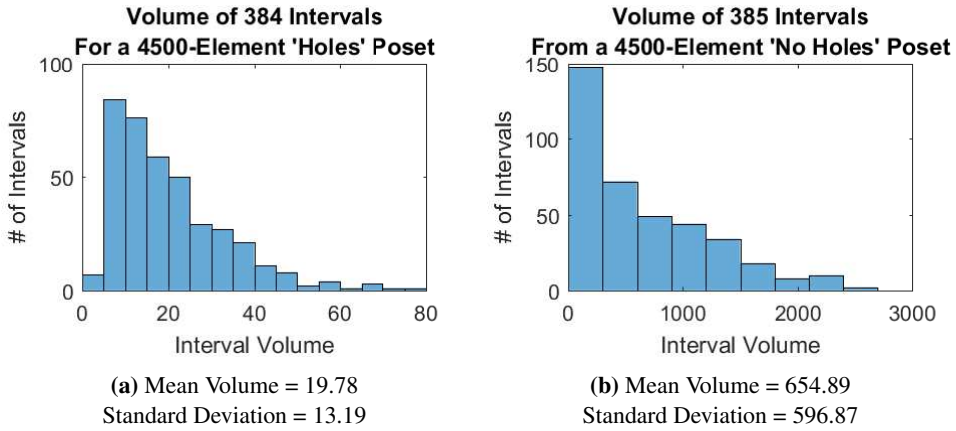
Figure 4.5: Distribution of interval volume in one poset

(a) Mean f = 0.99
Standard Deviation = 0.06

(b) Mean f = 0.74
Standard Deviation = 0.13
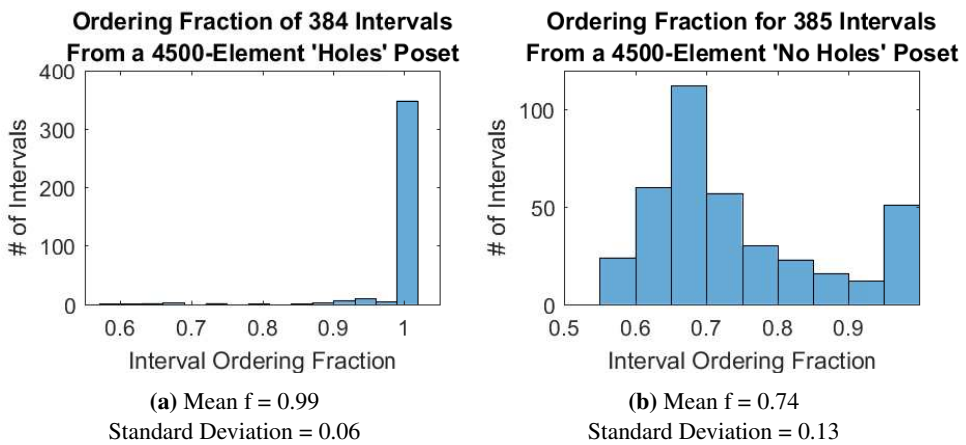
Figure 4.6: Distribution of interval ordering fraction in one poset

Finally, there appears to be no relationship between any of these values at this scale. The figures provided by the comparison between interval volume and ordering fraction in the *no holes* posets invite the possibility of a correlation between the two values, where the ordering fraction may converge on a single value in the limit of large volume. Moreover, the ordering fraction appears to converge to approximately 0.636, the "total" ordering fraction of the poset (reviewed in the following section). Figure 4.7 demonstrates the stark difference between the two regimes for both the smaller and larger posets.

Nonetheless, multiple attempts to fit curves on the data have indicated that no such relationship exists. Figure 4.8 provides a fitted curve on the entirety of the data set for the larger no holes poset. While the curve fits the data well, it fails to converge on a non-zero value of the ordering fraction. Figure 4.9 shows the results of comparing two fitted curves in two piecewise vertical regions of the data set, partitioned along the line $x = 0.636$, the conjectured value to which the curves might converge. In this case, the optimal curve for the lower region is a poor fit, and even then, the fit curves for both regions intersect and diverge rapidly rather than converge on a single value.
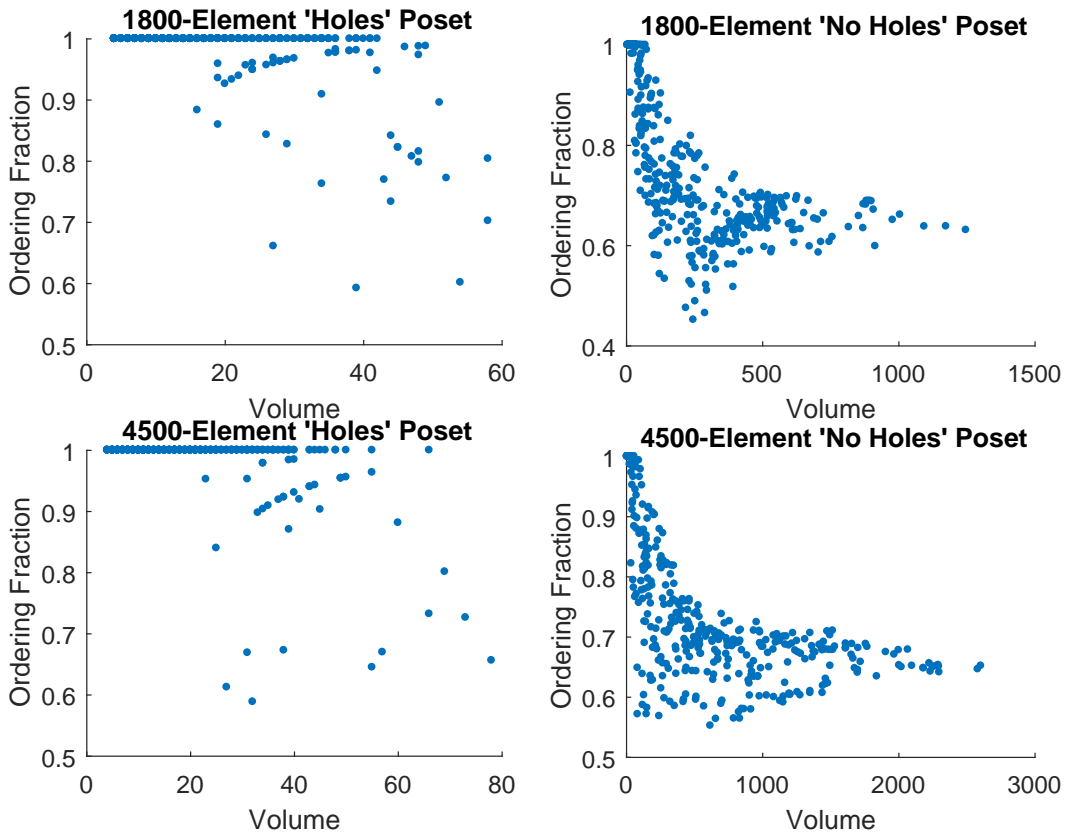

Figure 4.7: An apparent relationship exists between interval volume and ordering fraction for the *no holes* posets, but not for the *holes* posets, regardless of poset cardinality.

Fitted Curve For All Interval Volume vs. f Data Points
4500-Element "No Holes" Causet

Robust (LAR) Non-Linear Least Squares Fit
$y = 1.113x^{-0.219} + 0.436$
SSE: 0.052
R-square: 0.991

Volume vs. f
Fitted Curve
Shape-Preserving Extrapolation
Value at Volume =4500

X: 4500
Y: 0.6241
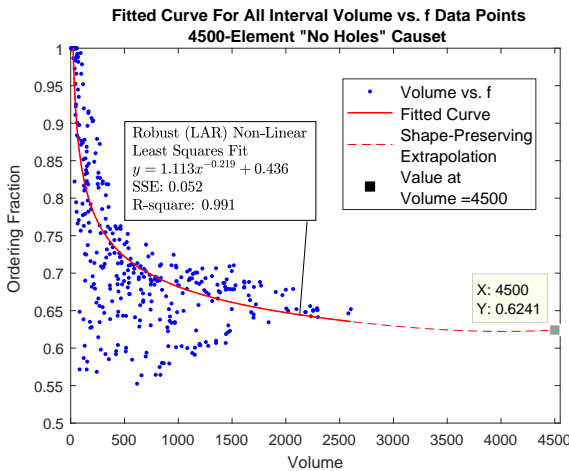
Figure 4.8: Fitted curve on the scatterplot displaying the relationship between interval volume and ordering fraction for the 4500-element no holes poset.

If such a relationship existed, it might provide insights on the transition behavior of a causet from a discrete theory to the continuum limit. However, the scale at which such a transition is thought to occur is ill-defined, but surely significantly above that of the 4500-element causet considered. Expecting continuum-limit evidence at this scale is wishful thinking, and the patterns observed at this scale are of undetermined significance. However, this phenomenon will be explored again when considering the coarse-grained causets, as these results are more likely to reveal continuum-limit behavior.

Appendix B includes the scatterplots for the comparison of the other interval observables for both regimes, as well as the distribution of interval observables for the smaller 1800-element posets. There are no significant results from these explorations, as the former simply demonstrate no correlation, while the latter distributions are similar (apart from scale) to those found for the larger 4500-element posets provided in this section.

Piecewise Curve Fitting of Interval Volume vs. Ordering Fraction
For a 4500-Element "No Holes" Causet

Robust (LAR) Non-Linear Least Squares Fit
$y = 0.008e^{-3.723x} + 0.697e^{-0.016x}$
SSE: 0.03484
R-square: 0.9916

Upper Region
Lower Region
Upper Region Fit
Lower Region Fit
Shape-Preserving Extrapolation
Approximate Intercept

X: 4350
Y: 0.6285

Non-Linear Least Squares Fit
$y = 0.563x^{0.013}$
SSE: 0.055
R-square: 0.064

Figure 4.9: Partitioned curve-fitting of the interval volume and ordering fraction scatterplot of the 4500-element no holes poset
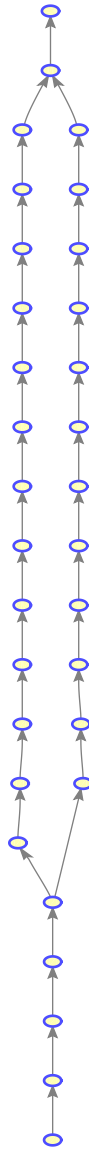
Figure 4.10: Hasse diagram for an isolated subinterval with an ordering fraction corresponding to two dimensions. This set is a subinterval of an 1800-element *holes* poset. The node labels are arbitrary and have no relation to their original labeling in the larger poset.
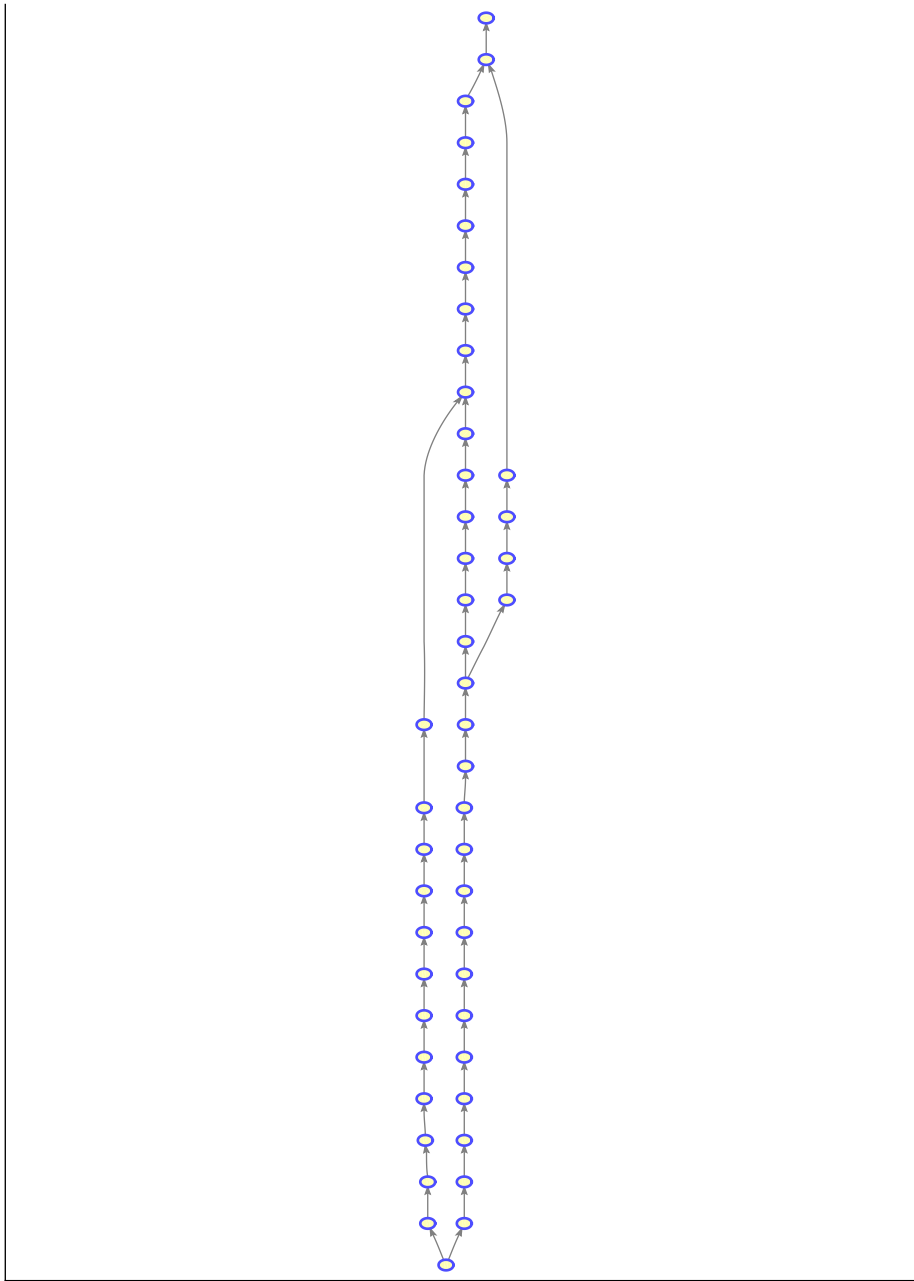
Figure 4.11: Hasse diagram for an isolated subinterval with an ordering fraction corresponding to two dimensions. This set is a subinterval of an 1800-element *no holes* poset. The node labels are arbitrary and have no relation to their original labeling in the larger poset.

4.1.2 Analysis of the Poset as a Subinterval

As subintervals of larger Alexandrov intervals, the posets become more interesting. Before coarse-graining is applied, the heights of the causets are significantly above the 3-level KR orders, as can be seen in Figures 4.12a and 4.12b for the smaller 1800-element *holes* and *no holes* causets, respectively. The 4500-element *holes* poset has a height of 70, while the 4500-element *no holes* poset has a height of 117.


(a) Mean height = 59.3
Standard Deviation = 14.38

(b) Mean height = 77.06
Standard Deviation = 9.24
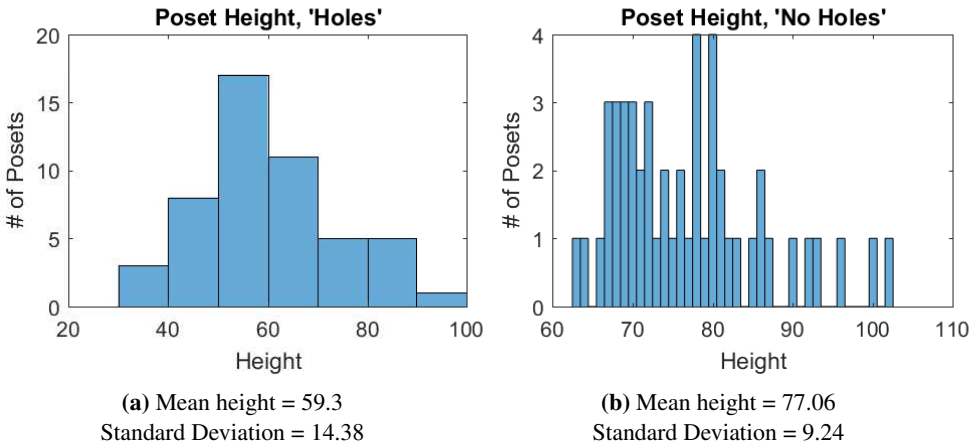
Figure 4.12: Height Distributions for 50 1800-Element Posets of each type

Additionally, the layer structure avoids the proportionality of KR orders, where roughly half of the events are distributed in the middle layer and the remaining half are roughly evenly distributed on the top and bottom layers, an optimistic result for the coarse-graining analysis that follows in the next section. Figure 4.14 provides a visual depiction of the level structure of each type of poset. One curiosity that arises is


Figure 4.13: An order where the number of levels is greater than its height.

that while the height of the *holes* poset is roughly equal to its number of levels, the number of levels in the *no holes* posets exceeds its height by nearly one order of magnitude. While this may be initially surprising, it becomes obvious if one considers the simple order depicted in Figure 4.13. It is plain to see that for any given order that is not an Alexandrov interval, there is a high probability that the number of levels will surpass the height of the poset, particularly as the kinematic complexity of the order increases. For an Alexandrov interval however, the number of levels is expected to be equal to the height plus one.[1]

---

[1]Mirsky's theorem states that the number of antichains that a given finite poset can be partitioned into is always greater than or equal to the height. One formulation of Mirsky's theorem states that a finite poset can always be partitioned into a number of antichains exactly equal to the height. However, layering requires each element of a given antichain to have the same distance from a common root element, so there is no guarantee that the number of a poset's layers will be equal to its height if an extremal event in the set is chosen.
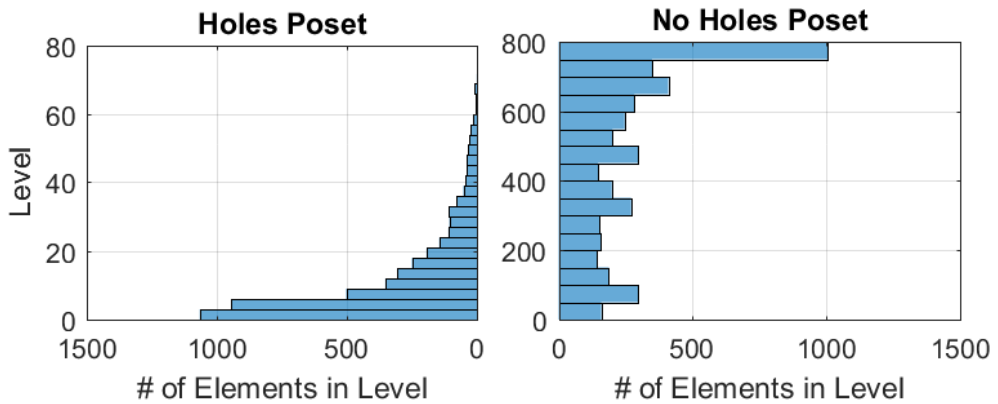
Figure 4.14: Level structure of both holes and no holes posets containing 4500 elements. Note the difference in scale between the two histograms. This reveals two interesting results: 1) the number of levels in a poset is not necessarily equal to its height and 2) the kinematic properties of the no holes posets leads to a greater degree of complexity reflected by the number of layers. Note: the direction of the levels has no significance in these figures and is a remnant of the plotting function used to create them. In general, both types of posets have monotonically decreasing cardinality as the level increases.

Upon promoting the open sets to subintervals of a closed set, the *holes* posets spontaneously exhibit 4-,5-, and 6-dimensional ordering fractions, while the *no holes* posets retain the 2- dimensionality of their constituent infrared orders. It must be critically noted that the former posets have significantly higher extrema-to-cardinality ratios than the latter, where on average roughly 25% of the elements in a *holes* poset are extremal, compared with 2.5% for the *no holes* posets. Figure 4.15 on Page 75 indicates the ordering fractions of each type of poset, alongside the ratio of extremal events. Nonetheless, taking into consideration Equation (3.18) provides a negligible margin of error that does not change the integer dimensionality of the sets, and these results are taken to be reliable indicators of dimensionality for the 1800-element sets *only*.

The larger 4500-element posets are consistent with the results found for the smaller posets. The 4500-element *holes* poset has an ordering fraction of 0.018, corresponding to roughly 6 Minkowski dimensions, a result that is approximately 1.5 standard deviations from the mean ordering fraction of the smaller posets. The 4500-element *no holes* poset has an ordering fraction of 0.615, corresponding to roughly 2 Minkowski dimensions, a result that is within less than one standard deviation from the mean ordering fraction of the smaller posets. However, the midpoint scaling approach provides an estimated dimension of 7 for the *holes* posets and an estimated dimension of 2 for the *no holes* posets.[2]

Recall that the Feynman posets were defined as having vertices with a *maximum* degeneracy of 3. If one imposes the stronger condition that the vertices must have a degeneracy *exactly equal* to three, then only the *holes* posets fit this condition, as *at least* 1.8% of the *no holes* poset's vertices are found to be two-degenerate, while 100% of the vertices

---

[2]See the caption for Table 4.1 for a disclaimer for this result.
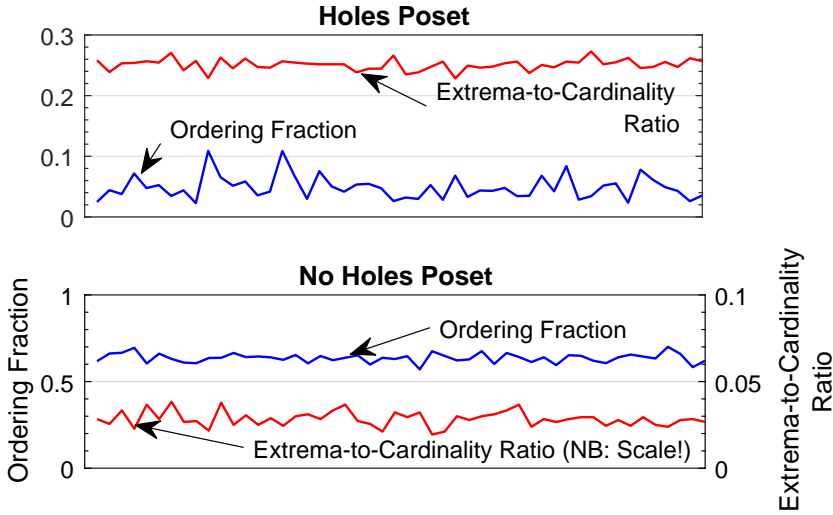
Figure 4.15: Ordering Fraction and Extrema-to-Cardinality Ratio for 50 1800-Element Holes and No Holes Posets. The mean ordering fraction is 0.0484 ± 0.0196 for the holes posets and 0.6362 ± 0.0267 for the no holes posets.

of a *holes* poset's vertices are exactly three-degenerate.[3] In fact, it is natural to conjecture that there can exist no *no holes* posets where 100% of the the vertices are exactly three-degenerate.

The vertices of the *holes* posets are diverse, and may contain both "Y"-shaped vertices and "fork"-shaped vertices (c.f. Figures 3.1 and 3.2 on Page 51), but in general, roughly 25% of the poset's vertices are "fork"-shaped, while the remaining are "Y"-shaped. As indicated by Figure 4.16, there exists no relationship between the ordering fraction and the proportion of vertex type. Similar null results are confirmed for the prospective relationship between height and proportion of vertex type.

Before turning to d-rigidity and coarse-graining, it is worth summarizing the findings thus far. Table 4.1 gives an overview of the dimension estimators and heights for both of the 4500-element posets constructed.

To determine the d-rigidity of the posets, the closed form expressions of $\langle N_m^d \rangle$ provided in [25] will be qualitatively compared with the interval abundance curves found for the larger posets constructed in this project. The expectation value for the abundance of m-inclusive intervals in a d-dimensional poset containing N elements is given by

$$\langle N_m^d \rangle (N) = \frac{N^{m+2}}{(m+2)!} \frac{\Gamma(d)^2}{(\frac{d}{2}(m+1)+1)_{d-1}} \frac{1}{(\frac{d}{2}m+1)_{d-1}}$$

$$\times \, _dF_d \left(\begin{matrix} 1+m, \, \frac{2}{d}+m, \, \frac{4}{d}+m, \, \ldots, \, \frac{2(d-1)}{d}+m \\ 3+m, \, \frac{2}{d}+m+2, \, \frac{4}{d}+m+2, \, \ldots, \, \frac{2(d-1)}{d}+m+2 \end{matrix} \, \middle| -N \right) \quad (4.1)$$

---

[3]One exception persists among all 50 *holes* posets constructed, where exactly one vertex is two-degenerate and all others are three-degenerate, but this will be considered to be an extreme outlier and neglected in the analysis.

where $(a)_d$ is the Pochhammer symbol and $_dF_d$ is the generalized hypergeometric function (see [25]).

Vertex Type vs. Ordering Fraction For 50 1800-Element 'Holes' Posets
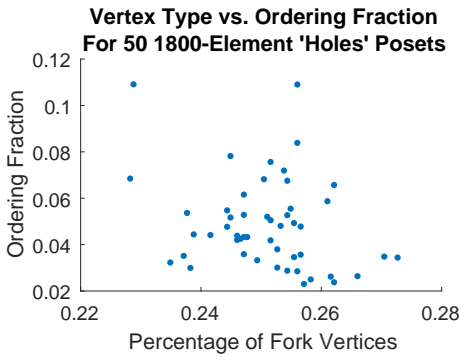
Figure 4.16: Percentage of vertices that are fork-shaped versus ordering fraction for 50 1800-Element Holes posets.

Figures 4.17 and 4.18 on Page 77 give the simulated interval abundance curves for the *holes* and *no holes* posets respectively, along with the analytic characteristic curves given by Equation (4.1) for $d = 2, 3, ..., 5$. These figures include the data for the poset in its *entirety* and amounts to a test for *strong d-rigidity*. To test for *weak d-rigidity*, a selection of the poset's largest subintervals were isolated and the abundance of m inclusive intervals within each of these subintervals have been compared with the characteristic curves given by Equation (4.1). Figures 4.19 and 4.20 on Page 78 give the results of this computation. As Equation (4.1) is a function of volume, only those subintervals with volume $N \geq N_{\max} - \sqrt{N_{\max}}$, where $N_{\max}$ is the volume of the set's largest subinterval were sampled and plotted. The solid lines represent the *mean* abundance of m inclusive intervals across all sampled subintervals, while the shaded region is defined by the minimum and maximum interval abundance for the sampled subintervals. Moreover, the posets were not partitioned according to their Myrheim dimensions, although Figure 4.7 on Page 69 indicates that the largest intervals in the holes posets are typically one or two dimensional, while those of the no holes posets are almost certainly two dimensional.

Dimension Estimators and Height for Each 4500-Element Poset					
Type of Poset	Ordering Fraction	Margin of Error	Myrheim Dimension	Midpoint Scaling Dimension	Height
Holes	0.018	$\pm 1.98 \times 10^{-3}$	6	7.05	70
No Holes	0.615	± 0.012	2	>1.66*	117

Table 4.1: Summary of results for dimension estimators and height for both 4500-element posets before coarse-graining. The Myrheim dimension has been rounded to the next nearest whole number.
*The midpoint scaling dimension estimator is not available at the time of writing, as simulations are still in progress. Intermediate results give $N_2 \leq 1425$, with a volume difference of $N_1 - N_2 = 658$, implying that the midpoint dimension is *at least* 1.66. Results given in Table 4.2 on Page 84 corroborate the conjecture that the midpoint dimension ≈ 2 with no coarse-graining. This preliminary results reflects the midpoints between in the top 14% largest intervals in the set and all other smaller intervals.
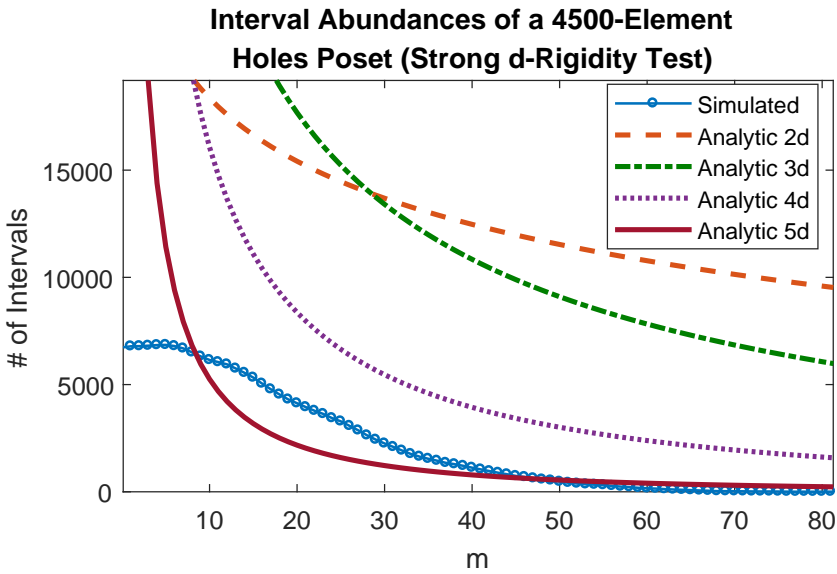
Figure 4.17: Interval abundance curves for a holes poset compared with the expectation value for characteristic curves for $d = 2, ..., 5$.
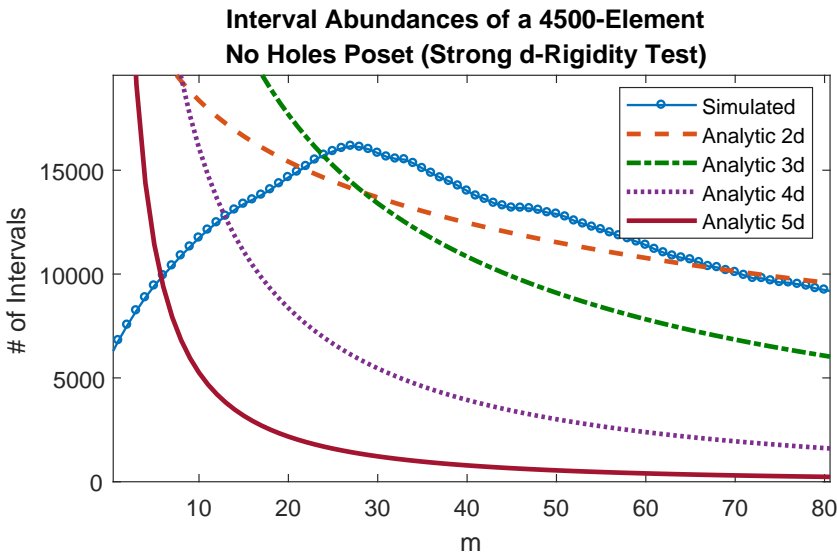

Figure 4.18: Interval abundance curves for a no holes poset compared with the expectation value for characteristic curves for $d = 2, ..., 5$.
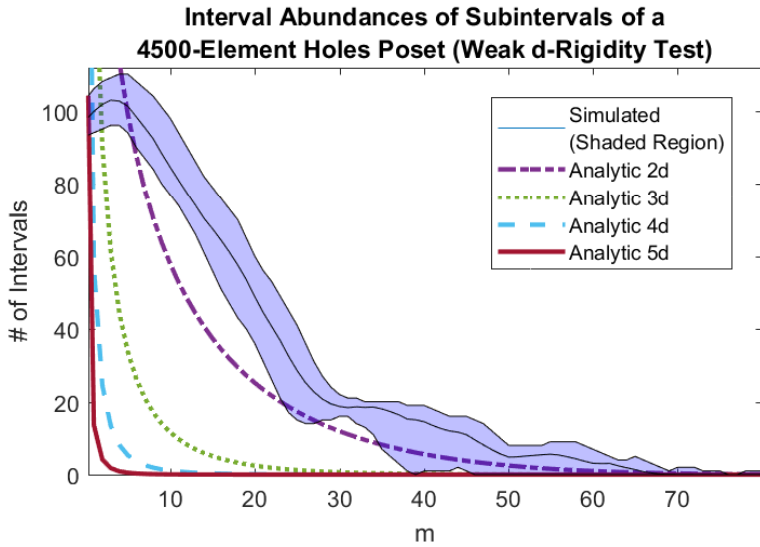
Figure 4.19: Interval abundance curves for a *sampling* of a 4500-element poset's largest subintervals. The shaded regions indicate the minimum and maximum number of subintervals at each value of m for a sampling of the *holes* poset's largest intervals. Each sampled interval contains approximately 90 elements.
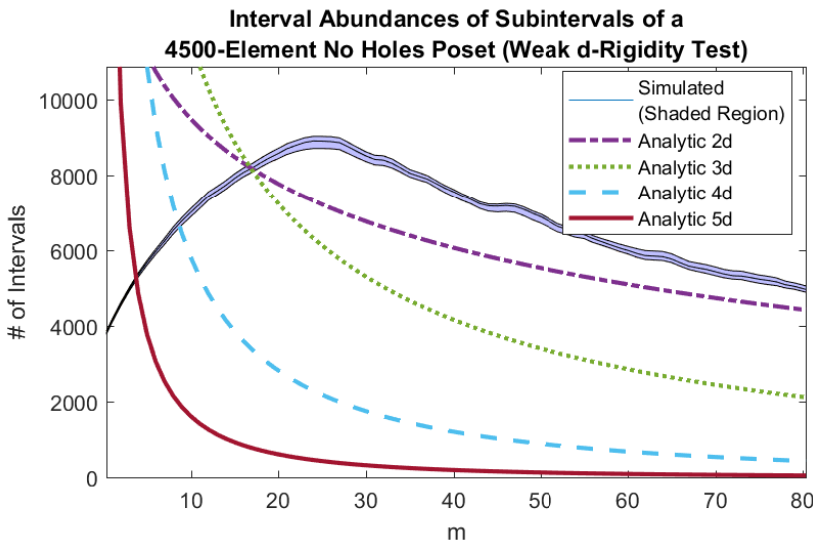

Figure 4.20: Interval abundance curves for a *sampling* of a 4500-element *no holes* poset's largest subintervals. The shaded regions indicate the minimum and maximum number of subintervals at each value of m for a sampling of the poset's largest intervals. Each sampled interval contains approximately 2660 elements.

4.1.3 Coarse-Graining

In Section 4.1.1, a potential relationship between interval volume and ordering fraction was explored with null results. Despite the suggestive appearance of Figures 4.7, no curve fitting on the data points (c.f. Figures 4.8 and 4.9 on Page 70) revealed convergence to a nonzero value of the ordering fraction. Figure 4.21 shows the results of this comparison for the 4500-element *no holes* poset after coarse-graining, where the volume has been scaled by the coarse-graining parameter. Note moreover that the density of data points has increased, as the entirety of the coarse-graining's intervals were measured rather than a representative sample to ensure accurate results. A curve was fitted to the data points (excluding intervals with an ordering fraction of identically 1 to avoid ultraviolet errors) and indicates a convergence to $f \approx 0.57$ in the limit of infinite volume, reinforcing the original conjecture that this subclass of Feynman posets demonstrates a relationship between interval volume and ordering fraction.
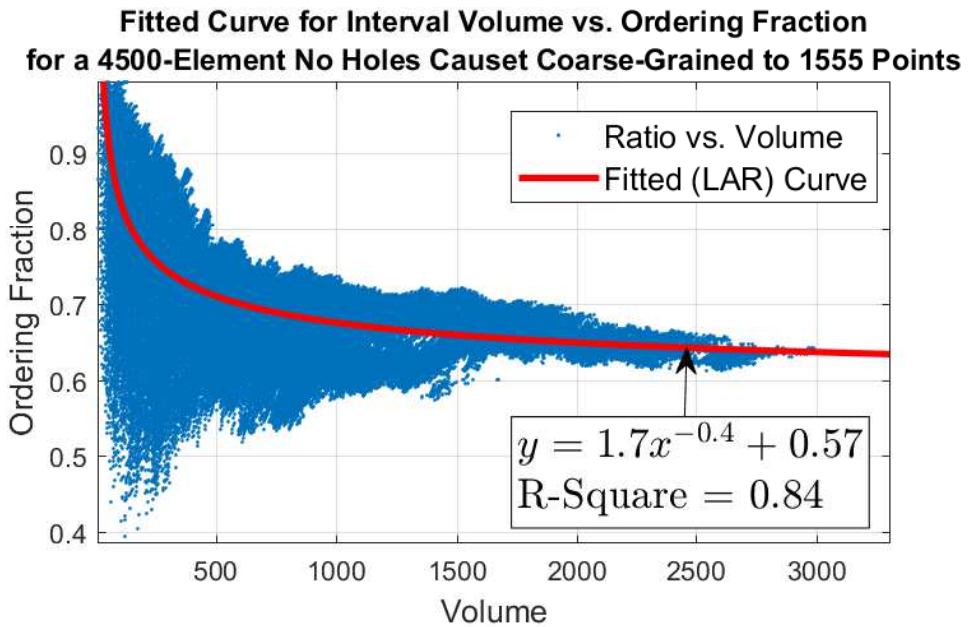
Figure 4.21: Fitted curve on the scatterplot of the interval volume and ordering fraction for the 4500-element no holes poset, now *including* data points from post-coarse-graining

To understand the prospective transition behavior of each poset, the total ordering fraction and heights of the posets were measured at each stage of coarse-graining. In Figure 4.22, the height of each type of poset is plotted against the coarse-graining level, while Figures 4.23 plot the total ordering fraction of each type of poset against coarse-graining along with the proportion of extremal events in the set. Figure 4.25 gives the approximate level structure for each type of poset after the last coarse-graining.

Each of the five coarse-grainings of both posets were tested for weak and strong d-rigidity. As the last coarse-graining containing roughly 33% of the posets' original
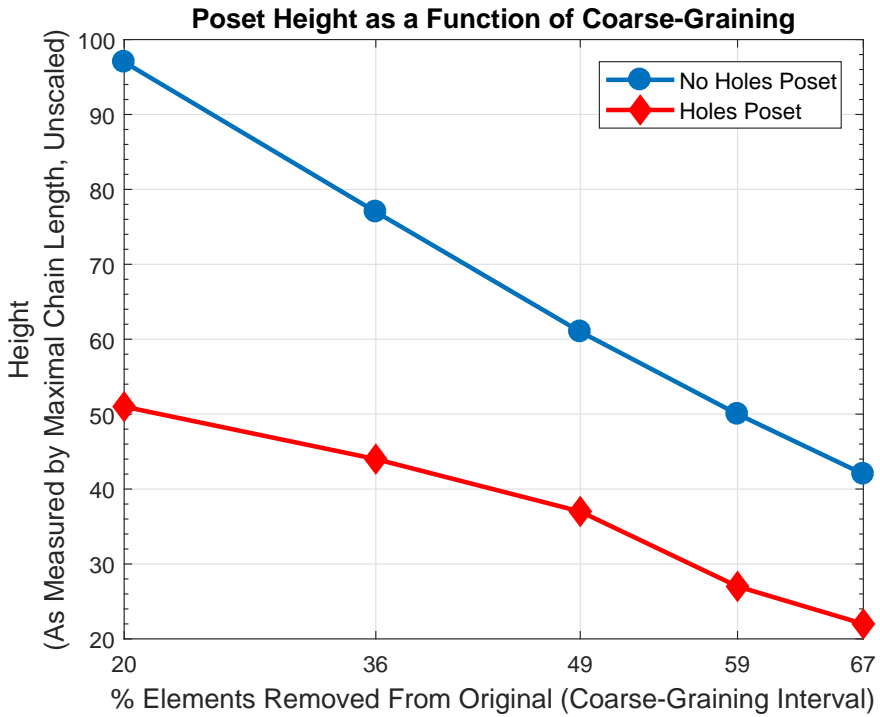
Figure 4.22: Change in the height of each type of poset as a function of coarse-graining.
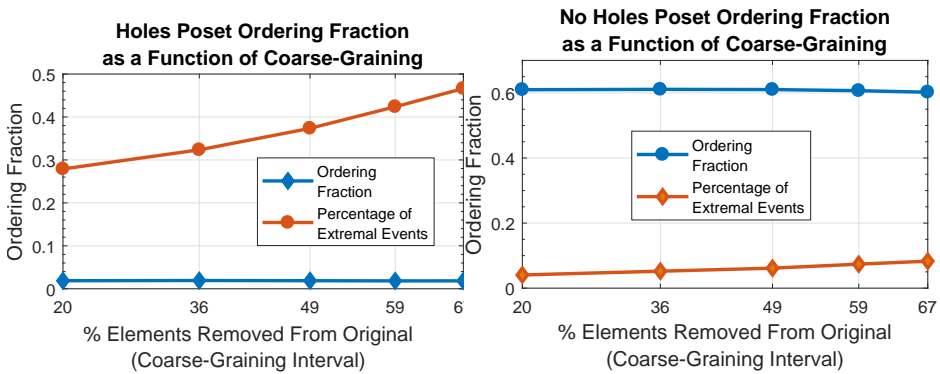
**(a)** Change in ordering fraction of holes posets   **(b)** Change in ordering fraction of no holes posets

Figure 4.23: Change in the ordering fraction of each type of poset as a function of coarse-graining, including the extrema-to-cardinality ratio of each corresponding poset.

elements gives the best continuum-limit approximation, the results from the other four coarse-grainings will be provided in Appendix B. Figures 4.26 and 4.27 on Page 82 give the characteristic curves for the *entire* coarse-graining's interval abundances (strong d-rigidity), while Figures 4.28 and 4.29 on Page 83 give the characteristic curves for the coarse-graining's largest subintervals (weak d-rigidity).
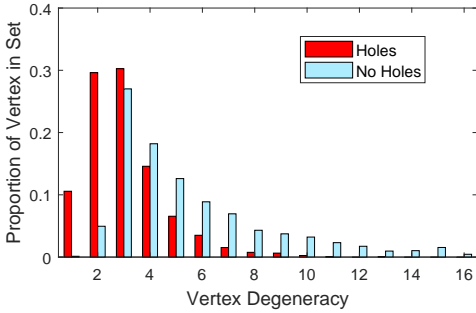

Figure 4.24: Distribution of vertex degeneracy for each 4500-element poset after coarse-graining.

Of particular interest in this part of the project is whether or not the sets maintain their causal structure after this relatively modest coarse-graining. As the results of this section indicate, coarse-graining has little influence on the ordering fractions and level structure of the posets and each coarse-graining can be said to represent the causal structure of its smaller counterparts.

Nonetheless, each coarse-graining exhibits fairly strong changes to its kinematic properties. While the original sets admitted 3-degenerate vertices, the coarse-grained *holes* posets contain up to 13-degenerate vertices, while the *no holes* posets contain up to 35-degenerate vertices. Figure 4.24 shows the distribution of n-degenerate vertices for each of the types of posets at the highest level of coarse-graining (limited to 16-degeneracy for clarity; the incidence falls off rapidly beyond this point).
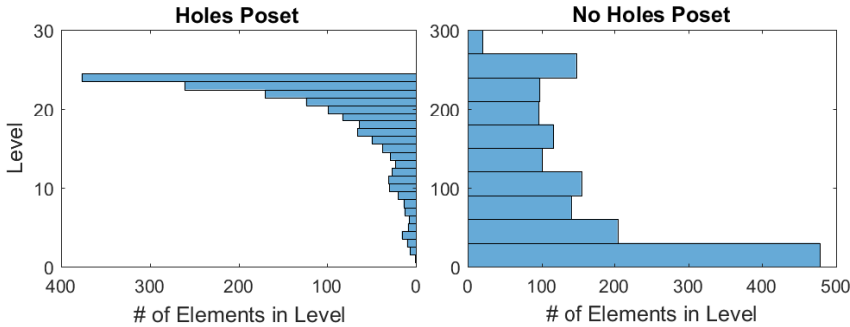
Figure 4.25: Histograms giving the level distribution of both types of posets after the last coarse-graining. Note: the direction of the levels has no significance in these figures and is a remnant of the plotting function used to create them. In general, both types of posets have monotonically decreasing cardinality as the level increases.

**Interval Abundances for the Entirety of a 4500-Element
Holes Poset (Coarse-Grained to 1570 Points)**
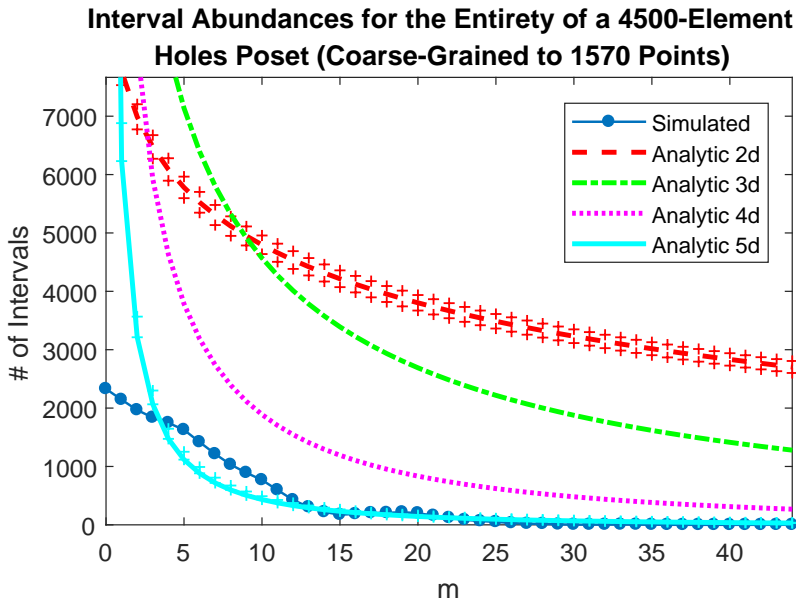
Figure 4.26: Interval abundance curves for the *entirety* of coarse-graining of a 4500-element holes poset containing roughly one-third of its original points. This amounts to a test for *strong d*-rigidity.

**Interval Abundances for the Entirety of a 4500-Element
No Holes Poset (Coarse-Grained to 1555 Points)**
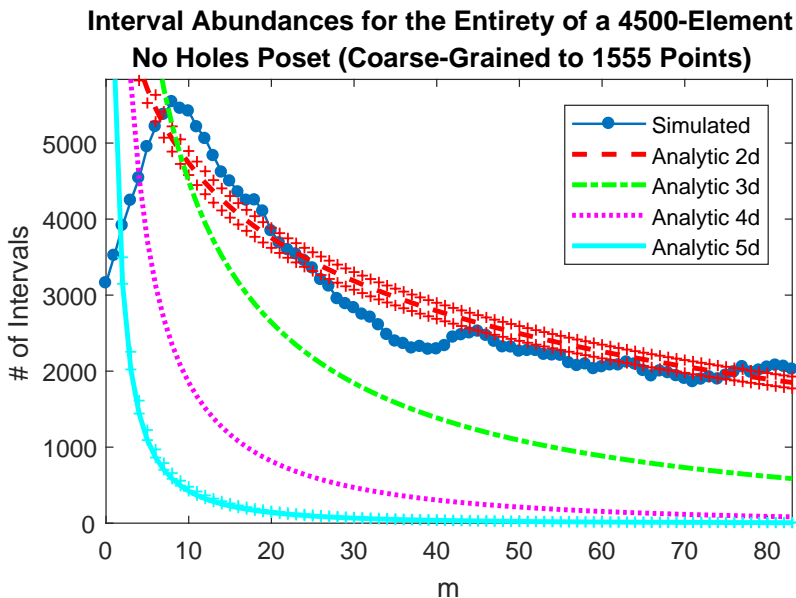
Figure 4.27: Interval abundance curves for the *entirety* of coarse-graining of a 4500-element no holes poset containing roughly one-third of its original points. This amounts to a test for *strong d*-rigidity.

Interval Abundances for Largest Subintervals of a 4500-Element Holes Poset (Coarse-Grained to 1570 Points)
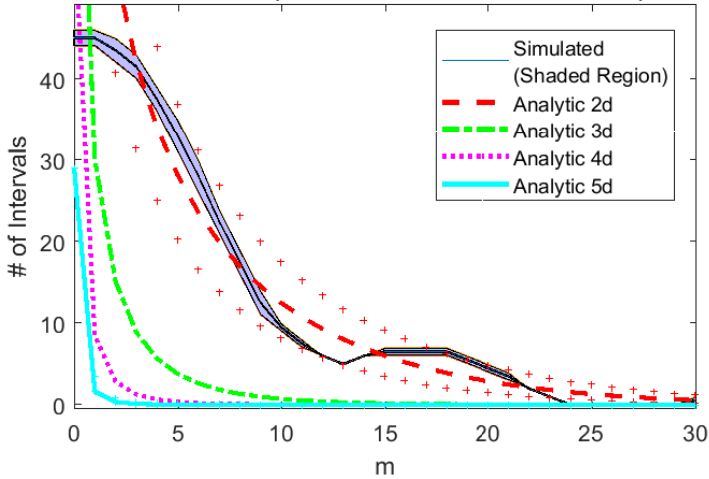
Figure 4.28: Interval abundance curves for the *sampling of subintervals* of coarse-graining of a 4500-element holes poset containing roughly one-third of its original points. This amounts to a test for *weak d*-rigidity.

Interval Abundances for Largest Subintervals of a 4500-Element No Holes Poset (Coarse-Grained to 1555 Points)
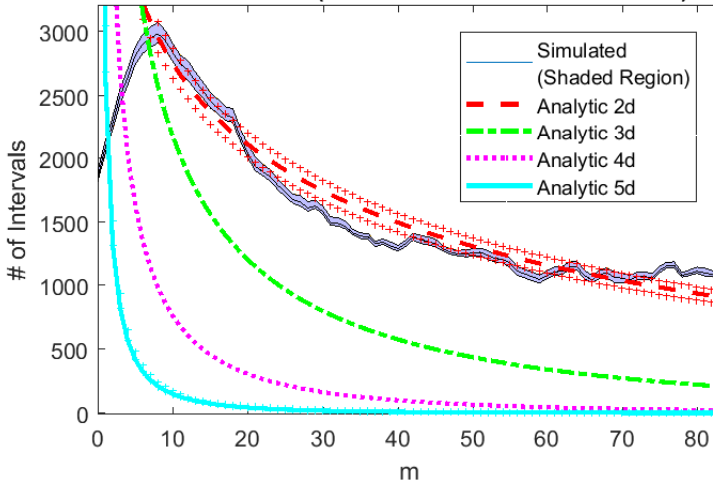
Figure 4.29: Interval abundance curves for the *sampling of subintervals* of coarse-graining of a 4500-element no holes poset containing roughly one-third of its original points. This amounts to a test for *weak d*-rigidity.

Finally, Table 4.2 gives an overview of the results found for the coarse-graining of each type of poset for the dimension estimators and height. Note that the height has not been scaled according to the coarse-graining parameter. The resulting heights will not be explicitly scaled in this document, but it is easy to see that each height in the table is roughly equal to the original height before coarse graining multiplied by the percentage of elements that were removed from the original set. This is an important measure for ensuring that coarse-graining does not drastically alter the causal structure of the posets.

Dimension Estimators and Height for Each 4500-Element Poset						
Poset Type	# Original Elements	Ordering Fraction	Margin of Error	Myrheim Dimension	Midpoint Dimension	Height
Holes	3624	0.0187	$\pm 2.2 \times 10^{-3}$	6	7.18	51
	2992	0.0192	$\pm 2.5 \times 10^{-3}$	6	7.09	44
	2412	0.0188	$\pm 2.8 \times 10^{-3}$	6	6.84	37
	1930	0.0184	$\pm 2.6 \times 10^{-3}$	6	6.59	27
	1570	0.0184	$\pm 3.2 \times 10^{-3}$	6	6.35	22
No Holes	3650	0.61	$\pm 1.2 \times 10^{-2}$	2	N/A*	97
	2955	0.611	$\pm 1.5 \times 10^{-2}$	2	1.97	77
	2360	0.614	$\pm 1.8 \times 10^{-2}$	2	1.97	61
	1911	0.607	$\pm 2.1 \times 10^{-2}$	2	1.97	50
	1555	0.602	$\pm 2.4 \times 10^{-2}$	2	1.98	42

Table 4.2: Summary of results for dimension estimators and height for both 4500-element posets at each level of coarse-graining. The Myrheim dimensions have been rounded to the next nearest whole number.

As in Table 4.1, the midpoint scaling dimension estimator is not available at the time of writing for this coarse-graining, as simulations are still in progress. Unfortunately, intermediate results are not available for this coarse-graining. This author suggests that the estimated dimension ≈ 2 for the missing data, as it would be rather surprising to find the most mild coarse-graining dimension to differ drastically from both the non-coarse-grained dimension *and* higher levels of coarse-graining.

4.2 Quasi-Quantum Model

As alluded to previously, the action-minimizing growth model did not produce appropriate posets. However, the resulting sets offer theoretic insights as to why this occurs, and the resulting posets are illustrated in the following pages in order to motivate the discussion in the next chapter. Figure 4.30 illustrates the graphs (NB: these are not Hasse diagrams, as they have not been topologically sorted, and therefore not ordered by levels) for the one of the posets created at varying values for $\beta = 1.4$. The other posets are similar to the one illustrated by Figure 4.30, but are not included in this document for space considerations. The key difference between Figure 4.30 and the remaining graphs is that they tend to have a larger number of disconnected singleton subsets.
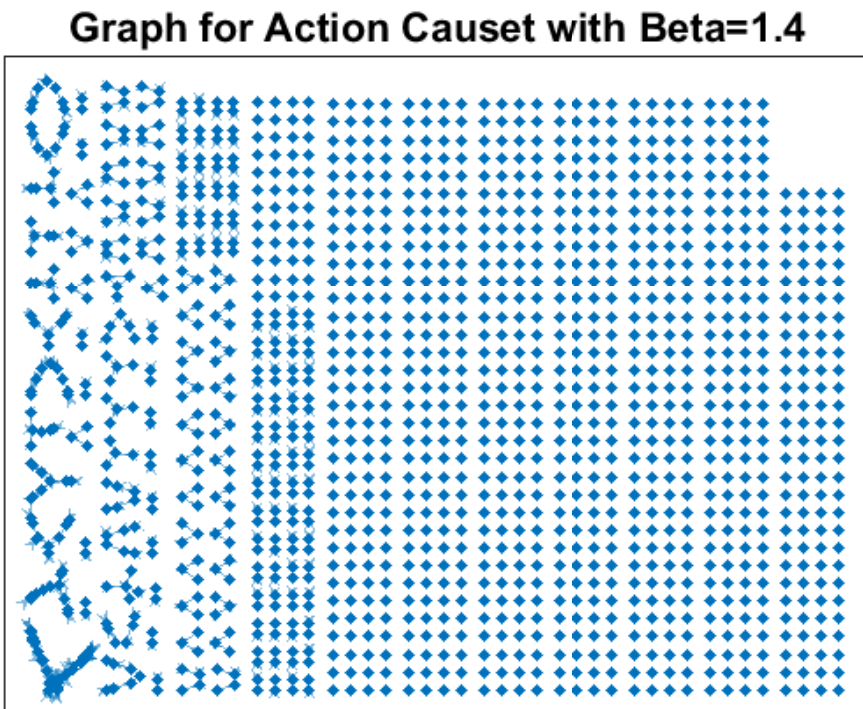
Figure 4.30: Graph for the poset constructed using the action principle with a thermalization temperature $\beta = 1.4$

Although the causet does not technically include the multitude of disconnected, singleton subsets, they have been included in this figure to illustrate the scope of the problem: namely, very few of the "external" elements are ever connected to the complete causet. For this reason, this document will eschew a more in-depth analysis of the causets until further improvements to the growth model have been made during future studies.

It must be emphasized that with the assumptions made in Chapter 3, there is no reason these sets cannot be understood as causets. After all, if the singleton subsets are simply understood as events that "do not exist" with respect to the resulting posets, the union of the remaining disconnected posets can easily be conceptualized as a subinterval of a larger interval. These sets are not rejected because they are "too non-manifoldlike". The small cardinality is not a reflection of their non-manifoldlikeness, but rather a reflection of the failure of the growth model at its present stage to construct posets. Although one could conceivably perform an analysis of the manifoldlikeness of these sets, they are rejected because they are unlikely to have been constructed with the particular kinematic and dynamic restrictions that this author had in mind when initializing the study, and this should not be understood as a statement of the physics behind them.

The Hasse diagram for the set with the largest cardinality of disconnected non-singleton subsets was found at $\beta = 1.4$ and its Hasse diagram is given in Figure 4.31.
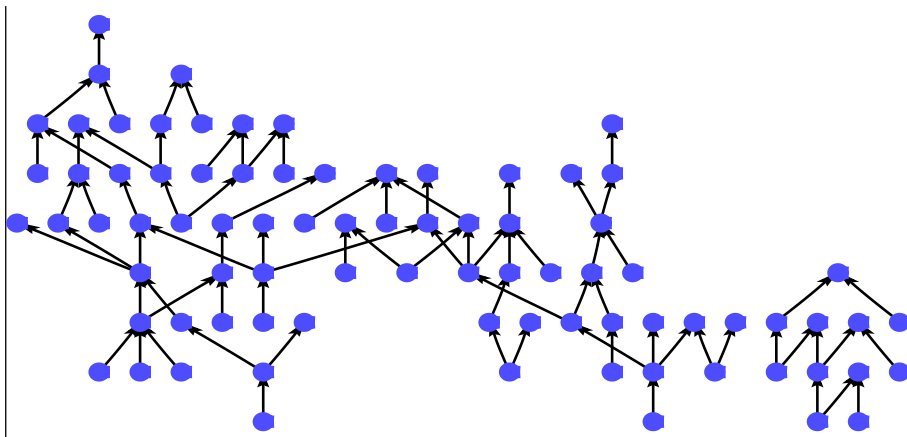

Figure 4.31: Hasse diagram for the resulting poset constructed with the action at a thermalization temperature of $\beta = 1.4$. Note that only those subsets containing at least 10 elements were included in this figure. The subset on the left-hand side contains 70 elements, while the subset on the right-hand side contains 11 elements.

5

Discussion and Analysis

Although this document has alluded to several measures that serve as partial indicators of the manifoldlikeness of the sets created, no definitive tests for manifoldlikeness have been offered thus far. The reason for this is twofold. The first is that many of the indicators were unknown to the author at the time of writing, and have therefore not been explored due to time limitations. The second is that in truth, the subject of "measuring" a poset's manifoldlikeness by reference to measurements within the causet remains a work in progress in the field, and the available tests are subject to severe limitations, both in their range of application and the accessibility of their use.

Section 5.1 will explore this issue closer and offer a preliminary analysis of the manifoldlikeness of the posets created in this project. Moreover, this section will deal with some other kinematic considerations of the poset not related to manifoldlikeness–simple observations of the structure and properties of the sets in their own right.

Section 5.2 offers a critical review of the methodology of this project, including both the guiding principles, as well as the technical details of numerical simulations. Section 5.3 outlines the future direction of this work, including work in progress and planned research in the near future.

5.1   Resulting Posets

5.1.1   Manifoldlikeness of Feynman Posets

Before we consider the battery of tests that have been (partially) developed for determining the manifoldlikeness of the poset, let's take a moment to consider what it means for a causet $\mathcal{C}$ to be "manifoldlike". Recall that if some causet $(\mathcal{C}, \prec)$ is approximated by the manifold $(\mathcal{M}, g)$, then the embedding of $\mathcal{C}$ is a high probability Poisson distribution in $\mathcal{M}$.

The most obvious solution is of course to try to make some hypothesis about the kind of manifold that $\mathcal{C}$ could be embedded into based on observations of the kinematic properties of $\mathcal{C}$, generate an ensemble of sprinklings from the respective $\mathcal{M}$, and determine whether or not the sprinkling and the causet are isometric. The computational machinery is already in place for such a strategy, as MatLab offers a efficient algorithm for doing so.

However, even with the most efficient algorithm, this approach would be extremely impractical; for a sufficiently large region of spacetime, there are countably infinite possible sprinklings, and only a handful of these may be isomorphic to the causet it is being compared to. Taken from the other direction, another approach offered by Henson in [27] is to simply embed the causet in a small region of Minkowski spacetime, using the geometric information that has been defined in the set to induce a new partial order, $\mathcal{C}'$ (in a sense, it is a "reverse sprinkling"). Calculating the proportion of relations in $\mathcal{C}$ that are "lost" in $\mathcal{C}'$ provides a test for the manifoldlikeness of $\mathcal{C}$. While this process can be generalized to n dimensions and arbitrary curvature, it has only been performed for flat 2D spacetime, and generalizing to arbitrary spacetimes is rather complicated. A contender for this test might be found in the *no holes* posets, which are highly likely to be embeddable in 2D Minkowski spacetime, but this exploration will be left for future studies.

A less direct and less reliable approach is afforded by the notion of "self-similarity", or scale invariant properties of the manifold that may be observed in a manifoldlike causet. Major, et. al. have developed a method of recovering the topology from a causal set with reference to higher-level structures–the homology groups of the causet, although this method is beyond the scope of this project (the reader can find more information about this test for manifoldlikeness in [36, 35]). A more minimalistic but highly selective approach in the same direction has been recently explored by Aghili, et. al., where properties of the chain length distribution within the causet as a function of causet cardinality form a parameter that exclude the most non-manifoldlike causets in the continuum limit [1].

Conversely, the implicit measures that have been used throughout this project (agreement of dimension estimators, d-rigidity, etc.) offer a test for *non-manifoldlikeness*. The strongest statement that can be made about this class of causets is that they are *likely* to be embeddable in the manifold (note that almost all causets immediately pass these "non-manifoldlikeness" tests, so this result is by no means trivial). Henson argues in [28] that these collective conditions "might yield a necessary and sufficient condition [for manifoldlikeness]." A weaker, yet more appropriate claim is that almost all of the *no holes* posets are not prohibited from manifoldlikeness, while the *holes* poset may not be manifoldlike, although there may prove to be exceptions for other posets in the same class.

This author concludes with a high level of confidence that the *no holes* posets are likely to be embeddable in flat 2D spacetime after coarse-graining and quite possibly in 2D curved spacetime as well. First, they avoid the entropic space of infrared orders. Second, dimension estimators agree at all levels of coarse-graining within integer rounding. Third, their interval abundance curves are in close agreement with the characteristic curves for flat and curved 2D spacetime, although weak d-rigidity is likely to be an unreliable indicator. Additionally, as the level of coarse-graining increases, the interval abundance curves come into closer agreement.

A weaker case is made for the manifoldlikeness of the *holes* posets. Unfortunately, due to time constraints, only one poset containing 4500 elements was constructed from

the *holes* posets. For this set, the dimension estimators did *not* agree at smaller scales. While the poset had a constant Myrheim dimension of 6 at all levels of coarse-graining, its midpoint scaling estimated dimension fluctated between 6 and 7. Despite promising ultraviolet-level agreement in the interval abundance curves for the *holes* posets, the effects of coarse-graining do not place the curves significantly closer to agreement with the characteristic curves for flat 6D spacetime (not illustrated due to graphical complications). However, even at this very modest coarse-graining parameter, the *holes* posets have interval abundance curves that are in perfect agreement with the characteristic curves for curved 2D spacetime at all levels of coarse-graining. At the time of writing, this author can offer no insights into the physical implications this has for the subclass of *holes* posets, save that these inconsistencies reveal non-manifoldlikeness for this particular poset. It may be argued that the disagreement between strong and weak d-rigidity should be discarded as an indicator for non-manifoldlikeness, as weak d-rigidity is unlikely to be a reliable indicator.

Since this subclass offers such a wide diversity of estimated topological properties, further study is needed. An improved action principle, either applied to a stochastic growth model or a Monte-Carlo simulation will most certainly reveal more conclusive results about the nature of the type of events that make up the *holes* poset. It is also possible that the open interval approximation of a closed interval has introduced errors that affect dimension estimator agreement. However, the margin of error is greatest at the smaller scales where the disagreement is the most acute, and the computations provided by Equation (3.18) cross referenced with Table 4.2 do not support this conjecture.

For both types of events, even the most rigorous coarse-graining undertaken in this project produces causets on the scale of 10^4 Planck volumes. This author conjectures that simulations involving larger posets will a) verify the manifoldlikeness of the *no holes* posets more rigorously and b) shed light on the mercurial behavior of the *holes* posets. Such a study will also allow us to more concretely answer questions about the continuum limit of each type of poset.

5.1.2   Effects of Coarse-Graining

As indicated previously, coarse-graining on the posets maintained the causal structure to a large degree, but changed the kinematic properties of the set quite considerably, with drastic effects for the vertex degeneracy of the posets. Each coarse-graining of the causet $\mathcal{C}$ can be viewed as a new and unique causet $\mathcal{C}'$, even when the causal structure is shown to be scale-invariant. The dimensionality, level structure, and even subinterval statistics remain invariant throughout each coarse-graining with nearly negligible variation, and yet, after coarse-graining, the posets are not, by definition, of the same class as when they started (the class of Feynman posets).

This phenomenon is easily explained in the context of the *Hauptvermutung* of causal set theory. Recall that the goal is to produce a partially ordered set that can be embedded in a manifoldlike region of spacetime. If the partially ordered set is a closed Alexandrov interval and is manifoldlike, its embedding in the spacetime manifold places its elements within the intersection of the past and future light cones of the maximal and minimal events in the Alexandrov interval, respectively, according to a Poisson distribution with the hypersurfaces of the resulting region determined by the topology of that manifold. Yet, if causal set events are Planckian, then surely the causet is bound to contain "redundant"

information that is not observed at the macroscopic continuum limit. Spacetime is conjectured to be an *approximation* of the causal set, and a coarse-graining that approaches the continuum scale will therefore be a causal set whose elements may in turn be causal sets in their own right with massive cardinality. That the vertex degeneracy increases is simply a reflection of the degree to which the coarse-grained sets are approximations of their smaller-scale constituents, and ultimately that the continuous manifold is an approximation of the discrete causal set.

Incidentally, the preservation of other causet properties after coarse-graining provides a partial indication of manifoldlikeness, as discussed in the preceding section. Consider the interval abundance curves in Appendices B.3.1 and B.3.2 beginning on Page 113. For the *no holes* poset, as the coarse-graining increases, the curves fall into greater agreement with the corresponding analytic curves for the dimension of the manifold that the causet is conjectured to be approximated by.

Moreover, Figures 4.23 on Page 80 show that the Myrheim dimension is scale invariant under coarse-graining, another indication that the coarse-graining has appropriately preserved causal structure. On the other hand, Figure 4.23a may foreshadow a potential barrier to these results for the *holes* posets if simulations are carried out for larger intervals and larger coarse-graining parameters. Unlike the *no holes* poset, the percentage of extremal events in the coarse-graining appear to increase rapidly, leading to larger error margins for the ordering fraction approximation offered by Equation (3.18). For an extrema proportion of $\alpha = 0.5$, there is a 28% margin of error in the ordering fraction. For $f \approx 0.02$, the ordering fraction of a typical *holes* poset, this is threateningly close to changing the integer dimensionality of the poset. On the other hand, while $f \approx 0.02$ corresponds with a Minkowski dimension of 6, at higher coarse-grainings, the margin of error includes a range of ordering fractions corresponding with 5 Minkowski dimensions, an optimistic sign given the context of Figure 4.18 on Page 77, where the interval abundance curve is closest to that of the characteristic curve for 5D spacetime.

Yet, the agreement of individual dimension estimators at different coarse-grainings is not the condition for manifoldlikeness (rather, it is only evidence that coarse-graining has not changed the causal structure); as suggested by Rideout in [46], the variance of causet dimension may prove to be a manifoldlike property after all. It is the agreement of *different* dimension estimators that serves as the condition.

In summary, the *no holes* poset do not only meet the dimension estimator condition for manifoldlikeness, but also feature invariant dimensionality across coarse-grainings, suggesting that the causal structure of the manifold that the *no holes* posets are approximated have comparable topologies at both the discrete and continuum levels. On the other hand, the *holes* posets do not meet either of these conditions; results remain inconclusive until a study of closed intervals is undertaken.

On a final note, this author speculates that the topological behavior of the *no holes* posets under coarse-graining suggests that the causal structure for the manifold that approximates these types of posets is *scale invariant*. In other words, it is possible that this particular manifold (assuming the poset is in fact embeddable) at the continuum limit is perhaps topologically indistinguishable from its discrete limit. More rigorous coarse-graining should be carried out to varify this conjecture.

5.1.3   Detailed Features of the Posets

In Section 4, it was conjectured that there may exist no *no holes* posets where all event vertices are exactly three-degenerate. This does not require a rigorous proof, as it can rather quickly be informally deduced with a simple drawing exercise. The reader is encouraged to try for themselves to verify this conjecture by trying to draw a *no holes* poset where each vertex is exactly three-degenerate (remember–the poset must respect the causal set axioms on Page 18–namely, there cannot be any closed loops!). It may perhaps be straightforward to prove this conjecture formally, but a proof will not be provided in this space.
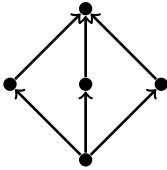

Figure 5.1: An immediate example of a closed interval containing fork-shaped vertices with an ordering fraction corresponding with 2 Myrheim dimensions.

However, a more frustrating phenomenon to explain has been the behavior of the "skinny orders" depicted on Pages 71 and 72 for the *holes* and *no holes* poset, respectively. Recall that if at any point in the analysis of the subintervals of each poset there existed a sufficiently large closed subinterval with an ordering fraction corresponding with two Myrheim dimensions, they were immediately isolated and stored as subgraphs. Figures 4.10 and 4.11 are the resulting Hasse diagrams from this analysis. Of note is that regardless of the allowed vertex degree of the overall poset, these special regions of the posets contain only *no holes*

type vertices. Even in the *holes* poset that admits "fork" shaped vertices, the two-dimensional subinterval that arises contains only "Y"-shaped vertices! The reader may at this point object that these subintervals are surely just one of a great multitude of two-dimensional subintervals that exist within any given poset and they would be correct! However, this behavior appears to be typical among all subintervals, although this author must concede that a rigorous analysis to this effect has not been carried out. The most obvious counter-example is offered by the union of a fork-shaped vertex with its time-symmetric counterpart, as illustrated in Figure 5.1. However, while it is the infrared behavior that is of interest in this exploration, this order is perhaps "too" infrared.

This author has been inclined to suggest that this behavior may speak to the fundamental kinematic properties of 2D Minkowski spacetime, although the discussion has been admittedly premature. The reader will be spared the lengthy foray into the tedious process of fitting these types of events into embeddings of 2D spacetime and the conclusion will simply be cited. Figure 5.2 gives an example of the sprinkling of 32 points in flat 2D Minkowski spacetime. The reader should not make the mistake (as this author has) of supposing that the discreteness implies that causal set events are necessarily quantized. The statistical geometry developed by Myrheim in [41] makes the following claims about the Hasse diagram that can be created from the events sprinkled in Figure 5.2. First, using Equation (2.15), which was given as

$$V = k^n N \tag{2.15}$$

it may be said that the volume of the region of spacetime that these points have been sprinkled into is *proportional* to $N = 32$, up to the discreteness scaling factor, k^2, *up to*

local fluctuations. Next, using Equation (2.17), which was given as

$$L = hk \tag{2.17}$$

it may be said that the length of the geodesic between the endpoints of this region of spacetime is *proportional* to $h = 8$, up to the discreteness scaling factor, k, *up to local fluctuations*.

Let's put a number to these fluctuations. The *Hauptvermutung* of causal set theory is that the appropriate causet may be embedded into the manifold according to a Poisson distribution. Thus, for $N = 32$ sprinkled points, the volume and proper length offered by Equations (2.15) and (2.17) hold with a relative error of

$$\eta = \frac{1}{\sqrt{N}} \tag{5.1}$$

i.e. if k is on the order of 1 Planck length, the causal set in Figure 5.2 describes a region of spacetime with a volume of 32 ± 5.5 squared Planck lengths where the proper length of the geodesic between its endpoints is 8 ± 1.5 Planck lengths. It is the statistical nature of discrete geometry that prohibits the tempting literalist approach to the interpretation of these "skinny orders" that this author has been inclined to undertake. It will not do to simply sprinkle points into the region "by hand" according to a continuum notion of
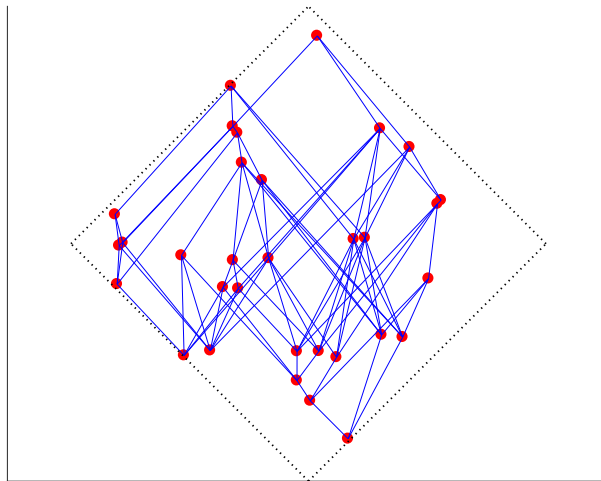

Figure 5.2: Example of a sprinkling of 32 points in flat 2D Minkowski spacetime. From this example, it can be seen that many sprinklings can describe the same causet. Suppose, e.g. the points were projected along two total orders on the u and v axes. As long as the *order* of the points along the axes do not change, we may make any arbitrary changes to their positions along the axes. The Hasse diagram from this sprinkling can then be constructed by maximizing the distance between the points along each of the two orders, and placing them back within the region. The result represents a unique sprinkling with the same causet, but the resulting Hasse diagram represents both sprinklings. This figure was produced with the code provided in Appendix C.3, courtesy of Jan Myrheim.

geometry, because distances are at this scale meaningless by construction. Thus, a closer examination of the "fundamental" nature of 2D Minkowski space as it relates to these skinny orders must await further exploration that treats the Planckian spacetime region statistically, rather than empirically.

Finally, consider the poset depicted in Figure 5.3. This is a *holes* poset whose vertices are all three-degenerate and which forms a closed interval. While much of the methodology and discussion has focused heavily on *ensuring* that the posets form closed intervals and this poset is at first glance rather appealing, it reveals a paradox if we are stringent in the original hypothesis that its elements are fundamental events defined by their vertex degeneracy. If the topology of the manifold region approximating this set truly arises from this fundamental event alone, then it must describe some region of spacetime that is *wholly inaccessible* and spacelike separated from any other region of spacetime, since one of the axioms of causal set theory states that the sets must be locally finite. This is not an entirely unsalvageable paradox, however.
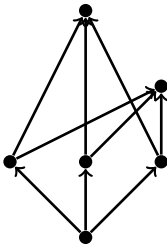

Figure 5.3: *Holes* poset containing only 3-degenerate vertices that forms a closed interval.

One possibility–the most likely explanation– is that three-degenerate vertices are not the only fundamental event types and that at the endpoints of this interval there exists some other (> 3)-degenerate event that "links" the two regions together. From this possibility arise several new interpretations. The first is that the cardinality of any given closed and "saturated" interval is proportional to the number of Planck volumes at the discreteness limit (although this immediately raises the question of quantifying the limit) and that the fundamental causal events are the building blocks of some larger building blocks that are in turn (> 3)-degenerate vertices. In other words, the proposition is that causet approaches the continuum limit precisely at the point that it becomes an "inaccessible" region. This would explain topology changes in coarse-grainings. Another closely related interpretation is that these closed intervals represent the faces of a higher dimensional object, a 2-complex, and that the fundamental units of causal set theory are in turn the building blocks of what other approaches to quantum gravity call fundamental (like loop quantum gravity–although now the topology change may be represented by these "connecting" special vertices rather than closed timelines, as proposed in loop quantum gravity). Henson offers an interpretation in this direction in [28], although sadly, this author is not well-versed in spin-foam theories or loop quantum gravity enough to push the correspondence between causal set theory and other approaches to quantum gravity any further at this stage. Entertaining this idea can easily constitute an entirely separate program of study.

Another possibility (and a personal favorite of the author) is that the the entire history of the universe *is* bounded by the volume of this (necessarily finite) interval. This is a cosmological model known as the *ekpyrotic universe* that is finite in temporal and spatial extent and perhaps cyclic. This is similar to the conclusion reached by Rideout and Sorkin in [47] for the causets constructed with their transitive percolation growth model. If these

closed intervals have a cosmological explanation, one could no longer ignore the effects of Λ in the Einstein field equations or the Einstein-Hilbert action as it was done in this treatment, and the growth model would have to be revisited with a renewed kinematic rigor.

This is a by no means exhaustive enumeration of possible interpretations. The most obvious alternative is that three-degenerate events are not the only building blocks of geometry or perhaps that vertex degeneracy is not a fundamental property of causal events at all. While this is certainly the most important interpretation, there is not enough information on the topic in the literature to answer this question at this stage. This document represents only a small sliver of the work that is needed to conclude this prospect.

5.2 Critical Review of Methodology

In this section, I offer an overview of the most urgent shortcomings of this project and a few ideas on how to improve the methodology for future studies. The first concerns the theoretic justification for the methodology; these are observations of how several tools, although sound, have been used less than optimally. It reflects a renewed understanding of the Benincasa-Dowker action and Glaser and Surya's tests for locality for this author and constructive ways in which this hindsight can be used to improve upon the existing model. The second is a very informal discussion on the computational portion of the project. While the scripts employed throughout this project have evolved and become progressively more efficient and readable, there is plenty of room for improvement.

5.2.1 Guiding Principles

Action

By far the greatest weakness of the methodology used in this project has been the application of the Benincasa-Dowker action. The most notorious snag in the development of the action-minimizing growth model has been the dimensional reduction of infrared orders, leading to glaring inconsistencies in the definition of the causet. On the one hand, the intermediate posets were seen as subintervals of a closed, connected interval of fixed cardinality, $N_{\mathcal{C}}$, and fixed Minkowski dimension, $d = 4$. On the other hand, the disconnected orders with a collective cardinality of N are clearly one-dimensional in the first transitions. The initial motivation for this deliberate choice rested upon the assumption that the Benincasa-Dowker action would rectify this inconsistency by building up the set in such a way that the resulting, complete, connected poset featured the desired Minkowski dimension, although in hindsight this is a simply naïve (although by no means serious) misuse of the action.

A more serious issue is the abuse of the smearing function. Consider the most likely case after the first transition is introduced during the growth procedure: two incomparable links. What does ϵ do for the action? Recall from Equation (2.39) that we have

$$\epsilon = \left(\frac{l}{\xi}\right)^d \tag{2.39}$$

(a) Two incomparable orders that remain disconnected. The dotted lines indicate additional events not illustrated.

(b) $N_\mathrm{I} \approx N$. Dashed lines indicate a small number of additional events and relations.

(c) $N_\mathcal{A} \gg N$. The dotted lines indicate a large number of intermediate events between the orders and the maximal event.
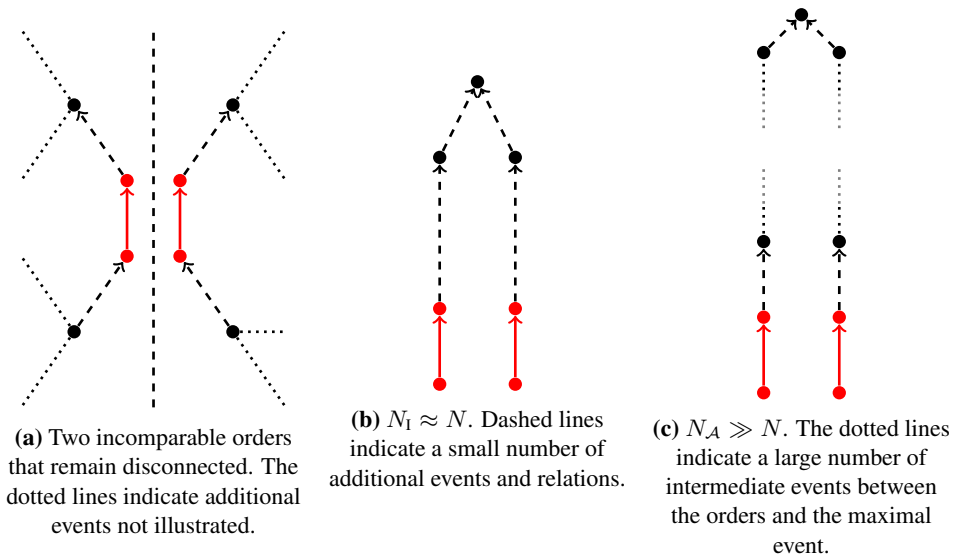
Figure 5.4: Three possible interpretations of the causet at an intermediate stage of the growth process. In Figure 5.4a, the two orders remain disconnected throughout all stages of the growth process and the Benincasa-Dowker action is not properly applied with $\xi = 4$. In Figure 5.4b, $\xi \approx 4$ and the growth process is restricted to interpreting the two orders to be connected by a common maximum at a fairly small scale. Figure 5.4c represents the optimal theoretic situation when applying the Benincasa-Dowker action to the growth process with $\xi = N_\mathcal{C}$.

where $l = 1$ in natural units and ξ is the non-local scale. By placing $\xi = 4$, we are essentially saying that events in up to three layers to the causal past of the set's maximal events may be assigned to different layers when subject to a Lorentz boost, thereby changing the distribution of intervals according to length. Again, the inconsistency reveals itself: it is implied that the set in reference is the disconnected set with cardinality $N = 4$. The use of the 4-dimensional Benincasa-Dowker action presupposes that the *interval* with cardinality $N_\mathcal{A} \gg 4$ is being measured, and not this subinterval of disconnected elements. The case with 4 elements may of course never be 4-dimensional (c.f. Equation (2.62), which gives a maximum ordering fraction of ≈ 0.17 corresponding with 3 Minkowski dimensions, if we reasonably assume that there is no such thing as "half" of a covering relation), but even if there is assumed to be some intermediate interval with cardinality $N < N_I < N_\mathcal{A}$ that may have a 4-dimensional ordering fraction, this clearly assumes too much of the causal structure of the set. Figure 5.4 provides an illustration of three possible interpretations:

1. The two orders are non-nonlocal, i.e. they are incomparable and disconnected now and forever, even under Lorentz transformations and represent completely disconnected subsets of the larger poset, as indicated by Figure 5.4a. This represents a nonsensical case where the non-locality scale, $\xi = N = 4$ in the Benincasa-Dowker action.

2. They are non-local to within three layers to the causal past of some event that both

orders precede, as indicated by Figure 5.4b. This is a specious assumption in an asymptotically large poset, as there is no reason to presume that the segments occupy the same temporal position with respect to the maximum event that connects the two orders.

3. They are non-local to within an arbitrarily large number of layers to the causal past of some event that both orders precede, as indicated by Figure 5.4c. This is the ideal case with $\xi = N_{\mathcal{A}}$ because a) there are made no *a priori* assumptions about the closed interval that the two orders are common to and b) the "smearing" remains agnostic on the matter of the relative temporal position of these segments with respect to the maximal event in the closed interval, i.e. the cardinality of the intermediate events between the two orders and the maximal event is not necessarily equal for each order.

By "temporal position" I mean the following: In Figure 5.4b, the two total orders, which we will label $i = 1, 2$, are separated from their common maximum by chains of length i_1 and i_2. In Figure 5.4b, imposing $\xi = 4$ means stipulating that $i_1 \approx i_2$. Meanwhile, in Figure 5.4c, where $\xi = N_{\mathcal{C}} = 4500$, $i_1 \neq i_2$ in general.

In fact, even the so-called optimal case depicted in Figure 5.4c does not fully encapsulate the realm of possibilities that the designation $\xi = 4$ inappropriately prohibits. Refer back to Figure 5.2, which provides a sprinkling of 32 points in 2D flat Minkowski spacetime. Figures 5.5a and 5.5b show an even greater range of possibilities when the intermediate causal set is understood in the context of their prospective embedding. When ξ is set to the cardinality of the "complete" poset, the smearing over potential local regions allows all existing elements to be (possibly) comparable, and minimizing the action will
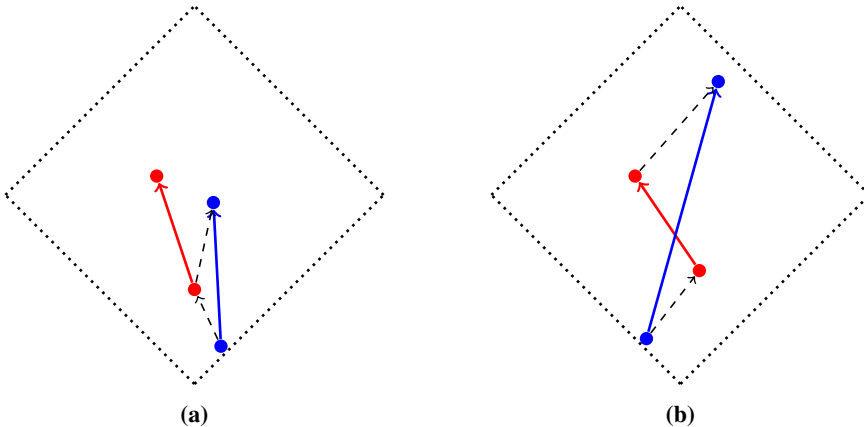

Figure 5.5: Further possibilities for the construction of causal structure during the growth process that are inappropriately excluded when the locality scale is not set equal to the cardinality of the "total" set. The four elements may also be comparable under Lorentz boosts. The solid colored lines indicate the two intermediate orders, while the dashed black lines indicate possible causal orderings in local regions, expressed as Hasse diagrams.

in theory guide the causal structure towards manifoldlike configurations with appropriate dimensionality.

Figure 5.4b is precisely what is reflected in the resulting posets using the action principle. A stochastic model is simply too much to ask of this method for calculating the observable without having designated some *a priori* timelike hypersurfaces by which the causet is partitioned. If the Benincasa-Dowker action is to be applied to the growth model, it stands to reason that each disconnected subinterval needs to be considered in its own right, the action calculated using the bi-local additive property, and the dimension of the causet, however defined, must be dynamic with respect to the growth process. Alternatively, one may start with a sprinkling of d-dimensional Minkowski spacetime and perform exchanges in a Monte-Carlo simulation as in [55], but with the kinematic restrictions of the Feynman posets imposed in each sweep.

Another more immediate possibility is fixing ξ to the number of elements in the "total" poset. Simulations with this adjustment are presently being carried out for the *holes* posets.

Locality

Another shortcoming of this project has been the treatment of weak d-rigidity. While the strong d-rigidity tests are fairly straightforward and follow precedence for reasonable applications from the prior literature [25], the procedure for determining weak d-rigidity has been rather haphazard. As Glaser and Surya have pointed out, "weak d-rigidity is a rather weak necessary condition for $\mathcal{C}$ to faithfully embed into a d-dimensional curved spacetime, since the only requirement is that there exist a local or strongly d-rigid sub-causal set $\mathcal{C}'$ in $\mathcal{C}$ [25]."

In this treatment, I have merely selected a handful of subintervals subject to no conditions other than that they are among the largest in the set. Clearly, if weak d-rigidity is to serve as a condition for embeddedness in a curved spacetime, "one should expect a whole family of strongly d-rigid sub-causal sets $\mathcal{C}'$ [25]", but the families must certainly be subject to more than the abundance of their members. Rather, the condition for embeddedness in flat spacetime borne out by strong d-rigidity hinges on the assumption that the scale of the causet is far below the scale of flatness. Were weak d-rigidity to serve as a condition for embeddedness in curved spacetime, the analysis would need to include a discussion on precisely "where" the scale of the causet reaches the flatness scale, a much more involved and complicated consideration.

Thus, the results found for the weak d-rigidity of the causets constructed in this project should be taken with a grain of salt. In reality, strong d-rigidity is a much more reliable condition for manifoldlikeness.

5.2.2   Computational Approaches

As Appendix C makes clear, the scripts used in this project leave much to be desired. While this issue does not affect the results of this project, it suffices to say that even modest improvements to the algorithms would significantly reduce runtime, with the immediate consequence of being able to produce a larger statistical sample (i.e. more posets) with larger cardinality. This latter improvement is particularly important when considering manifoldlikeness in the context of coarse-graining and the continuum limit. If we were

able to produce larger posets, even if by one order of magnitude, we would not only be dealing with a region of spacetime ten times larger to begin with, but the coarse-graining of such a set to the scale of the present posets would represent a region of spacetime with a volume on the order of half a million planck volumes. Such a set coarse-grained to 500 points would bring the scale of the poset to within just a few orders of magnitude of the resolving power of the LHC.

Appendix C represents a collection of missed opportunities that result from an initial lack of familiarity with the packages that MatLab has to offer. Readers who are well-versed in computational physics will surely notice several portions of the algorithms that are written using strategies that have been made obsolete by new functionalities. Even at the time of writing, new packages are being developed and released that offer new possibilities in graph theory. While most of the consequences have been largely superficial and regard readability and runtime, many of these extended capabilities offer exciting, new possibilities for constructing different types of sets with more specific and systematized properties.

This author prefers to take an optimistic view in the face of these considerations. What this project lacks in ease of reproducability it makes up for with the prospective new directions to explore in the immediate future.[1]

5.3 Future Work

5.3.1 Further Exploration into Fundamental Event Types

Uncovering the potential existence of fundamental event types has only just begun. So young is this proposition (and yet as timeless as Wheeler's *geons*) that the preliminary question is not "what are the fundamental event types?", nor "how are fundamental event types distinguished?", but rather if geometrodynamics is an appropriate candidate for describing quantum gravity and if so, if causal set theory can be used to identify its particles. The options moving forward are so numerous, it is almost overwhelming. The following is an outline of the most prudent next steps in the study in this author's estimation.

Deeper Analysis of Feynman Posets

Given the results produced in this project, it would certainly be premature to move onto generalized n-degenerate event vertices and beyond. While we have learned a great deal about the kinds of possibile topologies on Feynman posets, the study is far from complete. In particular, there remain an abundance of tests and conditions for manifoldlikeness that must be carried out before making any conclusive statements about 3-degenerate events. The most immediate tasks include applying the stable homology tests and embedding the most promising posets into the manifold. This is a study that will be tremendously aided by the construction of larger posets for each type. Understanding the geometric properties of posets containing these types of events will also benefit greatly from a more rigorous analysis of their infrared orders.

---

[1]http://xkcd.com/1053/

Other Parameters

Event degeneracy is just one of the possible distinguishing characteristics of fundamental event types, if they exist. Given the diversity of posets, vertex degeneracy seems to be an almost arbitrary specification. As mentioned briefly in earlier chapters, there are plenty of different types of posets and directed graphs with many properties that can be explored. One direction is to restrict the properties of each node in a graph or element in a set. Some examples are are multitrees (DAGs such that any two given chains in the poset with a common minimal event may not share a common maximal event; these may not, by definition, form closed intervals) and colored graphs (each node or edge in the graph is assigned a color and and the graph is constructed in such a way that no node or edge of the same color may be adjacent). This latter option is particularly appealing from a physicist's perspective, because it allows us to turn the tables on the narrative. By exploiting the mathematical concept of coloring graphs, the kinematic properties of the set become more direct analogies for particular event *types* that behave like coloring, but are not identical to these mathematical objects. This stands in stark contrast to the current stage of causal set theory, where the mathematics that ought to be the *model* for physical reality are presently the *defining* objects, barring more explicit developments in the discovery of event properties.

Given the analogy to the path integral approach to quantum mechanics, one need not necessarily be restricted to those mathematical objects that satisfy the exact axioms given on Page 18. As long as the mathematical object may potentially be embedded in any topology, and not necessarily a manifoldlike one, this author maintains that it contributes to the sum over histories. Suspending the condition that it must be possible to express incomparable events, for instance, gives rise to an entirely new class of sets that are *undirected*. In that case, another possibility may include specifying the properties of *finite structures* within the graph, of which Figure 5.6, the so-called Bull graph, is just one of countless examples.
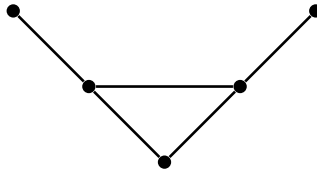

Figure 5.6: A Bull graph

Until an appropriate dynamics can be fully developed, causal set theory has focused primarily on posets, as these are thought to be the only sets that are manifoldlike in the continuum limit. Yet another direction is afforded by introducing the concept of *modes of influence* to the causet, wherein there may exist two independent and distinct chains between two events, where one chain is a link, as has been proposed by Dribus in [20]. Isham has also developed a theory similar to causal sets by means of higher-order structures that generalize the partially ordered set as *categories* ([20] citing [30]).

The possibilities are endless and this author could not hope to enumerate them in this space. These considerations represent a long-term research project that will likely be re-

visted at a later time in the study of fundamental causal events, although it should be emphasized that some of the approaches mentioned here represent independent approaches to quantum gravity in their own right, and not necessarily in regards to causal set theory.

5.3.2 Quantum Stochastic Model

While the *no holes* posets are the most promising class explored in this space, the *holes* posets are likely to pose a more stubborn challenge for manifoldlikeness tests owing to their diversity. While a deeper exploration into the *no holes* posets may begin immediately with essentially any given poset constructed, there is a much smaller likelihood of selecting a *holes* poset that happens to be manifoldlike. One approach may be to continually construct posets until one with an ordering fraction corresponding with 4 Minkowski dimensions is offered, although this is of course no guarantee that it will be manifoldlike (only that *if* it is manifoldlike, it happens to be embeddable in the particular manifold we are most interested in).

The most promising strategy for finding manifoldlikeness among the *holes* posets, if it exists, is undoubtedly by revising the stochastic growth model in hopes that this will produce the most manifoldlike that the subclass has to offer. Due to the implementational obstacles presented by the bi-local nature of the action in its present form, Monte-Carlo simulations are expected to offer a more straightforward and efficient model than the growth models employed in this project.

6
Conclusion

This project provides encouraging signs that *no holes* posets are manifoldlike and can be embedded into 2D Minkowski spacetime, as they have passed several preliminary conditions that an entropic space of posets tend to fail. Nonetheless, conclusive statements await direct embeddings. Results for the *holes* posets are on the other hand inconclusive, although the possibility remains open that the space of this subclass suffers from its own entropy problem that might be resolved via an action principle.

Despite inconclusive results, the consideration of each poset's infrared orders suggests that whether or not these posets are manifoldlike, a more detailed and statistical analysis of posets in this class may inform the question of fundamental causal event types and vertex degeneracy as one of their distinguishing features. This project has also outlined a few of the next steps that will be taken in this direction.

This project has also provided a critical self-review of the action-guided stochastic growth model that was used. From these results, this author offers an example of what *not* to do when quantizing the growth model, and offers a few suggestions for improvements in future studies.

As a closing remark, I'd like to simply offer to the reader that this project has merely scratched the surface not only of what lies in store for the future of causal set theory, but also what causal set theory can offer to the development of a theory of quantum gravity. The potential of the theory does not come without its risks. During one of our conversations, Jan Myrheim likened the study (with the liberty of creative license, of course) to the parable of the blind men and the elephant. The story describes a group of blind men who stumble upon an elephant. Each one touches a different part of the elephant–the tusk, the hoof, a side–and tries to describe the animal to the others, finding themselves in complete disagreement about the nature of an elephant. In our version of the story, I have measured the height and the volume, and characterized some of the curves of some very tiny portion of an animal, but I have not said very much about whether or not it is an elephant. Without

stretching the analogy too far, it may perhaps be said that I have rigorously shown that my animal does, in fact, have tusks; but tusks do not an elephant make.

Caution must be taken twofold. In the first, it is easy to lose track of the motivation of the project and find oneself running down highly specialized mathematical tangents that have little physical content. To be clear: this is not a reflection of what the theory has to offer, but rather a reflection of the limitations and biases the physicist may hold. Secondly, it is easy to take many of the images produced very literally, focusing on minute details that may hide the so-called "true" nature of the elephant within its folds, when in fact, one has not been observing an elephant at all.

Above all, dropping the metaphor, the greatest danger must surely be dogmatism. At all times when studying causal set theory, it must be borne in mind that the theory is at its current stage a purely mathematical (but no less valid) conceptualization of the physical. Whether the event is simply a label or "something more" remains to be seen. Again, this project has merely scratched the surface of causal sets. In turn, however, causal set theory has merely scratched the surface of geometrodynamics. If we keep digging and find nothing but dirt–i.e. nothing in our study appears to speak to the physical nature of the fundamental objects of the gravitational force–then we might as well stop digging. The key is knowing when to stop. To this author, the richness of Malament's theorem combined with the simplicity of Myrheim's statistical geometry makes the theory deserving of further investigation. I conceal no bias when I claim *there is gold in them thar hills!* When compared with what is left to be done, the potential of causal set theory is far too great to discount just yet.

Afterword

To conclude, I'd like to refer to the quote offered in the preface:

> *An adventure lacking in prospect or a rush made blindly, however, would in most cases end in failure. The adventure that really trains the theory and leads to correct cognition must have an accurate prospect more than anything else. The perspective adventure, even if it fails, is able to teach certainly lessons from the failure and secures the success in the next adventure.*

> - Shoichi Sakata, 1948

Upon a final review, I must admit that there have been occasions where this project has approached "a rush made blindly". This adventure was fortunate enough to have had a firm and patient leader. Jan Myheim has offered a strong prospect that has led to results that in turn promise future prospects. On the other hand, this author's adventurism has been consistently kept in check, such that few opportunities have been missed for learning from mistakes made in this project. For this reason, the next adventure is surely better equipped than the present.

A

d'Alembertian in Two Dimensions

For any scalar function ϕ, the d'Alembertian is given by

$$\Box\phi = \frac{1}{\sqrt{-g}}\partial_\mu\sqrt{-g}g^{\mu\nu}\partial_\nu\phi \tag{A.1}$$

A completely general line element for any 2D spacetime in any coordinate system, (p, q), is given by

$$ds^2 = A(p, q)\,\mathrm{d}p^2 + 2B(p, q)\,\mathrm{d}p\,\mathrm{d}q + C(p, q)\,\mathrm{d}q^2 \tag{A.2}$$

Consider then the line element for the topological space with light-cone coordinates, (u, v). Along the null geodesic of the light cone, the line element must be zero, so

$$ds^2 = 0, \quad \begin{cases} \mathrm{d}u = 0 \\ \mathrm{d}v = 0 \end{cases} \tag{A.3}$$

It follows that

$$ds^2 = D(u, v)\,\mathrm{d}u\,\mathrm{d}v \tag{A.4}$$

The metric tensor is then

$$g_{\mu\nu} = \begin{pmatrix} 0 & g_{uv} \\ g_{vu} & 0 \end{pmatrix} = \begin{pmatrix} 0 & D \\ D & 0 \end{pmatrix} \tag{A.5}$$

The determinant, $g = \det g_{\mu\nu}$ is then given by

$$-D^2 = g$$
$$\sqrt{-g} = D, \quad (D > 0) \tag{A.6}$$

Returning to Equation (A.1), we then have the covariant vector

$$\partial_\nu \phi = \begin{pmatrix} \partial_u \phi \\ \partial_v \phi \end{pmatrix} \tag{A.7}$$

and the contravariant vector

$$g^{\mu\nu}\partial_\nu \phi = \begin{pmatrix} \frac{1}{D}\partial_v \\ \frac{1}{D}\partial_u \end{pmatrix} \tag{A.8}$$

Next,

$$\sqrt{-g}g^{\mu\nu}\partial_\nu \phi = \begin{pmatrix} \partial_v \phi \\ \partial_u \phi \end{pmatrix} \tag{A.9}$$

Finally,

$$\Box \phi = \frac{2}{D}\partial_u \partial_v \phi \tag{A.10}$$

It is straightforward to make the discrete approximations

$$\psi(u,v) = \partial_u \phi(u,v) \approx \frac{\phi(u,v) - \phi(u - l_p, v)}{l_p}$$

$$\partial_v \psi(u,v) \approx \frac{\psi(u,v) - \psi(u, v - l_p)}{l_p}$$

$$\Box \phi \approx \frac{2}{D}\frac{\phi(u,v) - \phi(u, v - l_p) - \phi(u - l_p, v) + \phi(u - l_p, v - l_p)}{l_p^2} \tag{A.11}$$

More generally, the discrete approximation to the d'Alembertian in Equation (A.11) is given by

$$\Box \phi \approx \frac{2}{D}\frac{\phi(u,v) - \phi(u, v - b) - \phi(u - a, v) + \phi(u - a, v - b)}{ab} \tag{A.12}$$

B
Additional Results

This appendix includes additional results from the analysis that are either superfluous in the discussion, or too numerous to include in the main body of the document. Section B.1 includes some statistical distributions of heights, volumes, and ordering fractions for the smaller 1800-element posets and largely reflect those found for the larger 4500-element posets and are therefore included in this appendix for completeness only.

Section B.2 includes the scatterplots for volume, length, and ordering fraction for the smaller posets. These are included simply to demonstrate that there is no apparent relation between these properties in any of the posets. The corresponding scatterplots for the 4500-element posets feature nearly identical behaviors and are therefore not included in this document for space considerations.

Section B.3 includes the figures associated with the interval abundance curves for intermediate stages of the coarse-graining procedure for both types of posets. These figures are important for revealing the strong and weak d-rigidity of the posets, tests for the existence of local regions in flat and curved spacetime, respectively.

B.1 Additional Interval Statistics (1800-Element Sets)
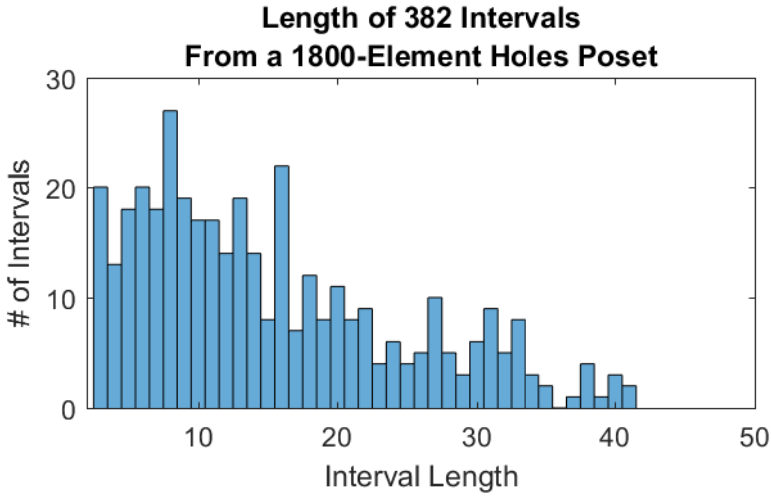
Figure B.1: Distribution of subinterval length for 1800-element *holes* poset.
Mean = 15.17
Standard Deviation = 9.42
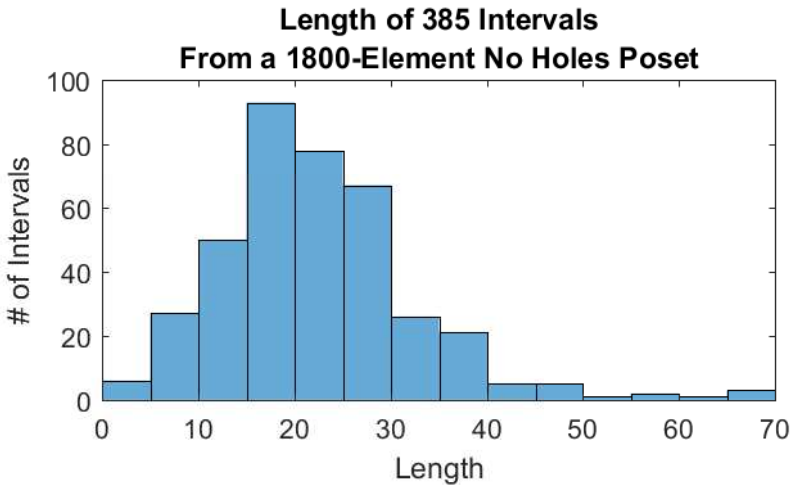
Figure B.2: Distribution of subinterval length for 1800-element *no holes* poset.
Mean = 21.74
Standard Deviation = 10.38
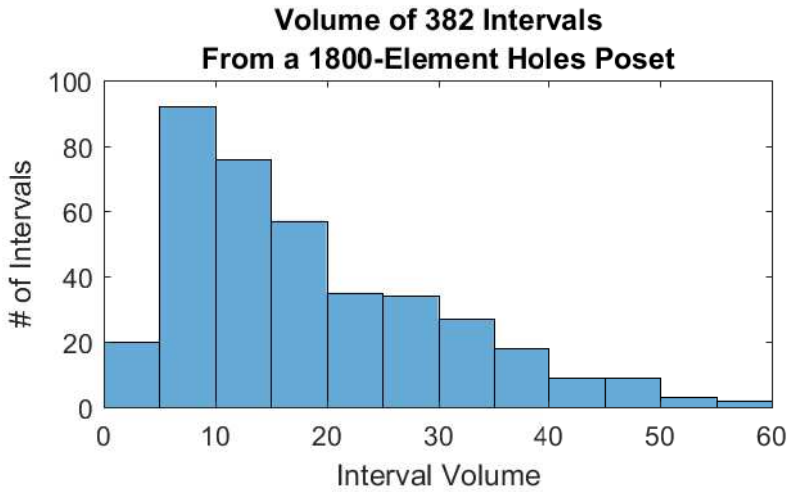
Figure B.3: Distribution of subinterval volume for 1800-element *holes* poset.
Mean = 18.15
Standard Deviation = 11.81
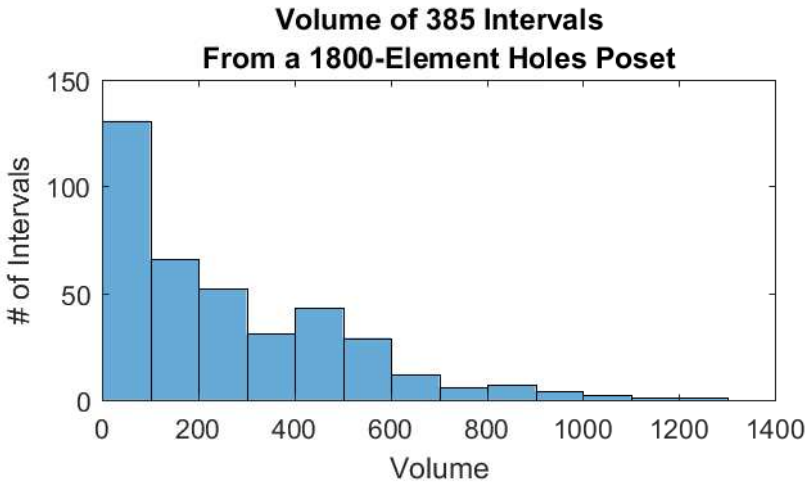
Figure B.4: Distribution of subinterval volume for 1800-element *no holes* poset.
Mean = 259.92
Standard Deviation = 238.99
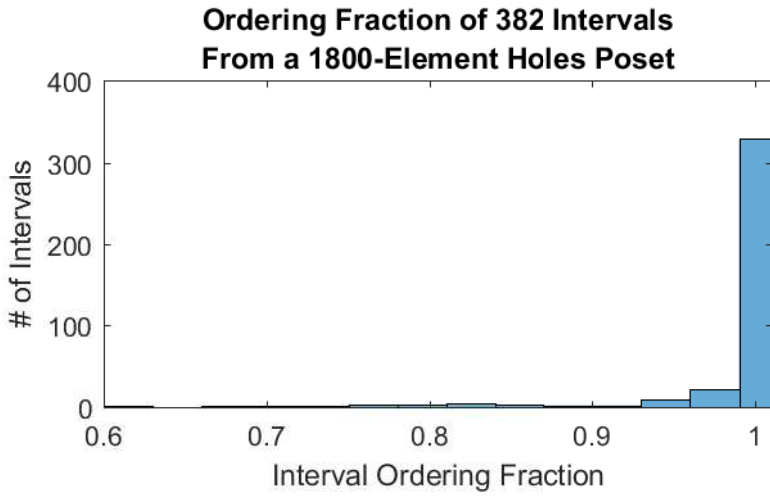
Figure B.5: Distribution of subinterval volume for 1800-element *holes* poset.
Mean = 0.99
Standard Deviation = 0.05
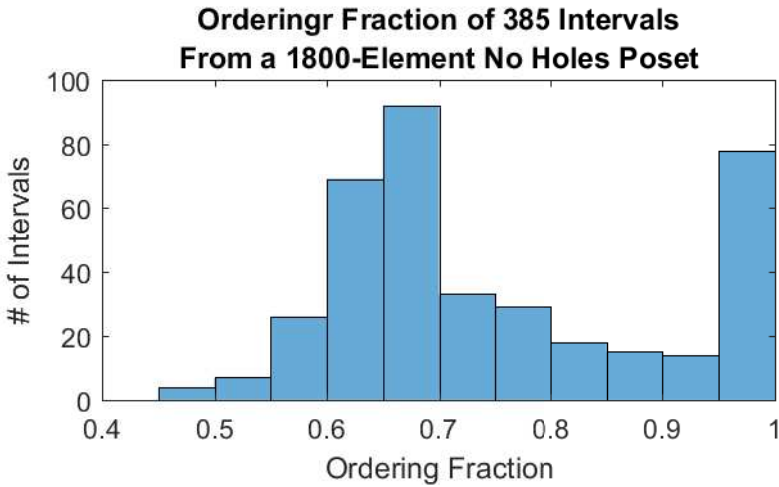
Figure B.6: Distribution of subinterval ordering fraction for 1800-element *no holes* poset.
Mean = 0.76
Standard Deviation = 0.15

B.2 Scatterplots for Smaller Posets
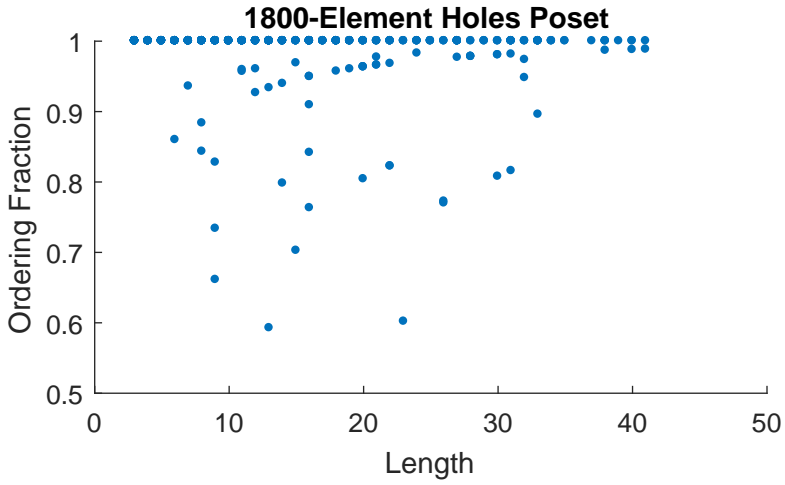
Figure B.7: Scatterplot of interval length versus ordering fraction for 1800-element *holes* poset.
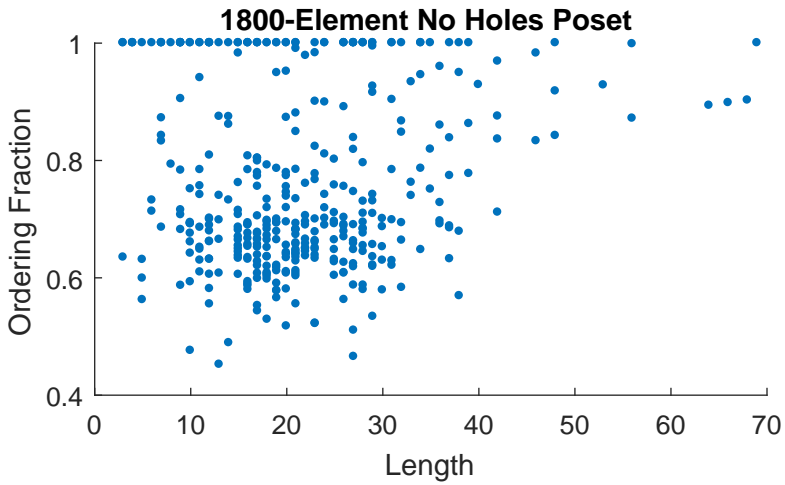

Figure B.8: Scatterplot of interval length versus ordering fraction for 1800-element *no holes* poset.
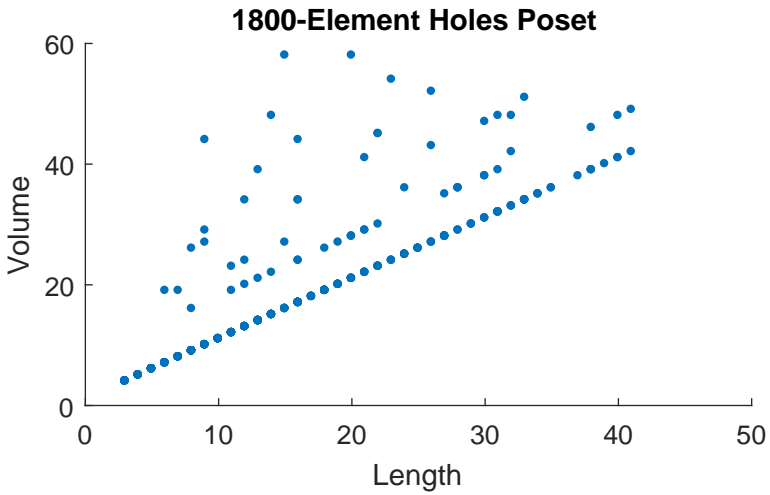
Figure B.9: Scatterplot of interval length versus volume for 1800-element *holes* poset.
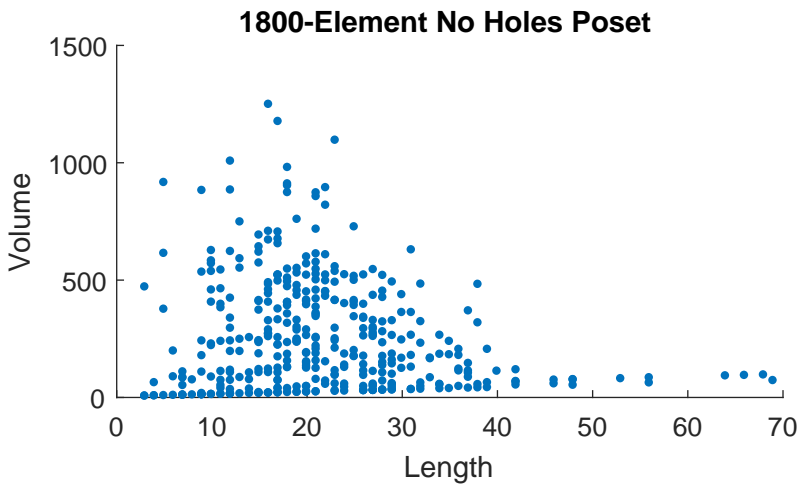

Figure B.10: Scatterplot of interval length versus volume for 1800-element *no holes* poset.

B.3 Rigidity Tests at Intermediate Coarse-Grainings

B.3.1 Strong d-rigidity
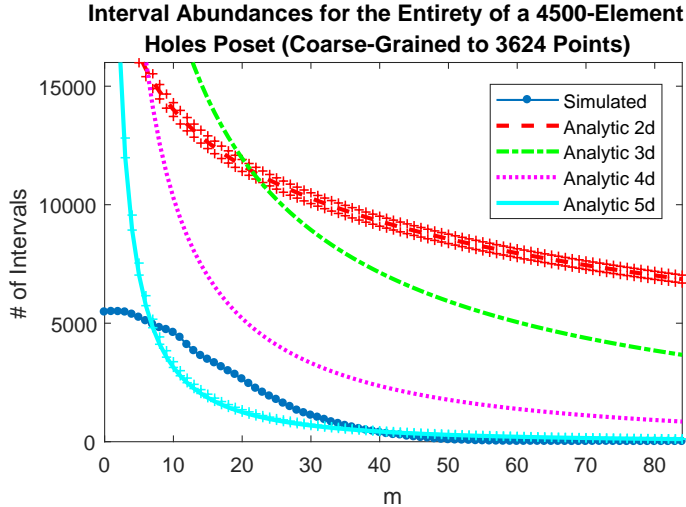
Figure B.11: Interval abundance curves for the *entirety* of coarse-graining of a 4500-element holes poset containing roughly 80% of its original points. This amounts to a test for *strong d-rigidity*.
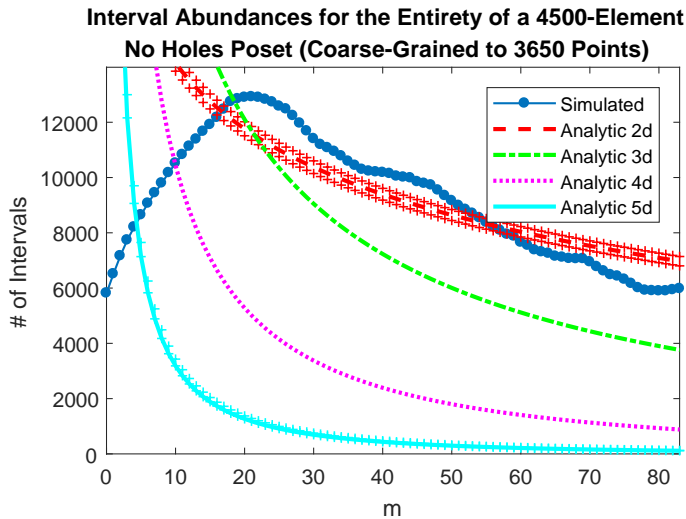

Figure B.12: Interval abundance curves for the *entirety* of coarse-graining of a 4500-element no holes poset containing roughly 80% of its original points. This amounts to a test for *strong d-rigidity*.
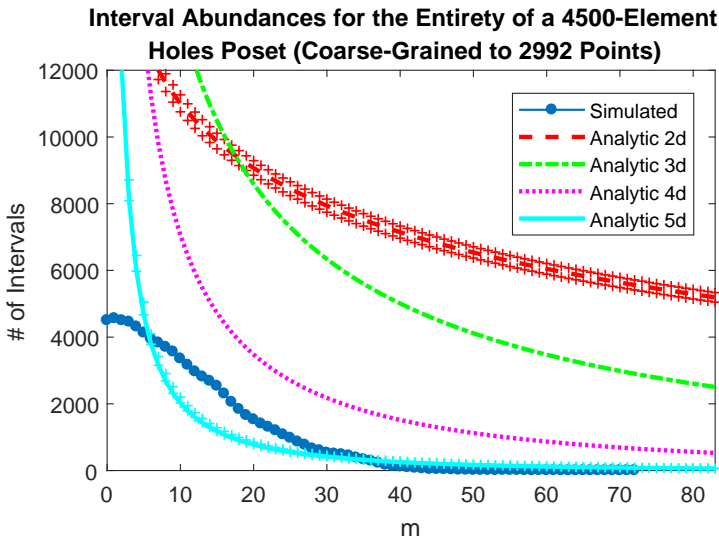
Figure B.13: Interval abundance curves for the *entirety* of coarse-graining of a 4500-element holes poset containing roughly 64% of its original points. This amounts to a test for *strong d*-rigidity.
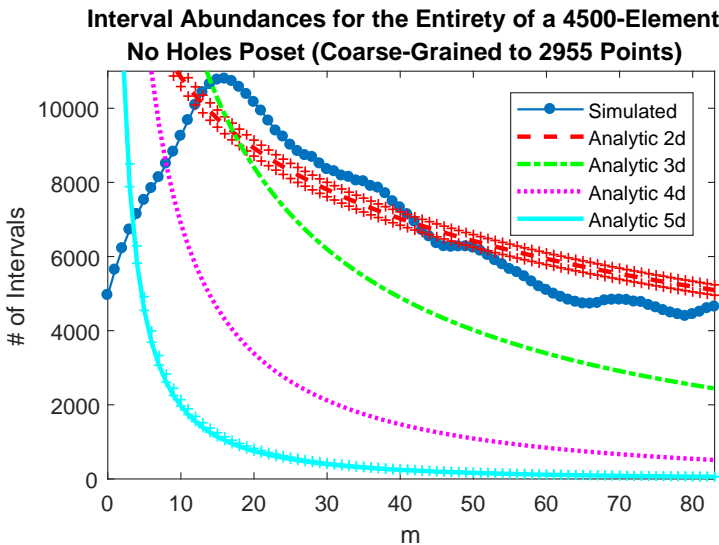
Figure B.14: Interval abundance curves for the *entirety* of coarse-graining of a 4500-element no holes poset containing roughly 64% of its original points. This amounts to a test for *strong d*-rigidity.
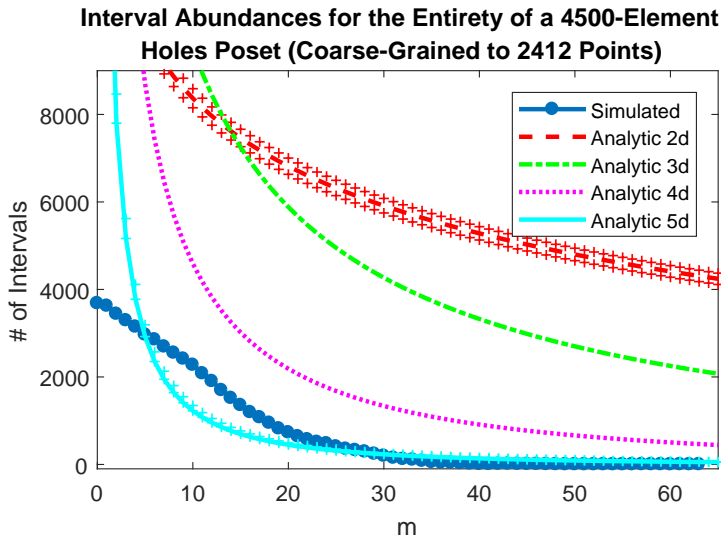
Figure B.15: Interval abundance curves for the *entirety* of coarse-graining of a 4500-element holes poset containing roughly 51% of its original points. This amounts to a test for *strong d*-rigidity.
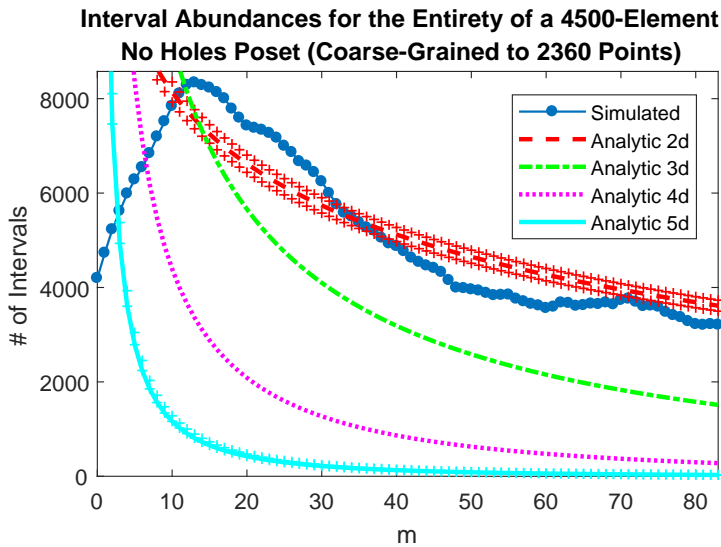

Figure B.16: Interval abundance curves for the *entirety* of coarse-graining of a 4500-element no holes poset containing roughly 51% of its original points. This amounts to a test for *strong d*-rigidity.
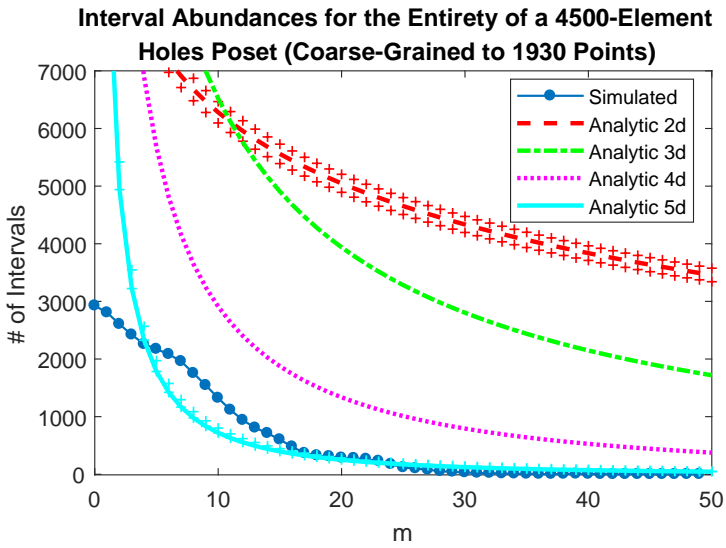
Figure B.17: Interval abundance curves for the *entirety* of coarse-graining of a 4500-element holes poset containing roughly 41% of its original points. This amounts to a test for *strong d*-rigidity.
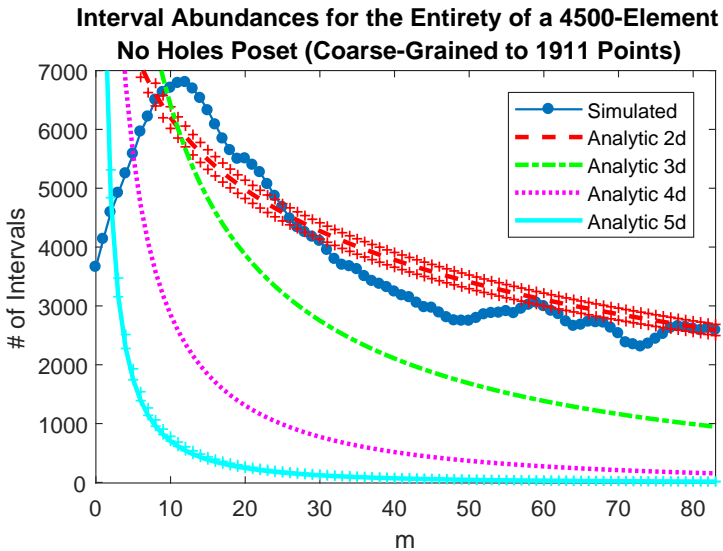

Figure B.18: Interval abundance curves for the *entirety* of coarse-graining of a 4500-element no holes poset containing roughly 41% of its original points. This amounts to a test for *strong d*-rigidity.

B.3.2 Weak d-rigidity
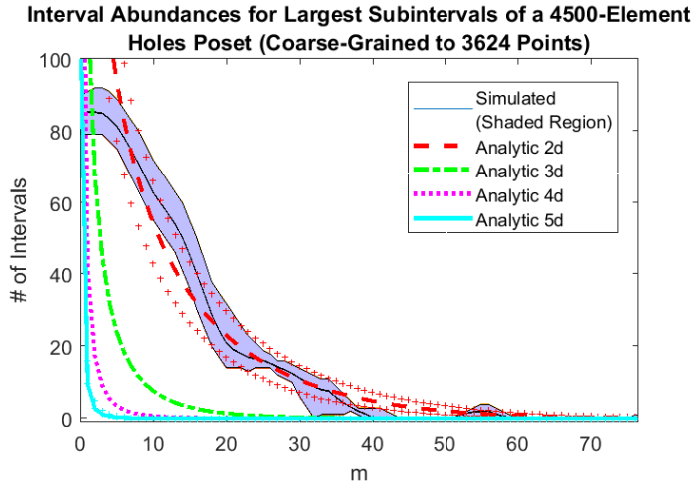
Figure B.19: Interval abundance curves for the *sampling of subintervals* of coarse-graining of a 4500-element holes poset containing roughly 80% of its original points. This amounts to a test for *weak d*-rigidity.

Figure B.20: Interval abundance curves for the *sampling of subintervals* of coarse-graining of a 4500-element no holes poset containing roughly 80% of its original points. This amounts to a test for *weak d*-rigidity.
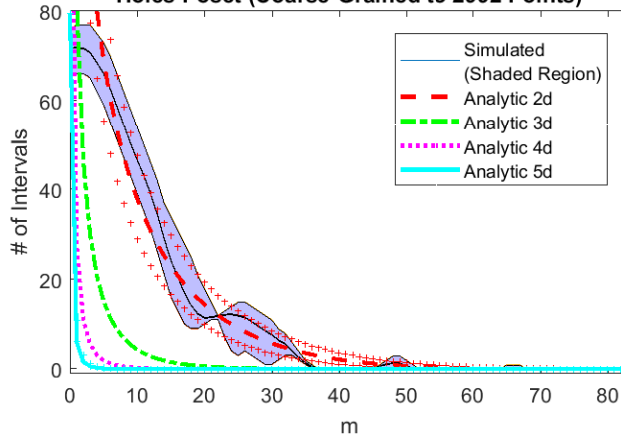
Figure B.21: Interval abundance curves for the *sampling of subintervals* of coarse-graining of a 4500-element holes poset containing roughly 64% of its original points. This amounts to a test for *weak d*-rigidity.
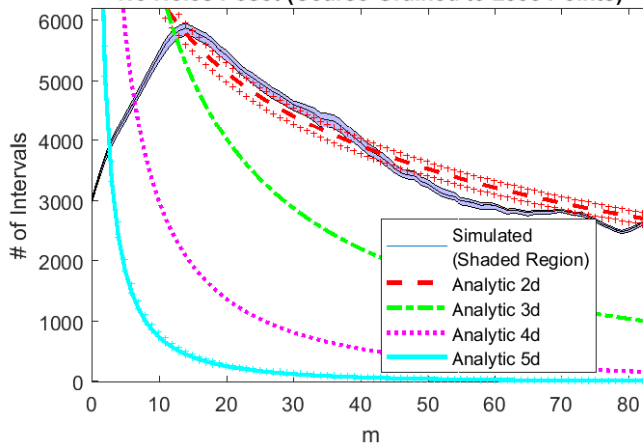
Figure B.22: Interval abundance curves for the *sampling of subintervals* of coarse-graining of a 4500-element no holes poset containing roughly 64% of its original points. This amounts to a test for *weak d*-rigidity.
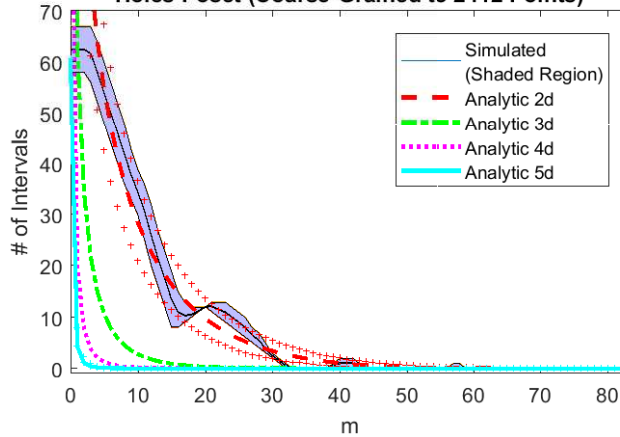
Figure B.23: Interval abundance curves for the *sampling of subintervals* of coarse-graining of a 4500-element holes poset containing roughly 51% of its original points. This amounts to a test for *weak d*-rigidity.
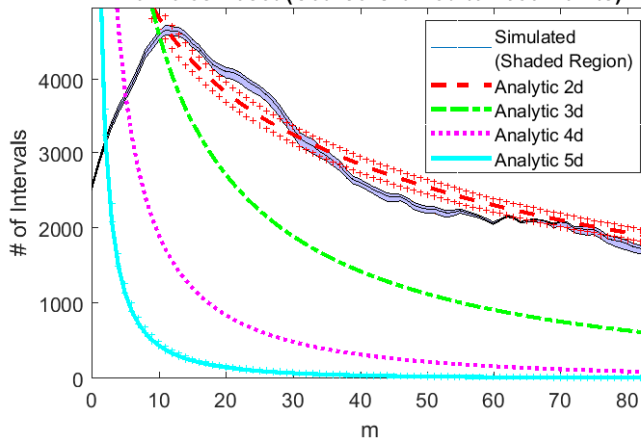

Figure B.24: Interval abundance curves for the *sampling of subintervals* of coarse-graining of a 4500-element no holes poset containing roughly 51% of its original points. This amounts to a test for *weak d*-rigidity.
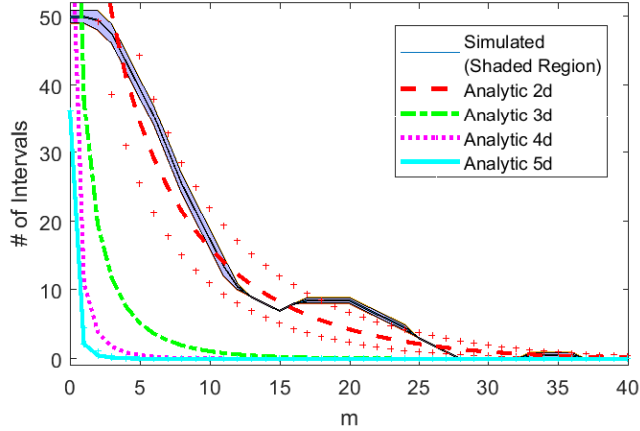
Figure B.25: Interval abundance curves for the *sampling of subintervals* of coarse-graining of a 4500-element holes poset containing roughly 41% of its original points. This amounts to a test for *weak d*-rigidity.
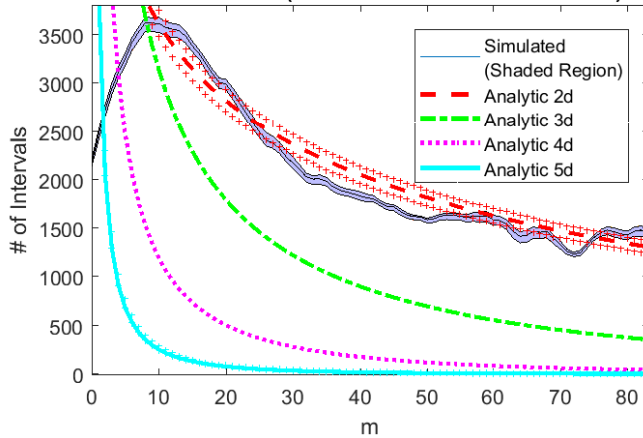

Figure B.26: Interval abundance curves for the *sampling of subintervals* of coarse-graining of a 4500-element no holes poset containing roughly 41% of its original points. This amounts to a test for *weak d*-rigidity.

C

Overview of Algorithms

This appendix contains a more detailed description of the algorithm used in this project. All scripts are written in MatLab and all results were produced using MatLab R2017a. This release contains additional functions that are not present in earlier releases of MatLab, and newer releases may have changed the functionality of some of the functions used in these scripts. These scripts are adapted for Windows environments running Java; the results were produced by running these scripts on the Linux cluster at NTNU. Introducing the script to a Linux environment leads to small changes in syntax, typically related to file structure and Java support. The source codes for both Windows and Linux adaptations are provided at `https://github.com/conorak/Causet-Generator`, along with more detailed instructions that can be followed to reproduce the results with appropriate release versions of MatLab.

The scripts provided on GitHub are not identical copies of those used in this project, but are rather adaptations based on the original scripts with functionality, readability, and efficiency improvements. The author is currently working on further improvements that will be updated in future releases on GitHub.

On a final note, it should be borne in mind that the following scripts are riddled with readability and efficiency issues, as even those with beginner-to-intermediate knowledge with MatLab will recognize. In that respect, the reader is cautioned that variable names are often confusing or unnecessarily lengthy, and extraneous steps plague the scripts. The releases on GitHub represent far more advanced versions of the code included in this document, but since these original scripts were those used to produce the results in this project, they have been added here for completeness. Those who are interested in reading through the details of the script are highly encouraged to consult those that have been released on GitHub instead of those included here.

C.1 Classical Model

The basic outline of this script is given as follows:

1. Create:

   - 50 posets containing 1800 elements
   - One poset containing 4500 elements

2. From each poset constructed, enumerate and sample its intervals. If a subinterval contains greater than 30 and less than 80 element and has an ordering fraction corresponding to two dimensions, extract its adjacency matrix (done only once for the 50 smaller posets). Store the distribution subinterval lengths, ordering fractions, and volume for the larger poset and the smaller poset from which the subinterval with dimensionality 2 was extracted. Calculate also the total ordering fraction, the height, the number of extremal events, the number of 'V'-shaped vertices, 'pitchfork'-shaped vertices, and 'Y'-shaped vertices for the entire poset.

Causet Construction

The first step in the algorithm is to construct the initial adjacency and relation matrices with a fixed cardinality N: a simple script creating two identical $N \times N$ matrices of zeroes with a '1' in the first row and second column, and a corresponding '-1' in the second row and first column. Additionally, the computation time of the algorithm is considerably aided by a corresponding `allowed` matrix that keeps track of transitions that will ultimately be rejected (i.e. between any elements that are already three-degenerate, etc.) initialized as an $N \times N$ matrix of ones with zeros on the diagonals and zeros where there exists a '1' or '-1' in the adjacency matrix (as this reflects a link which has already been added). Later, a '0' will be added when a transition between any events labeled (a, b) in the `allowed` matrix creates a loop, a hole (where applicable), or a vertex that is more than three-degenerate. Algorithm C.1 gives the script.

Algorithm C.1: Initial Poset Construction

```
1   m=4500;
2
3   %——Link matrix——
4   linkMatrix = zeros(m,m); %empty set
5   %————————————————————————————————————
6
7   %——Matrix enumerating allowed additions——
8   allowed = ones(m,m);
9   x=1;
10  while x<m+1
11      allowed(x,x)=0;
12      x=x+1;
13  end
14  %————————————————————————————————————
```

```matlab
15
16  %——Create initial subset with 1 link——
17  i = 1;
18  j = 1;
19  while i<n+1
20      while j<n+1
21          if i<j
22              linkMatrix(i,j)=1;
23              allowed(i,j)=0;
24          elseif i>j
25              linkMatrix(i,j)=—1;
26              allowed(i,j)=0;
27          end
28          j=j+1;
29      end
30      j=1;
31      i = i+1;
32  end
33  %————————————————————————————————
34
35  reltrans = linkMatrix; %Initial transitive relation matrix
```

The algorithm then immediately begins to apply transitions within a while loop specified by `countlimit`. While the `count` variable is less than `countlimit`, the algorithm will continue to add transitions. By setting `countlimit` to a large constant (e.g. ten times the cardinality of the set), the while loop will break after an arbitrarily large number of attempts to make a transition, such that the algorithm will terminate in the event there is an unforeseen condition that prohibits any additional transitions from being made. Other conditions for breaking the while loop includes a set whose vertices are all three-degenerate and an `allowed` matrix filled with zeros.

In addition to the `allowed` matrix, the algorithm also saves two arrays containing the elements that are already "saturated" with the maximum number of links in order to avoid picking these elements randomly when choosing a transition. Thus, the first step for each pass is to check for these conditions and break if they are met, as reflected in Algorithm C.2.

Algorithm C.2: Check for Exhausted Transitions

```
1   %—Add relations—
2   countlimit=m*10
3   count = 1;
4   while count<countlimit
5       %—Filter out saturated points—
6       rowadd = [1:m];
7       coladd = [1:m];
8       for b=1:m
9           if  sum(abs(linkMatrix(b,:)))>2
10              rowadd(b) = 0;
11              allowed(b,:) = zeros(1,m);
12          end
13          if sum(abs(linkMatrix(:,b)))>2
14              coladd(b) = 0;
15              allowed(:,b) = zeros(m,1);
16          end
17      end
18      rowadd = rowadd(rowadd~=0);
19      coladd = coladd(coladd~=0);
20      %————————————————————
21
22      %—Condition for finished construction—
23      if length(coladd)<2
24          break
25      end
26      %————————————————————
27
28      ...
29
30  end
```

Next, a distance matrix is created (each element of the matrix gives the chain length between the event labeled by the row to the event labeled by the column, returning ∞ if the events are incomparable and 0 along the diagonals. This is used to avoid creating extraneous links, i.e. those already implied by transitivity (if there is a chain from event a to event b of length greater than one, then a transition between event a and event b introducing a link with length one is an automorphic transformation and is therefore redundant).

The algorithm then enters another while loop, this time breaking only when the algorithm has found an appropriate transition or has exhausted all possible transitions. Selecting two random elements from the list of allowed events, the while loop first checks to see if the transition is redundant. If the *no holes* posets are being constructed and the script encounters a potential hole created by the transition between two event pairs, it will check to see if the hole can be avoided by imposing the direction of the new relation, as reflected in Algorithm C.3.

Algorithm C.3: Check for Holes

```
1  while count<countlimit
2
3      ...
4
5      distMatrix = distances(digraph(abs(linkMatrix)));
6      %——Check for holes and loops, then add——
7      success = 0; %Success=1 means the transition does not create a
             hole or loop
8      while success==0
9          %——Condition for finished construction——
10         if sum(sum(allowed)) < 2
11             count = countlimit+1;
12             break;
13         end
14         %————————————————————————————————————————————
15
16         %——Pick random point from allowed list——
17         e = randi(length(rowadd));
18         randrowadd = rowadd(e);
19         f = e;
20         while f==e
21             f = randi(length(coladd));
22         end
23         randcoladd = coladd(f);
24         %————————————————————————————————————————————
25
26         %——Extraneous link avoidance——
27         if abs(distMatrix(randrowadd,randcoladd))>1 && isinf(
                distMatrix(randrowadd,randcoladd))==0 && abs(reltrans(
                randrowadd,randcoladd))==1
28             allowed(randrowadd,randcoladd)=0;
```

```matlab
29            allowed(randcoladd,randrowadd)=0;
30            continue
31        end
32        %————————————————————————
33
34        %—Hole avoidance—
35        if sum(linkMatrix(randrowadd,:))>1
36            direction=1;
37            free=0;
38            allowed(randrowadd,:) = zeros(1,m);
39            if sum(linkMatrix(:,randcoladd))<—1
40                allowed(randcoladd,:) = zeros(1,m);
41                continue
42            end
43        elseif sum(linkMatrix(randrowadd,:))<—1
44            direction=0;
45            free=0;
46            if sum(linkMatrix(:,randcoladd))>1
47                allowed(:,randcoladd) = zeros(m,1);
48                continue
49            end
50        elseif sum(linkMatrix(randcoladd,:))>1
51            direction=0;
52            free=0;
53            allowed(randcoladd,:) = zeros(1,m);
54        elseif sum(linkMatrix(randcoladd,:))<—1
55            direction=1;
56            free=0;
57            allowed(:,randcoladd) = zeros(m,1);
58        else
59            direction = randi([0,1],1);
60            free=1;
61        end
62        %—end hole avoidance—
63
64        ...
65
66    end
67
68    ...
69
70 end
```

Next, the script checks to see if the transition will create a loop, and again attempts to impose the direction of the transition. In the *no holes* script, the direction may have already been imposed, and if the loop cannot be avoided given the direction, the transition is rejected, as reflected in Algorithm C.4.

Algorithm C.4: Check for Loops

```
1   while count<countlimit
2
3       ...
4
5       while success==0
6
7           ...
8
9       %——Loop avoidance——
10      if free==1 && reltrans(randcoladd,randrowadd)==1
11          direction=1;
12      elseif free==1 && reltrans(randcoladd,randrowadd)==−1
13          direction=0;
14      elseif free==0 && direction == 1 && reltrans(randcoladd,randrowadd
            )==−1
15          allowed(randcoladd,randrowadd)=0;
16          continue
17      elseif free==0 && direction == 0 && reltrans(randcoladd,randrowadd
            )==1
18          allowed(randrowadd,randcoladd)=0;
19          continue
20      end
21      %——end loop avoidance——
22      success = 1;
23      end
24
25      ...
26
27  end
```

If these conditions are met, the `success` variable is set to one and the transition is implemented and the relation matrix updated correspondingly as in Algorithm C.5.

Algorithm C.5: Impose the Transition

```
1   while count<countlimit
2
3       ...
4
5       while success==0
6
7           ...
8
9       %—Implement link addition—
10          if success==1
11              if direction==0
12                  linkMatrix(randrowadd,randcoladd)=1;
13                  linkMatrix(randcoladd,randrowadd)=—1;
14                  reltrans(randrowadd,randcoladd)=1;
15                  reltrans(randcoladd,randrowadd)=—1;
16                  allowed(randrowadd,randcoladd)=0;
17                  allowed(randcoladd,randrowadd)=0;
18              else if direction==1
19                      linkMatrix(randrowadd,randcoladd)=—1;
20                      linkMatrix(randcoladd,randrowadd)=1;
21                      reltrans(randrowadd,randcoladd)=—1;
22                      reltrans(randcoladd,randrowadd)=1;
23                      allowed(randcoladd,randrowadd)=0;
24                      allowed(randrowadd,randcoladd)=0;
25                  end
26              end
27              %—Links added—
28
29              %—Create transitive (relation) matrix—
30              if direction==0
31                  a = randrowadd;
32                  b = randcoladd;
33              else
34                  a = randcoladd;
35                  b = randrowadd;
36              end
37              i = 1;
38              while i<m+1
39                  if reltrans(i,a)==1 && reltrans(i,b)~=1
40                      reltrans(i,b) = 1;
41                      reltrans(b,i) = —1;
42                      j = 1;
```

```
43                  while j<m+1
44                      if reltrans(b,j)==1 && reltrans(i,j)~=1
45                          reltrans(i,j)=1;
46                          reltrans(j,i)=-1;
47                      end
48                      j=j+1;
49                  end
50              end
51              if reltrans(b,i)==1 && reltrans(a,i)~=1
52                  reltrans(a,i) = 1;
53                  reltrans(i,a) = -1;
54              end
55              i=i+1;
56          end
57          %——Transitive (relation) matrix constructed——
58          if makes_many==0
59              count = count+1
60          end
61      end
62   end
63   %——Relation added (big while loop over)——
64
65 ...
66
67 end
```

It is easy to see that the *holes* posets are much simpler to construct and only trivial changes must be made to the algorithm to admit for holes. Rather than reproducing the entirety of the script here, it suffices to note that in Algorithm C.2, the the condition for filtering out the "saturated" points is that the sum of the corresponding columns and rows changes trivially:

Algorithm C.6: Minor Changes to the Condition to Remove Allowed Events

```
1   while count<countlimit
2          %—Filter out saturated points—
3          ...
4          for b=1:m
5                  if abs(sum(linkMatrix(b,:)))>2
6                  rowadd(b)=0;
7                  allowed(b,:)=zeros(1,m);
8          end
9          if abs(sum(linkMatrix(:,b)))>2
10                 rowadd(b)=0;
11                 allowed(b,:)=zeros(1,m);
12         end
13  end
```

The section of the algorithm that checks for holes (c.f. Algorithm C.3) is of course completely removed, while the algorithm for checking for loops (c.f. Algorithm C.4) is somewhat simplified:

Algorithm C.7: Simplified Check for Loops

```
1          %—Avoid Loops—
2          if direction==1 && relMat(addTwo,addOne)==−1
3              direction=0;
4          elseif direction==0 && relMat(addTwo,addOne)==1
5              direction=1;
6          end
7          %————————
8          success=1;
```

Causet Analysis

When the causet construction is complete, the script will begin to calculate various properties of the causet, with a more in-depth computation of a representative sample of the causet's subintervals. Since the algorithm makes use of MatLab's support for the digraph object, the matrix is immediately converted to a binary, rather than trinary, representation:

Algorithm C.8: Convert from Trinary to Binary Representation

```
1   %——Create adjacency matrix to use digraph——
2   linkbinary = linkMatrix;
3   linkbinary(linkbinary~=1)=0; %remove all −1
4   relbinary=reltrans;
5   relbinary(relbinary~=1)=0;
6   %————————————————————————————————
7
8   R = digraph(relbinary);
9   L = digraph(linkbinary);
```

Next, two matrices are created to express the past and future of each element in the set:

Algorithm C.9: Construction of Past and Future Matrices

```
1   %——Matrix of future and past events——
2   past=zeros(m,1);
3   future=zeros(m,1);
4   for a=1:m
5       past(a,1:length(predecessors(R,a))) = predecessors(R,a);
6       future(a,1:length(successors(R,a))) = successors(R,a);
7   end
8   %————————————————————————————————
```

For each pair of comparable elements in the set, $a \prec b$, the union of the future a and the past of b is used to define and enumerate all intervals in the set, stored in `all_pairs`:

Algorithm C.10: Construction of Past and Future Matrices

```
1  all_pairs=zeros(1,3);
2  %——Enumerates all extrema of intervals and keeps track of those done——
3  allowdist= distances(digraph(linkbinary));
4  for a=1:size(allowdist)
5      for b=1:size(allowdist)
6          if isinf(allowdist(a,b))==1
7              allowdist(a,b)=0;
8          end
9      end
10 end
11 all_pairs=[];
12 for a=1:length(future(:,1))
13     if sum(future(a,:)~=0)>0
14         for b=1:length(future(1,:))
15             if future(a,b)~=0
16                 all_pairs=vertcat(all_pairs,[a future(a,b) allowdist(a
                       ,future(a,b))]);
17             end
18         end
19     end
20 end
21 %
```

In accordance with sampling practices, the number of intervals to sample is given by Equation (3.20), and the sample space is restricted to those intervals with a length greater than 3 to avoid infrared errors, as reflected in Algorithm C.11.

Algorithm C.11: Determine the sample size and space

```
1  Z_score=1.96;
2  moe=0.05;
3  allowed_pairs=all_pairs;
4  allowed_pairs(allowed_pairs(:,3)<3,:)=[];
5  num_intervals=size(allowed_pairs,1); %number of intervals in set
6  sample_size=(0.25*(Z_score^2))/(moe^2);
7  trialnumber=ceil((num_intervals*sample_size)/(num_intervals+
       sample_size-1));
```

Finally, the volume, ordering fraction, and length of the sampled intervals are saved in a `num_intervals` $\times 3$ array, where each column corresponds with one interval and the rows are assigned respectively. In the event an interval features a Myrheim dimension of 2, the corresponding subset is saved for later use. In the event there are are several sets being created, the `sample` array is also stored for later use, as well as the causet that was constructed. Otherwise, each row in the `sample` array is averaged to return the interval statistics over each trial. This step is illustrated in Algorithm C.12

Algorithm C.12: Compute Statistics for Subintervals

```
1   for ii=1:trialnumber
2       random_pair=randi(length(allowed_pairs(:,1))); %pick random
            interval endpoints from whole set
3       interval = allowed_pairs(random_pair,:); %1x3 array of pairs
4       interval(3)=[]; %two points only
5       allowed_pairs(random_pair,:)=[]; %removes pair from allowed
6       interval_points = vertcat(nonzeros(interval),nonzeros(intersect(
            future(interval(1,1),:),past(interval(1,2),:))))); %
            intersection of light cones
7       interval_linkMat = linkMatrix(interval_points,interval_points);
8       interval_relMat = reltrans(interval_points,interval_points);
9       interval_size = length(interval_points); %length of subinterval
10      interval_pairs=all_pairs(ismember(all_pairs(:,1),interval_points)
            ==1,:); %selects subintervals whose min is in the interval
11      interval_pairs=interval_pairs(ismember(interval_pairs(:,2),
            interval_points)==1,:); %then of those, those that are in the
            max
12
13      %——Calculates ordering fraction for interval——
14      fmax = (interval_size*(interval_size−1))/2;
15      f = sum(sum(abs(triu(interval_relMat))));
16      ratio = f/fmax;
17      %——determines interval dimension——
18      if ismember(ratio,dim_mat(:,1))==0 %if the ordering fraction/dim
            pair not stored, calculate and store
19          syms myrheim
20          eqns=(3*gamma((myrheim/2)+1)*gamma(myrheim+1))/(2*gamma((3*
                myrheim/2)+1)) == ratio;
21          assume(myrheim, 'real');
22          solution=vpasolve(eqns, myrheim, [1 Inf]);
23          myrheim=round(double(solution));
24          dim_mat=vertcat(dim_mat,[ratio myrheim]);
25      else %otherwise, reuse dimension for corresponding ordering
            fraction
26          myrheim = dim_mat(((dim_mat(:,1)==ratio)==1),2);
27      end
28      %——Myrheim dimension determined——
```

```
29
30      %——Save matrix if the poset dimension is 2——
31      if isempty(sample)==1 && (makes_many==1)==1
32          if isempty(special_hasse)==1 && (myrheim==2)==1 && exist('
                rigid')==0 && interval_size<80 && interval_size>30
33              special_hasse = interval_linkMat;
34          end
35      end
36      %——————————————————————————————————————————
37      X(ii)=interval_size;
38      Y(ii)=ratio;
39      Z(ii)=allowdist(interval(1,1),interval(1,2));
40      myrheimDim(ii)=myrheim;
41      if isempty(sample)==1 && (makes_many==1)==1
42          special_sample = 1;
43      end
44  end
45  %Sampling of intervals finished
```

The `dim_mat` array has been imported from a text file that has calculated the correspoinding Myrheim dimension from the ordering fraction beforehand. The script that produced this file is given in Algorithm C.13.

Algorithm C.13: Produce an array of ordering fractions and their corresponding dimensions

```
1   dim_mat=zeros(10000000,2);
2   i=0;
3   for ratio=0:0.0000001:1
4     i=i+1
5     syms myrheim
6     eqns=(3*gamma((myrheim/2)+1)*gamma(myrheim+1))/(2*gamma((3*myrheim
          /2)+1))==ratio;
7     assume(myrheim,'real');
8     solution=vpasolve(eqns,myrheim,[1 Inf]);
9     myrheim=round(double(solution));
10    dim_mat(i,:)=[ratio myrheim];
11  end
12  save('dim_mat.dat','dim_mat','—ASCII');
```

C.1.1 Coarse-Graining and Rigidity

A final script is then run to both coarse-grain the causets, then determine the existence of local regions in each resulting causet by calculating the d-rigidity. The coarse-graining procedure is given in Algorithm C.14. Like the subinterval statistics procedure of the preceding section, a past and future matrix is constructed based on the binary adjacency matrix. This stage of the project was characterized by an improved familiarity with the MatLab language, and rather than making changes to the matrix representations, nodes are removed directly from the digraph object according to a probability determined by the coarse-graining parameter, P, while the preceding and succeeding events are promoted from length-2 chains to links. The new causet is then stored as relation and adjacency matrices.

Algorithm C.14: Coarse-Graining Completed Causets

```
1   %——Coarse Graining——
2       L=digraph(linkbinary);
3       R=digraph(relbinary);
4       P=20;
5       m=numel(linkbinary(:,1));
6       N=m;
7       for coarse=1:5
8           i=1;
9           while i<numnodes(L)
10              if randi([1 100],1)<P
11                  past=predecessors(L,i);
12                  future=successors(L,i);
13                  for a=1:length(past)
14                      for b=1:length(future)
15                          if findedge(L,past(a),future(b))==0
16                              L=addedge(L,past(a),future(b),1);
17                          end
18                      end
19                  end
20                  L=rmnode(L,i);
21                  %——
22              else
23                  i=i+1;
24              end
25          end
26          N = numnodes(L);
27          reltrans = full(adjacency(transclosure(L)));
28          linkCoarse=full(adjacency(L));
29          R=digraph(reltrans);
30          linklabel=strcat('linkBin',num2str(coarse),'.dat');
31          relLabel=strcat('relBin',num2str(coarse),'.dat');
32          save(linklabel,'linkCoarse','—ASCII');
```

```
33          save(relLabel,'relBin','-ASCII');
34          %--Coarse-Graining complete--
35
36          ...
37
38      end
```

The procedure for determining the d-rigidity of the sets is again similar to that of the subinterval statistics, where an array enumerating all intervals in the causet is constructed. As before, the array containing interval volume, ordering fraction, and length is stored in a separate file labeled `sample` for each coarse-graining. For the test for strong d-rigidity, the volumes of every interval in the set is enumerated, sorted by incidence, and stored in the file labeled `flat`. To determine weak d-rigidity, the script identifies the maximum volume among all subintervals. A new list of intervals, `subList`, is constructed based on `allPairs`, but stores only those subintervals with volume within $N \pm \sqrt{N}$, where N is the maximum volume of subintervals. For each interval considered, the script then identifies the subintervals of each interval and calculates the minimum, mean, and maximum incidence of each subinterval volume, which is then sorted by incidence and stored in the files labeled `curveMin`, `curveMean`, and `curveMax`. This procedure is outlined by Algorithm C.15

Algorithm C.15: Determine the strong and weak d-rigidity of each coarse-graining

```
1   for coarse=1:5
2
3       ...
4
5       %— Locality (Rigidity Tests) —
6       distMat = distances(L);
7       distMat(isfinite(distMat)==0)=0;
8
9       %—Create Past and Future matrices—
10      future=zeros(N,N);
11      past=zeros(N,N);
12      for a=1:N
13          past(a,1:length(predecessors(R,a))) = predecessors(R,a);
14          future(a,1:length(successors(R,a))) = successors(R,a);
15      end
16      %————————————————————————
17
18      %—Create list of all pairs—
19      allPairs=zeros(5, numedges(R));
20      pair=1;
21      for a=1:N
22          if sum(future(a,:))~=0
23              for b=1:N
24                  if relbinary(a,b)==1 && distMat(a,b)>1
25                      points = intersect(nonzeros(future(a,:)),
                            nonzeros(past(b,:)));
26                      pointsGreater = vertcat(points,[a b]');
27                      vol = numel(points)+2;
28                      numRelations = sum(sum(relBin(pointsGreater,
                            pointsGreater)));
29                      rmax = (vol*(vol−1))/2;
```

```
30              ratio = numRelations/rmax;
31              allPairs(1:5,pair) = [a b distMat(a,b) vol-2
                    ratio]';
32              pair=pair+1;
33            end
34          end
35        end
36      end
37      sample = allPairs([3:5],1:length(allPairs(1,:)));
38      sampleLabel=strcat('sample',num2str(coarse),'.dat');
39      save(sampleLabel,'sample','-ASCII');
40
41      %%Strong d-rigidity
42      flat=zeros(max(allPairs(4,:)),1);
43      for i=1:max(allPairs(4,:));
44          flat(i) = numel(nonzeros(allPairs(4,:)==i));
45      end
46      flatLabel = strcat('flat',num2str(coarse),'.dat');
47      save(flatLabel,'flat','-ASCII');
48
49
50      %%Weak d-rigidity
51      subList=allPairs;
52
53      %-Condition for sampling subintervals-
54      maxVol=max(allPairs(4,:));
55      max_vol_min=maxVol-sqrt(maxVol);
56      max_vol_max = maxVol+sqrt(maxVol);
57      TF1=subList(4,:)<max_vol_min;
58      TF2=subList(4,:)>max_vol_max;
59      TF3=subList(4,:)==maxVol;
60      TF4=subList(4,:)==0;
61      %-----------------------------------
62
63      %-List of all intervals to sample-
64      subList(:,(TF3==0 & (TF1==1 | TF2==1) | TF4==1))=[];
65      %-----------------------------------
66
67      %-Stores abundances for sample of intervals-
68      curveMean = zeros(3,maxVol); %row 1: mean, row 2: min, row 3:
                max
69      curve = zeros(numel(subList(1,:)),maxVol); %each row is a
                sampled interval
70      %-----------------------------------------
71      for i=1:numel(subList(1,:))
```

```matlab
72            points = intersect(nonzeros(future(subList(1,i),:)),
                  nonzeros(past(subList(2,i),:)));
73            pointsGreater = vertcat(points,[subList(1,i) subList(2,i)
                  ]');
74
75            %──finds only the subinterval pairs
76            TFsub1=ismember(allPairs(1,:),points);
77            TFsub2=ismember(allPairs(2,:),points);
78            TF=TFsub1 & TFsub2;
79            %────────────────────────────────────
80            %include improper subintervals only
81            TFreject1=allPairs(1,:)==subList(1,i);
82            TFreject2=allPairs(2,:)==subList(2,i);
83            TFrej=TFreject1==1 &TFreject2==1;
84            %────────────────────────────────────
85            interval=allPairs(:,TF==1 & TFrej==0); %this the sub──
                  subintervals
86
87            for ii=1:max(interval(4,:))
88                curve(i,ii)=numel(nonzeros(interval(4,:)==ii));
89            end
90            for k=1:length(curve(i,:))
91                curveMean(1,k)=mean(curve(:,k));
92                curveMean(2,k)=min(curve(:,k));
93                curveMean(3,k)=max(curve(:,k));
94            end
95        end
96            curveLabel=strcat('curve',num2str(coarse),'.dat');
97            save(curveLabel,'curveMean','──ASCII');
98
99 end %for coarse=1:5
```

In order to produce the characteristic curves of interval bundances at various dimensions to compare with those stored in `flat`, `curveMin`, `curveMean`, and `curveMax`, Algorithm C.16 was used to numerically plot the function provided in Equation (4.1).

Algorithm C.16: Numerical plotting of characteristic curves based on analytic argument

```
1   NExp = zeros(101,1);
2   NExp(1) = 0;
3   saveN = N; %when plotting weak rigidity, N is +/− sqrt(N), so this
        saves the original N
4   for d=2:5
5       abundanceExp = zeros(101,1);
6       if d==2 || d==5
7           spec=3;
8       else
9           spec=1;
10      end
11      for xx=1:spec
12          for ii=1:101
13              if xx==2
14                  N=saveN+sqrt(saveN);
15              elseif xx==3
16                  N=saveN−sqrt(saveN);
17              end
18              m=ii−1;
19              NExp(ii)=ii−1;
20              A = (N^(m+2))/(factorial(m+2));
21              B = ((gamma(d))^2)/(pochhammer(((d/2)*(m+1)+1),d−1)*(
                    pochhammer((((d*m)/2)+1),d−1)));
22              if d==5
23                  C = hypergeom([1+m, (2/d)+m,(4/d)+m,(6/d)+m, (8/d)+m],
                        [3+m, (2/d)+m+2,(4/d)+m+2,(6/d)+m+2, (8/d)+m+2],−
                        N);
24              elseif d==2
25                  C = hypergeom([1+m, 1+m], [3+m,3+m],−N);
26              elseif d==3
27                  C = hypergeom([1+m, (2/d)+m,(4/d)+m], [3+m, (2/d)+m
                        +2,(4/d)+m+2],−N);
28              elseif d==4
29                  C = hypergeom([1+m, (2/d)+m,(4/d)+m,(6/d)+m], [3+m,
                        (2/d)+m+2,(4/d)+m+2,(6/d)+m+2],−N);
30              end
31              abundanceExp(ii) = A*B*C;
32          end
33          if xx==1
34              if d==2
35                  plot(NExp,abundanceExp,'−−r')
```

```
36              elseif d==3
37                  plot(NExp,abundanceExp,'-.g')
38              elseif d==4
39                  plot(NExp,abundanceExp,':m')
40              elseif d==5
41                  plot(NExp,abundanceExp,'--c')
42              end
43          elseif xx==2 || xx==3
44              if d==2
45                  scatter(NExp,abundanceExp,10,'+r')
46              elseif d==5
47                  scatter(NExp,abundanceExp,10,'+c')
48              end
49          end
50      end
51  end
```

C.2 Quantum Model

The implementation of an action-minimizing growth procedure is the least developed of the scripts and involves adding an additional check before admitting a transition, alongside the checks for holes and loops. Algorithm C.17, a separate script entitled `Action.m` is simply added as an if loop *ala*

```
if success==1
  run('Action.m');
end
```

immediately after the check for loops in Algorithm C.4, while Algorithm C.5, the algorithm for addition the transition, is simply removed from the main program (as it is effectively included in the `Action.m` script, since the transitions need to be imposed to calculate the action anyway. At the beginning of this script, the original causet (as well as the allowed matrix) is stored in case it needs to be restored in the event the action conditions are not met and they are saved as `auxrel`, `auxlink`, and `auxall` for the relation, adjacency, and allowed matrices, respectively.

The script then initializes the matrices as `digraph` objects, as previously, and enumerates intervals in the set, calculating their volumes. The action for the original set is calculated, the transition is imposed, and the action is calculated for the new set. If the action is positive or if Equation (3.1) is not satisfied, the transition is rejected and all matrices are restored to their original values.

Note that Algorithm C.17 is designed for calculting the action of 4-dimensional causets only. However, the constants and expressions for calculating the action can be easily replaced with the corresponding form for the Benincasa-Dowker action in arbitrary dimensions, and the script can even be altered to choose the correct form based on the total ordering fraction of the causet, cross referenced with the `dim_mat` file that was created using Algorithm C.13. This constitutes the basis for ongoing work.

Algorithm C.17: Action Minimizing Check (`Action.m`)

```
alpha = (2/gamma(1.5))*((pi/6)^(.5)); %one of the constant prefactors
    for d=4

%——Saves matrices in case transition is rejected——
auxlink = linkMatrix;
auxrel = reltrans;
auxall = allowed;
%————————————————————————————————————————

%——Do twice: once for pre—transition, another for post—transition
for ActionCounter=1:2
    %——Make matrices ready and enumerate intervals
    linkbinary = linkMatrix;
    linkbinary(linkbinary~=1)=0;
    L = digraph(linkbinary);
    distMat = distances(L);
```

```
16      distMat(isfinite(distMat)==0)=0;
17
18      relbinary = reltrans;
19      relbinary(relbinary~=1)=0;
20      R=digraph(relbinary);
21
22      future=zeros(m,m);
23      past=zeros(m,m);
24      for a=1:m
25          past(a,1:length(predecessors(R,a))) = predecessors(R,a);
26          future(a,1:length(successors(R,a))) = successors(R,a);
27      end
28
29      allPairs=zeros(5, numedges(R));
30      pair=1;
31      for a=1:m
32          if sum(future(a,:))~=0
33              for b=1:m
34                  if relbinary(a,b)==1 && distMat(a,b)>1
35                      points = intersect(nonzeros(future(a,:)),nonzeros(
                            past(b,:)));
36                      pointsGreater = vertcat(points,[a b]');
37                      vol = numel(points)+2;
38                      allPairs(1:4,pair) = [a b distMat(a,b) vol-2]';
39                      pair=pair+1;
40                  end
41              end
42          end
43      end
44      %--All intervals accounted for--
45
46      N = numnodes(L);
47      limitFromHeight = max(allPairs(3,:)); %sum for smearing function
48      Smear = 0;
49      %--calculates smearing function--
50      for xx=1:limitFromHeight
51          Nn = numel(nonzeros(allPairs(4,:)==xx));
52          STimes = ((N-1)/(N^2))^xx;
53          SOne = 1-((9*xx*(N-1))/(N^2));
54          STwo = 8*((xx^2)-xx)*(((N-1)/(N^2))^2);
55          SThree = (4/3)*((xx^3)-3*(xx^2)+2)*((N-1)/(N^2))^3;
56          Smear = Smear + Nn*STimes*(1-SOne+STwo-SThree);
57      end
58      %------------------------------------------
59
```

```matlab
60         %Specify if pre or post transition
61         if ActionCounter==1
62             ActionBefore = alpha*sqrt(N)-(N^1.5)*Smear;
63         else
64             ActionAfter = alpha*sqrt(N)-(N^1.5)*Smear;
65         end
66         %————————————————————————————
67
68         %—Impose transition if it has not been done yet—
69         if ActionCounter==1
70             if direction==0
71                 linkMatrix(randrowadd,randcoladd) = 1;
72                 linkMatrix(randcoladd,randrowadd) = -1;
73                 reltrans(randrowadd,randcoladd) = 1;
74                 reltrans(randcoladd,randrowadd) = -1;
75                 allowed(randrowadd,randwcoladd) = 0;
76                 allowed(randcoladd,randrowadd) = 0;
77             elseif direction==1
78                 linkMatrix(randrowadd,randcoladd) = -1;
79                 linkMatrix(randcoladd,randrowadd) = 1;
80                 reltrans(randrowadd,randcoladd) = -1;
81                 reltrans(randcoladd,randrowadd) = 1;
82                 allowed(randrowadd,randcoladd) = 0;
83                 allowed(randcoladd,randrowadd) = 0;
84             end
85         end
86         %————————————————————————————————————————————
87 end
88
89 %this also allows for the case where the action does not change
90 if ActionBefore==ActionAfter
91     ee = randi([1 10000],1);
92     ee=ee/10000;
93     if ee>0.5
94         success=0;
95         adjMat=auxlink;
96         relMat = auxrel;
97         allowed = auxall;
98     end
99     %—If condition not met, reject and revert back to original set—
100 elseif ActionBefore>ActionAfter
101         if exp(-(abs(ActionBefore-ActionAfter)*beta(betaCount)))<ee
102             success=0;
103             adjMat = auxlink;
104             relMat = auxrel;
```

```
105              allowed = auxall;
106          end
107      %─────────────────────────────────────────────
108  else
109      success=0;
110      linkMatrix = auxlink;
111      reltrans = auxrel;
112      allowed = auxall;
113  end
```

C.3 Additional Tools

In addition to the main causet construction script, there were a few additional scripts that were used to calculate miscellaneous properties of the sets and/or produce figures. In the interest of space limitations, these will be made available as releases in the GitHub repository, but two of these are offered here. The first is a particulary simple and instructive script for generated sprinklings in flat 2D Minkowski spacetime. The second is an algorithm for calculating the midpoint scaling dimension estimator.

C.3.1 Simple Sprinkling Script

This script for producing sprinklings was offered to the author by Jan Myrheim and is reproduced here with minor cosmetic edits.

Algorithm C.18: Sprinkling Script

```
1   rng(1917) %select seed
2   np = 32; %number of points to sprinkle
3
4   %initialize light cone coordinate axes
5   u = rand(1,np);
6   v = rand(1,np);
7   x = u−v;
8   y = u+v;
9   hold on
10  scatter(x,y,'ro','filled')
11
12  rel = zeros(np,np);
13  list1 = [];
14  list2 = [];
15  for i1=1:np−1
16    for i2=i1+1:np
17      if((y(i1)−y(i2))^2−(x(i1)−x(i2))^2>0)
18        if(y(i2)>y(i1))
19          list1 = [list1,i1];
20          list2 = [list2,i2];
21          rel(i1,i2) = 1;
22        else
23          list2 = [list2,i1];
24          list1 = [list1,i2];
25          rel(i2,i1) = 1;
26        end
27      end
28    end
29  end
30  lnk = rel;
31
```

```
32  G = digraph(list1,list2);
33  H = transreduction(G)
34  link = H.Edges;
35  link = link.EndNodes;
36  n = size(link,1);
37  for i0=1:n
38    i1 = link(i0,1);
39    i2 = link(i0,2);
40    plot([x(i1),x(i2)],[y(i1),y(i2)],'b')
41  end
42
43  plot([ 0, 1],[0,1],':','LineWidth',1)
44  plot([ 1, 0],[1,2],':','LineWidth',1)
45  plot([ 0,-1],[0,1],':','LineWidth',1)
46  plot([-1, 0],[1,2],':','LineWidth',1)
47  axis equal
```

C.3.2 Midpoint Scaling Dimension Estimator

The midpoint scaling dimension estimator was introduced later in the project, well after the sample posets were created. For this reason, the algorithm is offered as a standalone script. Implementing this algorithm into the main program is a priority task, as it will considerably reduce the overall runtime if one wishes to complete a full analysis of the posets after construction. The script relies on much of the data calculated during the main program that is not stored after completion. If the reader should wish to reproduce the results of this project, they are strongly urged to use a machine that is equipped to handle the memory demands of the following script. On that note, this is another algorithm that suffers from some of the efficiency defects of the prior scripts.

The procedure for calculating the midpoint scaling dimension estimator is outlined in Algorithm C.19. First, the script prepares the adjacency and relation matrices for use with `digraph`. As a computational convenience measure, the posets will be placed within a closed interval (that does not nwecessarily respect the kinematic constraints of the posets) labeled `ClosedLink` and `ClosedRel` for the adjacency and relation counterparts, respectively. If there are any disconnected singleton sets after coarse-graining, they are immediately removed before placing the posets within the closed interval.

Next, the distance matrix is created and all intervals within the poset are enumerated, along with a list of elements within them and their volumes. ΔV, the difference in volume between two intervals, is set to an arbitrarily high constant significantly above the cardinality of the poset. Beginning with the largest interval in the set, the script then begins to compare it against every other interval in the set. The script first checks to see if there is any intersection between the two intervals considered (other than their endpoints), and if so, moves to the next interval in the list by descending ordering in volume. If any two intervals have a difference in volume less than any other ΔV, `Vsmall` is assigned to the smallest of the two, and `Vdiff` is refreshed with the new value.

In the event two intervals have exactly the same value, the script immediately breaks out of the loop by setting the `success` variable equal to one.

Asq a protective measure to ensure accuracy of results, the script will end its search for a suitable partition of intervals if the volumes become too small. If the only remaining intervals have volumes less than $V_{\max} - 2\sqrt{V_{\max}}$, the script will simply use th2e last value of `Vsmall` to calculate the midpoint scaling dimension estimate. In the event that no suitable partition has been found, the script will terminate without storing any values (this is a temporary debugging solution). For this script, the labels `link` and `rel` have been used to denote the binar3y adjacency and relation matrices, respectively.

Algorithm C.19: Midpoint Scaling Dimension Estimator

```
1        L=digraph(link);
2        R=digraph(rel);
3        ClosedLink = L;
4        ClosedRel = R;
5        %remove disconnected
6        if numel(nonzeros(indegree(L)==0 & outdegree(L)==0))>0
7            ClosedLink = rmnode(ClosedLink,find(indegree(L)==0 &
                 outdegree(L)==0));
```

```
 8          ClosedRel = rmnode(ClosedRel,find(indegree(L)==0 &
                outdegree(L)==0));
 9      end
10      %removed disconnected nodes
11
12      %add minima and maxima and impose relations
13      addmin = 0;
14      addmax = 0;
15      if numel(nonzeros(indegree(ClosedLink)==0))>0
16          addmin=1;
17          minima = find(indegree(ClosedLink)==0);
18      end
19      if numel(nonzeros(outdegree(ClosedLink)==0))>0
20          addmax=1;
21          maxima = find(outdegree(ClosedLink)==0);
22      end
23      if addmin==1
24          ClosedRel = addedge(ClosedRel,numnodes(ClosedRel)+1,minima
                ,1);
25          ClosedLink = addedge(ClosedLink,numnodes(ClosedLink)+1,
                minima,1);
26      end
27      if addmax==1
28          ClosedRel = addedge(ClosedRel,maxima,numnodes(ClosedRel)
                +1,1);
29          ClosedLink = addedge(ClosedLink, maxima, numnodes(
                ClosedLink)+1,1);
30      end
31
32      %--distance matrix
33      distmat=distances(ClosedLink);
34      distmat(isfinite(distmat)==0)=0;
35
36      %--find all pairs
37      [x, y] = find(distmat ~= 0);
38      allPairs = zeros(length(x),3);
39      allPairs(:,[1 2]) = [x y];
40      %column 1 is minima, column 2 is maxima, 3 is volume
41
42      %--find volumes--
43      for ii = 1:length(x)
44          subint = intersect(nonzeros(successors(ClosedRel,x(ii))),
                nonzeros(predecessors(ClosedRel,y(ii))));
45          vol = numel(subint);
46          allPairs(ii,3) = vol;
```

```matlab
47            ii
48        end
49        %————————————————

51        %——sort intervals according to volume
52        allPairs = sortrows(allPairs,3,'descend');
53        %————————————————————————————————

55        Vdiff=10000000; %arbitrarily large difference
56        success=0; %condition for good vol diff

58        for ii=1:length(allPairs(:,3))—1 %pick largest interval
59            k = ii+1;
60            for jj=k:length(allPairs(:,3)) %then compare with others
61                %if the maximum of the selected pair is not the
                       minimum of the other, skip
62                if allPairs(ii,2)~=allPairs(jj,1)
63                    continue
64                end
65                %————————————————————————————————
66                %if they are exactly equal, this is the best partition
67                if abs(allPairs(ii,3) — allPairs(jj,3))==0
68                    Vsmall = allPairs(ii,3);
69                    success=1;
70                    break
71                end
72                %————————————————————————————————
73                if abs(allPairs(ii,3) — allPairs(jj,3))<Vdiff
74                    Vdiff = abs(allPairs(ii,3) — allPairs(jj,3));
75                    Vsmall = allPairs(ii,3);
76                end
77            end
78            if success==1
79                break
80            end
81        end
82        %debugging
83        if Vdiff==10000000
84            Vsmall = 0;
85        end
86        %debug

88        midpoint = log2(numnodes(ClosedLink)/Vsmall);
```

Primary References

[1] M. Aghili, L. Bombelli, and B. Pilgrim. *A Measure for Manifoldlikeness of Causal Sets*. Presentation at APS Meeting, Slides. 2018.

[2] J. Ambjørn et al. "Second-Order Phase Transition in Causal Dynamical Triangulations". In: *Physical Review Letters* 107.21, 211303 (Nov. 2011), p. 211303. DOI: 10.1103/PhysRevLett.107.211303. arXiv: 1108.3932 [hep-th].

[3] D. Benincasa. "The Action of a Causal Set". PhD thesis. Imperial College London, 2013.

[4] Dionigi M. T. Benincasa and Fay Dowker. "Scalar Curvature of a Causal Set". In: *Phys. Rev. Lett.* 104 (18 2010), p. 181301. DOI: 10.1103/PhysRevLett.104.181301. URL: https://link.aps.org/doi/10.1103/PhysRevLett.104.181301.

[5] Bjarne Å. Bergtun. "Dynamical Simulation of Causal Sets". MA thesis. Norwegian University of Science and Technology, 2016.

[6] Tommaso Bolognesi. "Algorithmic Causal Sets for a Computational Spacetime". In: *A Computable Universe*. World Scientific, 2012, pp. 451–477. DOI: 10.1142/9789814374309_0024. eprint: https://www.worldscientific.com/doi/pdf/10.1142/9789814374309_0024. URL: https://www.worldscientific.com/doi/abs/10.1142/9789814374309_0024.

[7] Luca. Bombelli. "Space-Time As a Causal Set". PhD thesis. Syracuse University, 1987.

[8] Luca Bombelli et al. "Space-time as a causal set". In: *Phys. Rev. Lett.* 59 (5 1987), pp. 521–524. DOI: 10.1103/PhysRevLett.59.521. URL: https://link.aps.org/doi/10.1103/PhysRevLett.59.521.

[9] L. Brewin. "Riemann Normal Coordinates". Accessed 5/19/2018. Clayton, Victoria, Australia, 1996.

[10] S. Carlip. "Dimensional reduction in causal set gravity". In: *Classical and Quantum Gravity* 32.23, 232001 (Dec. 2015), p. 232001. DOI: 10.1088/0264-9381/32/23/232001. arXiv: 1506.08775 [gr-qc].

[11] T. Clifton et al. "Modified gravity and cosmology". In: *Physics Reports* 513 (Mar. 2012), pp. 1–189. DOI: 10.1016/j.physrep.2012.01.001. arXiv: 1106.2476.

[12] W. Cunningham and D. Krioukov. "Causal Set Generator and Action Computer". In: *ArXiv e-prints* (Sept. 2017). arXiv: 1709.03013 [gr-qc].

[13] Deepak Dhar. "Entropy and phase transitions in partially ordered sets". In: *Journal of Mathematical Physics* 19.8 (1978), pp. 1711–1713. DOI: `10.1063/1.523869`. eprint: `https://doi.org/10.1063/1.523869`. URL: `https://doi.org/10.1063/1.523869`.

[14] F. Dowker, J. Henson, and R. D. Sorkin. "Quantum Gravity Phenomenology, Lorentz Invariance and Discreteness". In: *Modern Physics Letters A* 19 (2004), pp. 1829–1840. DOI: `10.1142/S0217732304015026`. eprint: `gr-qc/0311055`.

[15] Fay Dowker. "Causal sets and the deep structure of spacetime". In: *100 years of relativity*. Ed. by A. Ashtekar. Nov. 2005, pp. 445–464.

[16] Fay Dowker. "Introduction to causal sets and their phenomenology". In: *General Relativity and Gravitation* 45.9 (2013), pp. 1651–1667. ISSN: 1572-9532. DOI: `10.1007/s10714-013-1569-y`. URL: `https://doi.org/10.1007/s10714-013-1569-y`.

[17] Fay Dowker and Lisa Glaser. "Causal set d'Alembertians for various dimensions". In: *Classical and Quantum Gravity* 30.19, 195016 (Oct. 2013), p. 195016. DOI: `10.1088/0264-9381/30/19/195016`. arXiv: `1305.2588 [gr-qc]`.

[18] H. F. Dowker and J. J. Halliwell. "Quantum mechanics of history: The decoherence functional in quantum mechanics". In: *Phys. Rev. D* 46 (4 1992), pp. 1580–1609. DOI: `10.1103/PhysRevD.46.1580`. URL: `https://link.aps.org/doi/10.1103/PhysRevD.46.1580`.

[19] Benjamin F. Dribus. "Discrete Causal Theory". In: Springer International Publishing, 2017. Chap. 2. ISBN: 9783319500836.

[20] Benjamin F. Dribus. "On the Axioms of Causal Set Theory". In: *ArXiv e-prints* (Nov. 2013). arXiv: `1311.2148 [gr-qc]`.

[21] G. W. Gibbons and S. N. Solodukhin. "The geometry of small causal diamonds". In: *Physics Letters B* 649 (June 2007), pp. 317–324. DOI: `10.1016/j.physletb.2007.03.068`. eprint: `hep-th/0703098`.

[22] L. Glaser, D. O'Connor, and S. Surya. "Finite size scaling in 2d causal set quantum gravity". In: *Classical and Quantum Gravity* 35.4, 045006 (Feb. 2018), p. 045006. DOI: `10.1088/1361-6382/aa9540`. arXiv: `1706.06432 [gr-qc]`.

[23] Lisa Glaser. *A Causal Set Action*. `https://www.perimeterinstitute.ca/videos/causal-set-action`. Video lecture accessed on 4/11/2016. Copenhagen, Denmark, 2013.

[24] Lisa Glaser. "A closed form expression for the causal set d'Alembertian". In: *Classical and Quantum Gravity* 31.9, 095007 (May 2014), p. 095007. DOI: `10.1088/0264-9381/31/9/095007`. arXiv: `1311.1701 [math-ph]`.

[25] Lisa Glaser and Sumati Surya. "Towards a definition of locality in a manifoldlike causal set". In: *Physical Review D* 88.12, 124026 (Dec. 2013), p. 124026. DOI: `10.1103/PhysRevD.88.124026`. arXiv: `1309.3403 [gr-qc]`.

[26] James B. Hartle. "Gravity: An Introduction to Einstein's General Relativity". In: Addison-Wesley, 2003. Chap. 23. ISBN: 9780805386622.

[27] J. Henson. "Letter To The Editor: Constructing an interval of Minkowski space from a causal set". In: *Classical and Quantum Gravity* 23 (Feb. 2006), pp. L29–L35. DOI: 10.1088/0264-9381/23/4/L02. eprint: gr-qc/0601069.

[28] J. Henson. "The causal set approach to quantum gravity". In: *ArXiv General Relativity and Quantum Cosmology e-prints* (Jan. 2006). eprint: gr-qc/0601121.

[29] J. Henson et al. "Onset of the Asymptotic Regime for Finite Orders". In: *ArXiv e-prints* (Apr. 2015). arXiv: 1504.05902 [math.CO].

[30] C. J. Isham. "Quantising on a Category". In: *Foundations of Physics* 35 (Feb. 2005), pp. 271–297. DOI: 10.1007/s10701-004-1944-3. eprint: quant-ph/0401175.

[31] S. Johnston. "Particle propagators on discrete spacetime". In: *Classical and Quantum Gravity* 25.20, 202001 (Oct. 2008), p. 202001. DOI: 10.1088/0264-9381/25/20/202001. arXiv: 0806.3083 [hep-th].

[32] D. Kleitman and B. Rothschild. "Asymptotic enumeration of partial orders on a finite set". In: *Trans. Amer. Math. Soc. 205 (1975), 205-220* (1975). DOI: 10.1090/S0002-9947-1975-0369090-9. URL: https://doi.org/10.1090/S0002-9947-1975-0369090-9.

[33] D. Kleitman and B. Rothschild. "The Number of Finite Topologies". In: *Proc. Amer. Math. Soc. 25 (1970), 276-282* (1970). DOI: 10.1090/S0002-9939-1970-0253944-9. URL: https://doi.org/10.1090/S0002-9939-1970-0253944-9.

[34] S. P. Loomis and S. Carlip. "Suppression of non-manifold-like sets in the causal set path integral". In: *Classical and Quantum Gravity* 35.2, 024002 (Jan. 2018), p. 024002. DOI: 10.1088/1361-6382/aa980b. arXiv: 1709.00064 [gr-qc].

[35] S. Major, D. P. Rideout, and S. Surya. "On recovering continuum topology from a causal set". In: *Journal of Mathematical Physics* 48.3 (Mar. 2007), pp. 032501–032501. DOI: 10.1063/1.2435599. eprint: gr-qc/0604124.

[36] S. Major, D. P. Rideout, and S. Surya. "Stable homology as an indicator of manifoldlikeness in causal set theory". In: *Classical and Quantum Gravity* 26.17, 175008 (Sept. 2009), p. 175008. DOI: 10.1088/0264-9381/26/17/175008. arXiv: 0902.0434 [gr-qc].

[37] David B. Malament. "The class of continuous timelike curves determines the topology of spacetime". In: *Journal of Mathematical Physics* 18.7 (1977).

[38] D.A. Meyer. "The dimension of causal sets". PhD thesis. Massachusetts Institute of Technology, 1989.

[39] Jan Myrheim. *Causal Sets: Physics of the 22nd Century*. Colloquium Presentation. 2017.

[40] Jan Myrheim. *Classical Theory of Fields*. Department of Physics, NTNU, 2011.

[41] Jan Myrheim. *Statistical geometry*. Tech. rep. CERN-TH-2538. Geneva: CERN, 1978. URL: https://cds.cern.ch/record/293594.

[42]   Roger B. Nelsen and Harvey Schmidt. "Chains in Power Sets". In: *Mathematics Magazine* 64.1 (1991), pp. 23–31. ISSN: 0025570X, 19300980. URL: `http://www.jstor.org/stable/2690450`.

[43]   H. J. Prömel, A. Steger, and A. Taraz. "Phase Transitions in the Evolution of Partial Orders". In: *Journal of Combinatorial Theory, Series A* 94.2 (2001), pp. 230 –275. ISSN: 0097-3165. DOI: `https://doi.org/10.1006/jcta.2000.3135`.

[44]   David D. Reid. "Introduction to causal sets: an alternative view of spacetime structure". In: *Canadian Journal of Physics* 79.1 (2001), pp. 1–16. DOI: `10.1139/cjp-79-1-1`.

[45]   David D. Reid. "Manifold dimension of a causal set: Tests in conformally flat spacetimes". In: *Phys. Rev. D* 67.2, 024034 (Jan. 2003), p. 024034. DOI: `10.1103/PhysRevD.67.024034`. eprint: `gr-qc/0207103`.

[46]   D. P. Rideout. "Dynamics of Causal Sets". In: *ArXiv General Relativity and Quantum Cosmology e-prints* (Dec. 2002). eprint: `gr-qc/0212064`.

[47]   D. P. Rideout and R. D. Sorkin. "Classical sequential growth dynamics for causal sets". In: *Physical Review D.* 61.2, 024002 (Jan. 2000), p. 024002. DOI: `10.1103/PhysRevD.61.024002`. eprint: `gr-qc/9904062`.

[48]   D. P. Rideout and R. D. Sorkin. "Evidence for a continuum limit in causal set dynamics". In: *Phys. Rev. D* 63 (10 2001), p. 104011. DOI: `10.1103/PhysRevD.63.104011`. URL: `https://link.aps.org/doi/10.1103/PhysRevD.63.104011`.

[49]   R. D. Sorkin. "Does Locality Fail at Intermediate Length-Scales?" In: *ArXiv General Relativity and Quantum Cosmology e-prints* (2007). eprint: `gr-qc/0703099`.

[50]   R. D. Sorkin. "Light, links and causal sets". In: *Journal of Physics Conference Series*. Vol. 174. Journal of Physics Conference Series. June 2009, p. 012018. DOI: `10.1088/1742-6596/174/1/012018`. arXiv: `0910.0673 [gr-qc]`.

[51]   R. D. Sorkin. "Quantum Mechanics as Quantum Measure Theory". In: *Modern Physics Letters A* 9 (1994), pp. 3119–3127. DOI: `10.1142/S021773239400294X`. eprint: `gr-qc/9401003`.

[52]   R. D. Sorkin. "Scalar Field Theory on a Causal Set in Histories form". In: *Journal of Physics Conference Series*. Vol. 306. Journal of Physics Conference Series. July 2011, p. 012017. DOI: `10.1088/1742-6596/306/1/012017`. arXiv: `1107.0698 [gr-qc]`.

[53]   R. D. Sorkin. "Toward a "fundamental theorem of quantal measure theory"". In: *ArXiv e-prints* (Apr. 2011). arXiv: `1104.0997 [hep-th]`.

[54]   Sumati Surya. "Directions in Causal Set Quantum Gravity". In: *ArXiv e-prints* (Mar. 2011). arXiv: `1103.6272 [gr-qc]`.

[55]   Sumati Surya. "Evidence for the continuum in 2D causal set quantum gravity". In: *Classical and Quantum Gravity* 29.13, 132001 (July 2012), p. 132001. DOI: `10.1088/0264-9381/29/13/132001`. arXiv: `1110.6244 [gr-qc]`.

References on Dialectic Materialism

[56] F. Engels. *Anti-Dühring*. Engelsh. Trans. German by E. Burns. Moscow, USSR: Progress Publishers, 1947. URL: https://www.marxists.org/archive/marx/works/1877/anti-duhring/index.htm.

[57] F. Engels. "Dialectics of Nature". English. In: *Marx/Engels Selected Works*. Vol. 1. Moscow, USSR: Marx-Engels Institute, 1925. URL: https://www.marxists.org/archive/marx/works/1883/don/index.htm.

[58] V. I. Lenin. "Materialism and Empirio-criticism". English. In: *Lenin Collected Works*. Trans. Russian by A. Fineberg. Vol. 14. Moscow, USSR: Progress Publishers, 1972, pp. 17–362. URL: https://www.marxists.org/archive/lenin/works/1908/mec/index.htm.

[59] V. I. Lenin. "On the Question of Dialectics". English. In: *Lenin Collected Works*. Trans. Russian by C. Dutt. 4th ed. Vol. 38. Moscow, USSR: Progress Publishers, 1976, pp. 357–361. URL: https://www.marxists.org/archive/lenin/works/1914/cons-logic/summary.htm.

[60] Tse-Tung Mao. "On Contradiction". English. In: *Selected Works of Mao Tse-tung*. Vol. 1. Peking, China: Foreign Languages Press, 1965. URL: https://www.marxists.org/reference/archive/mao/selected-works/volume-1/mswv1_17.htm.

[61] K. Marx. "Theses on Feuerbach". English. In: *Marx/Engels Selected Works*. Ed. by F. Engels. Trans. German by W. Lough. Vol. 1. Originally unpublished work written by Marx in the Spring of 1845 and edited by Engels; it was published by the Marx-Engels Institute in Moscow in 1924 in Russian, then translated and published in 1969 and distributed by marxists.org in 1995. Moscow, USSR: Progress Publishers, 1969, pp. 13–15. URL: https://www.marxists.org/archive/marx/works/1845/theses/theses.htm.

[62] Shoichi Sakata. "Taketani's "Three-Stage Theory"*". In: *Progress of Theoretical Physics Supplement* 50 (1971), pp. 9–11. DOI: 10.1143/PTPS.50.9. eprint: /oup/backfile/content_public/journal/ptps/50/10.1143/ptps.50.9/2/50-9.pdf. URL: http://dx.doi.org/10.1143/PTPS.50.9.

[63] Mitsuo Taketani. "Dialectics of Nature: On quantum mechanics". In: *Progress of Theoretical Physics Supplement* 50 (1971), pp. 27–36. DOI: 10.1143/PTPS.50.27. eprint: /oup/backfile/content_public/journal/ptps/50/10.1143/ptps.50.27/2/50-27.pdf. URL: http://dx.doi.org/10.1143/PTPS.50.27.